UNIVERSITÀ DEGLI STUDI DI TRIESTE

XXXII CICLO DEL DOTTORATO DI RICERCA IN BIOMEDICINA MOLECOLARE

ROLE OF $p27^{Kip1}$ IN MAMMARY GLAND DEVELOPMENT AND TUMORIGENESIS IN Δ16HER2 MODEL

Settore scientifico-disciplinare: BIO/11 BIOLOGIA MOLECOLARE

DOTTORANDO /
GIORGIA MUNGO

COORDINATORE
PROF.SSA GERMANA MERONI

SUPERVISORE DI TESI
DOTT. GUSTAVO BALDASSARRE

CO-SUPERVISORE DI TESI
DOTT.SSA BARBARA BELLETTI

ANNO ACCADEMICO 2018/2019

UNIVERSITÀ DEGLI STUDI DI TRIESTE

XXXII CICLO DEL DOTTORATO DI RICERCA IN BIOMEDICINA MOLECOLARE

ROLE OF $p27^{Kip1}$ IN MAMMARY GLAND DEVELOPMENT AND TUMORIGENESIS IN Δ16HER2 MODEL

Settore scientifico-disciplinare: BIO/11 BIOLOGIA MOLECOLARE

DOTTORANDO /
GIORGIA MUNGO

COORDINATORE
PROF.SSA GERMANA MERONI

SUPERVISORE DI TESI
DOTT. GUSTAVO BALDASSARRE

CO-SUPERVISORE DI TESI
DOTT. SSA BARBARA BELLETTI

ANNO ACCADEMICO 2018/2019

Table of contents

ABSTRACT

HER2-amplified Breast Cancers (HER2 BC) represent about 15-20% of invasive BC and have poor prognosis. A subset of HER2-positive BC expresses an HER2 splice variant (Δ16HER2) with enhanced transforming activity. In the context of BC, the CDKN1B gene, encoding for the cell cycle inhibitor $p27^{kip1}$ (hereafter p27) is a tumor suppressor whose low nuclear expression is associated with worse patients' prognosis and altered response to therapies. However, controversial clinical and preclinical evidences have been reported on the role of p27 in HER2 BC.

Here using the MMTV-Δ16HER2 transgenic mice crossed with Cdkn1BKO mice we showed that Cdkn1BKO females had an unexpectedly lower number of tumors but a marked anticipation of tumor onset and a significantly increased tumor growth rate, suggesting a possible dual role for p27 in tumor onset and growth. Using a syngeneic injection approach, we observed that Δ16HER2 tumor-derived epithelial cells, either WT or Cdkn1BKO, displayed increased growth rate when injected in Cdkn1BKO recipient mice, indicating that, in this context, p27 tumor suppressor activity is mainly due to cell non-autonomous activities. A proteomic characterization of mouse mammary and serum samples confirmed this possibility, revealing an altered expression of selected cytokines involved in inflammatory response and immune cell maturation and recruitment (e.g. CX3CL1, CTLA4, CCL25, PRL) in Δ16HER2/Cdkn1BKO, accompanied by a significant increase of CD45+ leukocyte (mainly activated T Cells) in pre-neoplastic tissue examined at 13 weeks of age. Intriguingly, at the same age, Δ16HER2p27KO mice displayed profound alterations of mammary gland structure, with hypertrophic and swollen ducts, resembling a lactating phenotype. Based on the notion that prolactin (PRL) plays a key role in both lactation and T-cell activation we investigated further its role in our model and showed that, when compared to Δ16HER2/Cdkn1BWT, Δ16HER2/Cdkn1BKO mammary glands had higher expression of PRL resulting in aberrant JAK2 phosphorylation and STAT5 activation.

Collectively, our data indicates that in Δ16HER2-driven BC, p27 plays key non cell-autonomous roles that affect not only tumor onset and development but also the mammary gland morphogenesis. Since the PRL-PRL receptor axis is currently proposed as a new possible target for anticancer therapies for BC patients (*e.g.* Prolanta), these results could have a high and immediate translational relevance.

1. INTRODUCTION

1.1 Breast Cancer

Breast Cancer (BC) is the most common malignancy in women, and is also the leading cause of cancer death in over 100 countries. BC incidence has been rising in some Northern and Eastern European countries, has remained stable in several others, and some declines were only registered in Southern European countries. In the EU BC is the second cause of cancer death in women, despite favorable mortality trends since 1990s (Malavezzi et al., 2019). The downward mortality trends are due to the introduction of population screening, the rise of early diagnosis and the improvement of therapies (Carioli et al., 2017; Massat et al., 2016).

Age, family history, early menarche and late menopause all represent risk factors of breast cancer incidence, while modifiable factors include post-menopausal obesity, use of combined estrogen and progestin menopausal hormones, breastfeeding and lifestyle factors, such as diet, alcohol intake and smoking (American Cancer Society, 2015-2016). Hormonal perturbations influence breast cancer risk due to their impact on mammary epithelial cell proliferation and cancer growth, therefore a woman's cumulative lifetime exposure to estrogen determines the level of this environmental risk (Benson et al., 2009). Nulliparity and late childbearing are well known risk factors of breast cancer.

Up to 10% of breast cancer in Western countries is due to genetic predisposition. The most relevant genes identified as high-risk are BRCA1 and BRCA2, both implicated in different biological processes including DNA repair and recombination, cell cycle control and transcription (McPherson et al., 2000; Venkitaraman et al., 2002). Within cells, the effects of BRCA1 and BRCA2 are recessive, and both copies of an allele must be lost or mutated for cancer progression. Individuals carrying germline mutation in these genes have a dominantly inherited susceptibility, the second hit occurring in the somatic allele. However, mutations in BRCA1 and BRCA2 are rare in sporadic breast cancer (Benson et al., 2009). Other breast cancer susceptibility genes include mutations in TP53, PTEN and, rarely, H-RAS gene. Heterozygous carriers of ataxia-teleangectasia (ATM) gene mutations have also been reported to have increased risk of breast cancer (Antoniou et al., 2002). Fanconi anemia pathway genes have also been reported in about 5% of familial breast cancer (Melchor and Benitez, 2013).

Summarizing, breast cancer is a very common disease, detection and treatment at an early stage improves the prospects for long-term survival (Richards et al., 1999), nevertheless we still lack a complete knowledge of the biologic heterogeneity of breast cancers with respect to molecular alterations, treatment sensitivity and cellular composition (Prat and Perou, 2010).

1.2 Breast cancer classification

Breast cancer is not a single disease, but rather it comprises of many biologically different entities with distinct pathological features and clinical implications (Spitale et al., 2008; Desmedt et al., 2009; Sotiriou and Pusztai, 2009; Weigelt et al., 2010). A large amount of evidence has suggested that BC with different histopathological and biological features exhibit distinct behaviors that lead to different treatment responses and should be offered different therapeutic options (Blows et al.; 2010).

Breast cancer can begin in different areas of the breast, the ducts, the lobules, or in some cases, the tissue in between, and develop with peculiar morphological features (medullary, tubular, cribriform, mucinous).

From a histological point of view, breast cancers are classified as follows:

I. **Invasive (infiltrating) carcinomas**, are a heterogeneous group of tumors differentiated into histological subtypes. The major invasive carcinomas include infiltrating ductal, invasive lobular, ductal/lobular, medullary, tubular, mucinous (colloid), Paget disease. Of these, infiltrating ductal carcinoma (IDC) is the most common, accouting for 70-80% of all invasive lesions (Malhotra et al., 2010; Li et al., 2005).

II. **Non-invasive intraductal carcinomas (DCSI),** are carcinomas of the mammary ducts which do not invade the surrounding mammary tissues, and are considerably more common than its lobular carcinoma in situ (LCSI) counterpart and encompasses a heterogeneous group of tumors (Malhotra et al., 2010). DCIS has traditionally been further sub-classified based on the architectural features of the tumor which has given rise to five well recognized subtypes: Comedo, Cribiform, Micropapillary, Papillary and Solid (Connolly et al., 2004).

Histological classification is however not sufficient to understand the heterogeneity of this neoplasia; therefore, breast cancers have been further sub-classified depending on hormone receptor expression (estrogen and progesterone receptors) and on the over-expression or amplification of the HER2/ErbB2 oncogene (Hergeta-Redondo et al., 2008). Assessed by immunohistochemistry, breast cancer can be subdivided into three major subtypes.

(1) **Hormone-Receptor positive breast cancers** are tumors expressing estrogen and progesterone receptor, which was the first example of cancer suitable to targeted therapies (Higgins and Baselga, 2011). Estrogen-dependent breast cancer was initially treated with estrogen antagonist, in particular tamoxifen, which inhibits the activation of ER (Ali and Coombes, 2002).

(2) **HER2-overexpressing tumors.** HER2 gene encodes for a tyrosine kinase receptor, which belongs to a family of transmembrane receptors, activated by numerous extracellular ligands. These

ligands mediate growth, differentiation and cell survival. Overexpression of HER2 protein or HER2 gene amplification occurs in 15-25% of aggressive breast cancers (Martine et al., 2005). Trastuzumab is a humanized monoclonal antibody, developed against the HER2 extracellular domain, utilized as monotherapy or in combination with chemotherapy to provide a survival advantage to women with HER2-overexpressing breast cancer (Vogel et al., 2002).

(3) **Triple negative breast cancers** (TNBC) are characterized by the lack of both hormone receptors as well as HER2 overexpression/amplification. TNBC has a worse prognosis and tends to relapse earlier, but displays enhanced chemosensitivity compared to other subtypes (Dawood, 2010).

Thanks to the improvement of genomic studies, our knowledge of molecular alterations in cancer cell has rapidly climbed. RNA expression studies, based on cDNA microarrays, have provided the basis for an improved taxonomy of breast cancer. Microarray platform helped to group tumors based on alterations in the expression of a set of predefined genes (Sorlie et al., 2001; Sorlie et al., 2003). Therefore, phenotypic diversity of breast tumors can be due to differences in gene expression patterns. The study of Perou et al. identified five intrinsic subtypes: the luminal A, the luminal B, the basal-like, the human epidermal growth factor 2-related (HER2-related) and the normal-like (Perou et al., 2000). Recently, other studies identified a new subtype called “claudin-low” (Prat et al., 2010).

1.2.1 Luminal Subtype

The expression of estrogen receptor (ER) and ER-associated genes characterizes the luminal breast cancers. Within luminal subtype, there are at least two biological distinct subtypes: luminal A and luminal B.

Luminal cancers are often low-grade tumors, even though luminal B tumors have usually a poorer prognosis (Cheang et al., 2009). Luminal subtypes display a gene expression pattern, which is comparable to the one of the luminal epithelial cells of the mammary gland; they show high expression of both luminal cytokeratin 8 and 18 and are defined by the expression of four transcription factors such as ER, GATA3, FOXA1 and XBP1 (Perou and Dale, 2011). GATA3 has a critical role in the morphogenesis of the mammary gland and in luminal cells differentiation (Asselin-Labat et al., 2006), while FOXA1 is a downstream target of GATA3 and it is required for the induction of most ER-regulated genes (Kouros-Mehr et al., 2006). Luminal A breast cancers generally display low expression of HER2-cluster genes and tend to be less proliferative than luminal B tumor, given that luminal A subtype shows low expression of Ki-67 (<20%) and other proliferative genes (Sorlie et al., 2001, 2003). Thus, a distinction between luminal A and luminal B is based on their proliferation status and on the expression of HER2-associated genes. Finally, luminal B tumors display a higher frequency of TP53 mutations (Jacquemier et al., 2009).

1.2.2 HER2-enriched Subtype

The HER2-positive breast cancers are defined by the DNA amplification of HER2 together with overexpression of multiple HER2-amplicon-associated genes, including GRB7 (The cancer genome Atlas network, 2012). Depending on their estrogen receptor status, HER2-amplified tumors are split into two groups: HER2-positive/ER-negative, which clusters near the basal-like tumor and displays low expression of hormone receptor regulated genes, and HER2-positive/ER-positive. The latter may also be progesterone receptor positive and clusters with tumors of luminal cell origins, therefore it falls into the luminal B intrinsic subtype (Carey et al., 2006). HER2 overexpressing tumors comprise 15-25% of all breast cancers and they are usually high-grade tumors (Perou et Dale, 2011), even though ER+/HER2+ has significantly better survival than the ER-/HER2+ subtype (Parise et al., 2009). As mentioned above, patients with HER2-positive disease have greatly benefit from anti-HER2 targeted therapy. Treatment with trastuzumab increases the clinical benefit of first-line chemotherapy in metastatic breast cancers that overexpress HER2 compared to the best available standard chemotherapy alone (Slamon et al., 2001).

1.2.3 Basal-like Subtype

According to immunohistochemical classification, this subtype is often referred to as triple-negative breast cancer (TNBC) because most of basal-like tumors are negative for hormone receptors and HER2 amplification. However, most but not all basal-like tumors are triple-negative and most but not all triple negative BC are basal-like (Perou et Dale, 2011). These cancers express gene characteristic of basal epithelial cells such as cytokeratins 5, 6, 14, 17, vimentin and P-cadherin. Many of the overexpressed basal-like genes are involved in cellular proliferation (MEK, ERK, PI3K, AKT, NF-kB, cyclin E1, c-kit and EGFR), suppression of apoptosis, cell migration or invasion (TGF-β2) and, as a whole, they contribute to an aggressive phenotype and a decreased cell differentiation. Moreover, basal-like subtype shows a reduced expression of ER, ER-responsive genes and other genes peculiar to luminal epithelial cells and rarely HER2 overexpression (Rakha et al., 2008). Basal-like subtype displays high frequency of TP53 mutations (80%) and loss of RB1 and BRCA1 are additional basal-like features (The Cancer Genome Atlas Network, 2012). Most of BRCA1 germline mutation carriers display basal-like cancers (80-90%); while sporadic basal-like breast cancers represent a minority percentage (15%) and most of the times, BRCA1 gene or protein does not show any alteration.

1.2.4 Claudin-low Subtype

In 2007, Prat et al. identified a new molecular breast cancer subtype, both in human and mouse tumors. This was characterized by low expression of various epithelial cell-cell adhesion molecules, such as claudin 3, 4 and 7, occludin and E-cadherin. The molecular characterization of the claudin-low subtype reveals that these neoplastic lesions have high mesenchymal features and low epithelial differentiation. Indeed, they show high expression levels of many mesenchymal genes, such as Vimentin, N-cadherin, Snail1 & 2, Twist1 & 2, ZEB1 & 2 and HIF-1α (Prat et al., 2010). Many of these genes encode for embryonic transcription factors, which are often upregulated in malignant cells and confer motility and invasiveness, leading to the activation of epithelial to mesenchymal transition program (EMT). The EMT can generate cells prone to dissemination and it is associated with chemotherapy resistance and increased properties of self-renewal (Mani et al., 2008). The claudin-low subtype is enriched in $CD44^{+}/CD24^{-/low}$ cell populations, which are defined as tumor initiating cells (TIC) due to their self-renewal capability.

1.3 The mammary gland

Breast cancer is a heterogeneous disease at histological and molecular levels and, as described above, includes at least six distinct subtypes. It is known that different subtypes originate from distinct breast epithelial cells, which function as the "cell of origin". Epithelial cells in normal mammary gland belong to different subtypes and are hierarchically organized. The study of the normal mammary gland epithelium and its hierarchical structure leads the way towards a better comprehension of differences among the molecular subtypes in breast cancer. It is possible that the molecular signature of different tumor subtypes reflects the properties of the cell of origin. Moreover, any dysregulated pathways and processes observed in breast cancer progression mimic those observed during normal mammary gland development and tissue remodeling (Visvader, 2009).

The mammary gland (MG) development is a multistage process that occurs mainly after birth under the influence of hormonal cues and requires the involvement of numerous signaling pathways with distinct regulatory functions. The MG is composed by many different cell types that proliferate, differentiate or undergo apoptosis, giving rise to significant changes of the glandular tissue architecture, during the different stages of MG development. A specialized subpopulation of mammary stem cells fuels the dramatic changes in the gland occurring in MG during pregnancy. Moreover, external factors in the mammary gland microenvironment, such as extracellular matrix and cell-cell interactions, strongly influence cell fate and function.

Referring to the mammary structure and the cellular composition, the MG consists of two main tissue compartments: the epithelium and the stroma, also called mammary fat pad. The epithelial compartment is constituted of ducts and alveoli with a central lumen that opens to the body surface through the nipple. The great part of epithelial compartment is constituted by luminal and secretory cells, that differentiate during pregnancy to produce milk. These cells are encased by a mesh-like system of basal, myoepithelial cells, which constitute the contractile compartment and are responsible for milk delivery. These structures are embedded in the mammary fat pad, mainly made up of connective tissue, adipocytes, fibroblasts and cells from the hematopoietic- and immune-system. Cells forming the epithelial compartment (Figure 1) are proposed to derive from mammary stem cells (MSCs) which are able to self-renew and also differentiate to epithelial precursor cells (EPCs). The epithelial precursors become then restricted to a ductal or alveolar fate. Ductal precursor cells (DPs) form basal and luminal cells, that constitute ducts organized in two layers: the apically oriented layer and the basally oriented layer, which consist of luminal epithelial cells and contractile basal myoepithelial cells, respectively. Basal myoepithelial cells are in direct contact with the basement membrane and they are characterized by the expression of keratins 5 and 14, as well as smooth muscle actin that mediates their contractile function. Luminal cells express keratins 8 and 18. During

pregnancy, mammary gland structure dramatically changes. Alveoli are generated from alveolar precursors (APs), which also give rise to both basal and luminal cells. The latter are differentiated milk-producing cells, able to synthetize and secrete milk components thanks to the contraction of basal myoepithelial layer. Loss of prolactin signal after suckling is stopped leads to massive alveolar epithelium apoptosis in a process called involution. This process restores a ductal system that contains multipotent and committed ductal and luminal precursor cells (Henninghausen and Robinson, 2005).

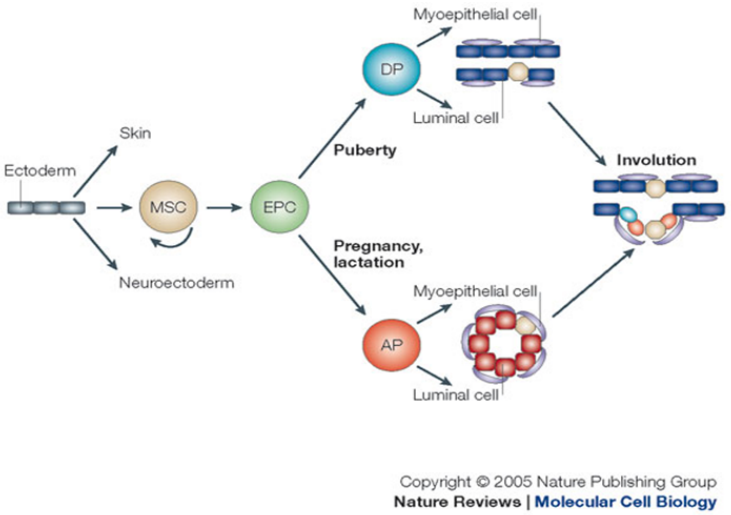

Figure 1. Cell lineages in mammary epithelium (Hennighausen and Robinson, 2005)

1.3.1 Postnatal development of mammary gland

Post-natal development of the mammary gland has been thoroughly investigated in mice. Following the embryonic stage, that in mice occurs between the embryonic day 10.5 and 18.5, and prepubertal stage, further changes of the mammary gland become hormone-dependent and continues at the onset of puberty. At this stage, under the control of hormones and other factors, the ductal epithelium of the mammary primordium invades the mammary fat pad, during a process referred to as branching morphogenesis (Figure 2). The terminal end buds (TEBs), club-shaped structures at the tips of growing ducts that penetrate the fat pad, lead the way. TEBs are formed by highly proliferative and invading epithelial cells that share some features with mesenchymal cells, suggesting that some degree of extremely regulated epithelial to mesenchymal transition (EMT) may occur at these sites. Two morphologically distinct cell types can be identified in TEBs: an outer layer composed of cap cells and a central localization of body cells. Cap cells line the end bud forming the cap of the structure, contact the surrounding stroma and appear to differentiate into myoepithelial basal cells. By contrast, the body cells fill the interior layer of the end bud. The central body cells then undergo apoptosis to form the lumen of the duct and the remaining body cells differentiate into luminal

epithelial cells, giving rise to the ductal epithelium of the adult mammary gland. Once the fat pad is filled, endogenous TGF-β pathway is activated to stop the branching process, most likely regulated by mechanical and local cues from the gland architecture (Nelson et al., 2006; Inman et al., 2015). In the gland of virgin mice, the mammary architecture changes during each estrus cycle thanks to a fine controlled proliferation and apoptosis loop of the epithelium.

During pregnancy, the mammary gland has to undergo further development and morphological changes to permit the preparation of lactation. Lactation requires the production of specific cells that can synthesize and secrete copious amount of milk. These changes require both gland maturation and alveologenesis and are primarily under control of two hormones: progesterone that induces extensive side-branching and alveologenesis, and, in combination with prolactin (PRL), promotes the differentiation of mature alveoli.

The first transformation that takes place during pregnancy is a drastic increase in secondary and tertiary ductal branching, that provides ductal arbors for the second occurring transformation, alveolar development. Alveolar buds, generated from proliferating epithelial cells, progressively cleave and differentiate into distinct alveoli, which become milk-secreting lobules during lactation. Interstitial adipose tissue disappears as the proliferating epithelial cells occupy the inter-ductal spaces.

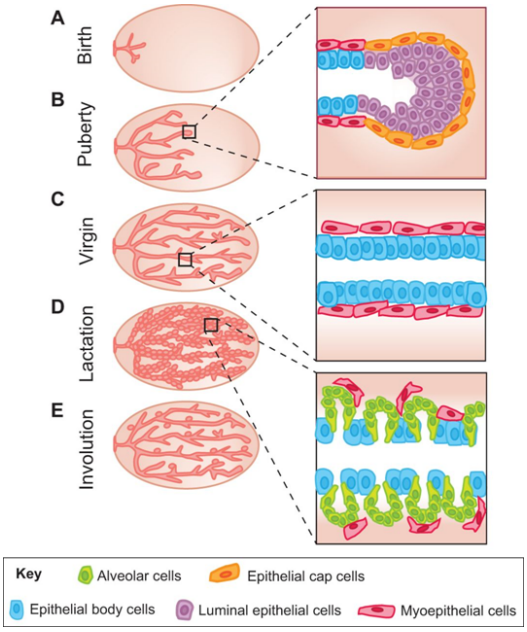

Figure 2. The branching morphogenesis of mammary gland (Inman et al., 2015)

1.3.2 Transcriptional regulators of mammary gland development

Several hormones and paracrine factors have been implicated in the regulation of postnatal mammary gland development, while less is known about signals that control embryonic mammary morphogenesis. It has been proposed that the Wnt signaling may play important roles in multiple steps in normal mammary gland development as well as in breast cancer (Chu et al., 2004). The morphogenetic changes that the mammary gland undergoes during puberty, pregnancy and lactation are primarily defined by steroid and peptide hormones, estrogen, progesterone and prolactin. Pubertal mammary development and the surge in growth that occurs during this period, that generate a functional mammary gland, are under the critical control of ovarian hormone estrogen. During puberty, branching mainly requires estrogen and estrogen receptor-α (ER-α) while adult tertiary side branching requires progesterone and its receptor (PgR). Branching is also coordinated by local crosstalk between the developing duct epithelium and nearby stromal cells. Estrogen binds to two distinct receptors encoded by two genes: ERα (Esr1) and ERβ (Esr2). They are nuclear receptors, functioning as transcription factors when bound to the steroid hormone. It has been demonstrated that the depletion of Esr1 in mice leads only to the formation of a rudimentary ductal system that fails to undergo the estrogen-mediated growth spurt that accompanies puberty, while depletion of Esr2 has no adverse effect on ductal development at this stage. Moreover, recent studies ascribe a role to estrogen during pregnancy in growth and maintenance of alveolar cell. In fact, the ablation of Esr1 in alveoli following ductal elongation results in defective development of lobuloalveolar compartment and inadequate milk production (Lubahn et al., 1993; Silberstein et al., 1994; Krege et al., 1998; Feng et al., 2007). On the contrary, the contribution of PgR to ductal branching is only minor but this receptor is essential for the expansion of the alveolar compartment. Mice lacking PR were shown to produce only a simple epithelial tree, even following the surge of growth at puberty, and upon pregnancy they do not undergo the associated ductal proliferation or lobuloalveolar differentiation (Lydon et al., 1995; Brisken et al., 1998). The proliferative effect of PR is mediated by a paracrine signaling that involves the Receptor Activator Nuclear factor kB-Ligand (RANK-L). Given its role in regulating skeletal calcium release, it is not surprising that this ligand should play an essential role in regulating alveologenesis, the first step in transmitting maternal calcium to infant mammals. It has been demonstrated that mice lacking RANK-L or its receptor RANK fail to undergo alveologenesis during pregnancy, similarly to PgR lacking mice (Fata et al., 2000).

During pregnancy, the generation of lactational competence is initially carried out by a single peptide hormone, prolactin (PRL), and its downstream intracellular partners, Jak2 and Stat5 (Figure 3). PRL fulfills its functions both indirectly, through its regulation of ovarian progesterone production, and directly via its effect on mammary epithelium. By binding to a member of the class

I cytokine receptor superfamily, Prolactin Receptor (PRLR), PRL induces receptor dimerization and conformational change that results in the associated Janus kinase-2 (JAK2) phosphorylating specific tyrosine residues in the receptor. Subsequently, also the transcription factors Stat5a and 5b are recruited through their SH2 domains and phosphorylated by JAK2. Phosphorylated Stat5a-Stat5b form homo- and hetero- dimers that translocate to the nucleus where they activate genetic programs necessary for cell proliferation and expression of milk proteins (Henninghausen and Robinson, 2005). Inactivation of the genes encoding for PRL and its receptor or the expression of mutant PRLR have helped to elucidate the role of this cytokine, at least during the early stages of pregnancy. Female mice with inactive PRLR alleles do not maintain pregnancies. Although ductal outgrowth during puberty was overtly normal in these mice, no functional alveolar compartment was formed during pregnancy, as a result of a lack of luminal cell proliferation. A threshold level of PRLR is required for normal development, as evidenced by haplo-insufficient mice where the presence of only one PrlR gene, alveolar proliferation and differentiation was stalled in second half of pregnancy (Ormandy et al., 1997; Brisken et al., 1999; Gallego et al., 2001). The JAK2/STAT5 signaling pathway is activated downstream of PRL/PRLR, and plays an essential role in establishing alveologenesis. Has been demonstrated that $Jak2^{-/-}$ and $Stat5^{-/-}$ mice display the same mammary defective phenotype as the one observed in Prlr deficient mice. Moreover, the conditional loss of Stat5 following PRL-induced differentiation of alveolar cells also showed that this pathway is required for maintenance of the pregnancy program (Han et al., 1997; Cui et al., 2004; Wagner et al., 2004). Downstream signaling of the PRLR/JAK2/STAT5 pathway culminates in the transcription of the milk protein genes, including β-casein (Csn2) and whey acidic protein (Wap).

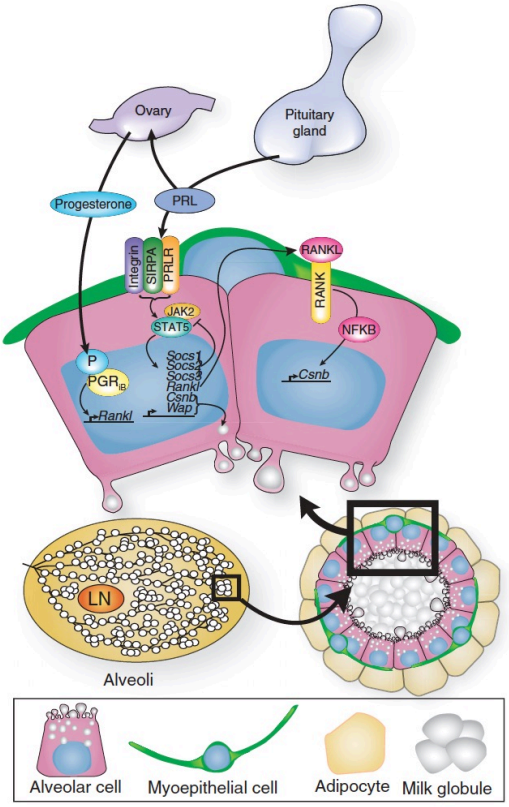

Figure 3. Schematic view of the events that generate lactation competence during pregnancy (Macias and Hink, 2012)

An important role in local regulation of branching morphogenesis is played by the HER/ErbB tyrosine kinase family members. It has been recently reported that ErbB2/HER2 is required for the initial stages of ductal outgrowth through a cell-autonomous mechanism. It is interesting to note that while lack of ErbB2/HER2 during puberty and adolescence results in delayed ductal outgrowth into the fat pad, elevated expression of ErbB2/HER2 is associated with human breast cancer and correlates with aggressive disease and poor prognosis. The work of Jackson-Fisher elucidated the role of HER2 receptor in ductal growth of mammary gland. The ErbB2$^{-/-}$ mammary buds advance slowly through the mammary fat pad owing to a penetration defect. ErbB2$^{-/-}$ terminal end buds display structural defects, characterized by a decrease in body cell number, an increased presence of cap-like cells in the pre-luminal compartment, and the presence of large luminal spaces. The importance of ErbB2 in promoting invasive penetration of the mammary fat pad is consistent with the aggressive properties of mammary carcinoma with ErbB2 amplification (Andrecheck et al., 2005; Jackson-Fisher et al., 2004). Other members of the HER/ErbB family, such as epidermal growth factor receptor (HER1/EGFR) and HER4/ErbB4, are implicated in growth and differentiation of mammary gland, as well as during pregnancy. EGFR and HER2 are expressed, phosphorylated in tyrosine residues, and colocalize in major cell compartments of mice mammary gland at puberty. After puberty, ErbB2 is localized in the epithelium and reduced in the stroma while EGFR is prominent in the stromal cells

surrounding the TEB. Ligands of the EGFR are believed to be particularly important downstream mediators of steroid hormone action in the mammary gland, acting locally to regulate mammary gland growth and development via stromal-epithelial interactions (Parmar and Cunha, 2004). HER4 is enriched in the ducts and has an essential role particularly in late pregnancy and lactation when it is strongly phosphorylated. The lack of HER4 in mammary epithelial cells impacts on alveolar differentiation and lactation due to an impaired activation of the transcription factor STAT5 (Hynes and Watson, 2010).

1.4 The HER tyrosine kinase family members

The Human Epidermal Receptor (HER) family of receptor tyrosine kinases (RTKs), also known as ErbB, plays an important role in both normal physiology and cancer, and its members are often mutated or amplified in breast cancer and other tumors. There are four members in the ErbB family: EGFR (HER1, ErbB1), HER2 (ErbB2, HER2/neu), HER3 (ErbB3) and HER4 (ErbB4) (Figure 4). They are typical RTKs belonging to the type I transmembrane protein, consisting of a heavily glycosylated and disulfide-bonded ectodomain that provides a ligand-binding site, a single membrane-spanning region and a large cytoplasmic region that comprises a tyrosine kinase and multiple phosphorylation sites (Hynes and McDonald, 2009). At least 12 known EGF-family peptides can bind the ErbB receptors and on the basis of their receptor specificity are divided in three groups. Ligand binding initiate signaling by causing specific dimerization between two identical (homodimerization) or different (heterodimerization) receptors belonging to the same family (Moasser, 2007).

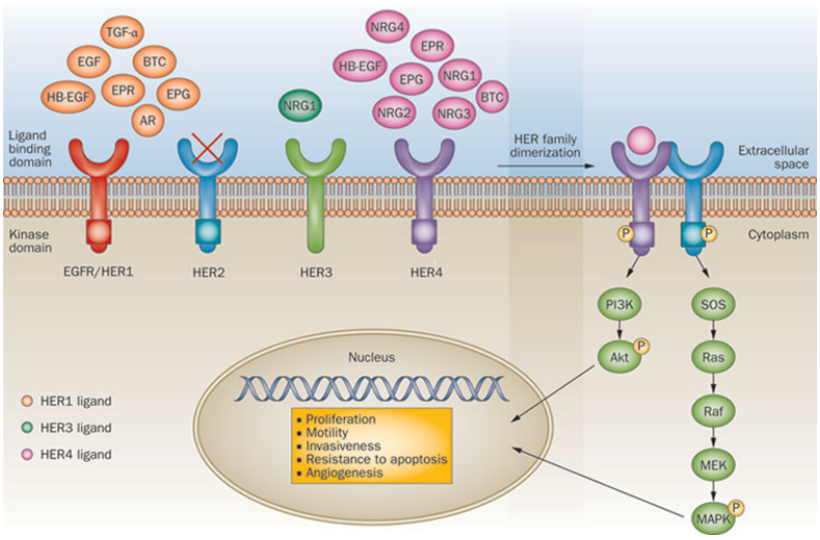

Figure 4. HER receptor family members. Note that HER2 has no ligand interaction (Carlos et al., 2012)

Homo- or hetero- dimerization leads to the intrinsic tyrosine kinase activity and triggers the auto-phosphorylation of specific C-terminal tyrosine residues that provides docking sites for proteins containing Src homology 2 (SH2) or phosphotyrosine binding (PTB) domains (Olayioye et al., 2000). Each ErbB receptor displays a distinct pattern of auto-phosphorylation sites in the C-terminal region. SHC and GRB2 adaptor proteins activate mitogen activated protein kinase (MAPK) pathway, which is a common downstream target of ErbB receptors, leading to cell-cycle progression. Similarly, the phosphatidylinosithol-3-kinase (p85 subunit of PI3K) pathway is activated by most ErbB receptors, through its SH2 domain. Transcription factors downstream HER signaling (c-Fos, c-Jun, c-Myc, NF-kB, Sp1, Stat) are involved in cell-proliferation, survival, adhesion, migration, cell polarity and differentiation (Holbro and Hynes, 2004).

ErbBs are good example of signal integrators because they are the target of signaling events emanating from other receptor classes. The transactivation is characterized by the rapid receptor tyrosine phosphorylation and subsequent stimulation of signaling pathways. Basically, two mechanisms control the ErbB transactivation: either ErbB receptors are phosphorylated by other kinases or ErbB receptors auto-phosphorylate as a consequence of increased kinase activity. The first mechanism is characterized by a "passive" behavior of the ErbBs: the receptors act as scaffolds and activation of their kinase domain is not necessary for downstream signaling. For example, binding of prolactin (Prl) to its receptor activates the constitutively associated janus kinase (Jak) 2 which phosphorylates the cytoplasmic domain of ErbB1 or ErbB2. ErbB transactivation, namely the ability of different receptors to indirectly stimulate the intrinsic kinase activity, has been intensively studied for G-protein coupled receptor (GPCR) agonist, such as endothelin-1 (ET-1), thrombin, bombesin, and lysophosphatidic acid (LPA). Mechanistically, this process involves rapid stimulation of metalloproteinases followed by cleavage of an EGF-like ligand precursor, whose binding activates ErbB1 and downstream signaling pathways, ultimately leading to a biological outcome.

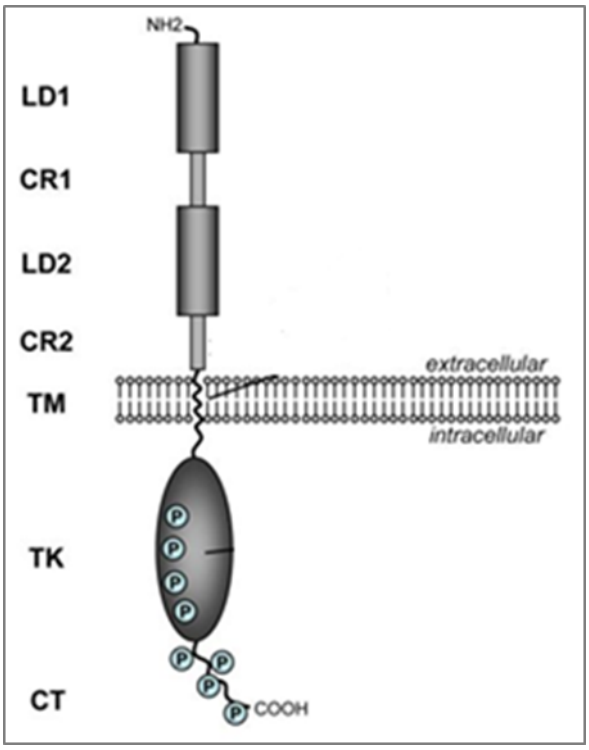

Figure 5. Structure of HER2 protein and its domains (Moasser, 2007).

1.4.1 The HER2 oncogene and its splice variants

HER2 was firstly identified in the early 1980s from rodent models and in humans. Referring to its nomenclature, ErbB2 refers both to the human and rodent gene while HER2 and *Neu* are used in reference to human and rodent gene, respectively. The extracellular domain of HER2 consists of two ligand-binding regions (LD1, LD2) and two cysteine-rich regions (CR1, CR2), followed by a short transmembrane domain and an intracellular tyrosine kinase domain, characterized by numerous tyrosine phosphorylation sites (Figure 5). Unlike the other members of ErbB family, the extracellular domain of HER2 receptor lacks a high-affinity ligand and it exists in an open and constitutively active conformation. Therefore, HER2 serves as a co-receptor and it is the preferred heterodimerization partner of all other ErbB ligand-bounded receptors (Moasser, 2007).

HER2 is usually referred to as a proto-oncogene. In human cancer the overexpression of HER2 protein, either through gene amplification or transcriptional deregulation, is observed in approximatively 20% of breast cancers, and confers more aggressive biological behavior. BC can have up to 25-50 copies of the HER2 gene and up to 40-100 fold increase in protein expression. HER2 amplification seems to be an early event in human breast tumorigenesis, and its status is maintained during progression to invasive disease, nodal and distal metastasis. This type of cancer presents a unique molecular portrait and it is preserved among the entire disease (Perou et al., 2000; Tsuda et al.,2001). The molecular mechanism underlying HER2 mediated tumorigenesis appears to be

complex and a unified model of transformation has not emerged. HER2-induced transformation of mammary epithelial cells is driven by two different mechanisms: (1) increased kinase activity and over-phosphorylation of itself and its cellular substrates or (2) increased total expression of HER2 and its splice variants, in particular the rare Δ16HER2 isoform.

Three naturally occurring HER2 splice variants have been previously characterized. The first HER2 variant described is an extracellular fragment named p100 (100 kDa). p100 mRNA encodes the first 633 amino acids of the HER2 extracellular domain of the full-length protein and it is a soluble, ligand-binding receptor form, which interferes with the oncogenic activity of HER2 wild-type receptor. This variant arises via an in-frame stop codon derived from intron 15 retention. It has been reported that p100 displays a decreased downstream signal activation of the MAP kinase pathway, and has the capacity to inhibit tumor cell proliferation (Sasso et al., 2011). A second HER2 secreted splicing product is a truncated 68 kDa protein known as Herstatin, resulting from intron 8 retention during the mRNA processing. The translated protein comprises the extracellular domain 1 (ECD1) and most of extracellular domain 2 (ECD2) of HER2, followed by a novel C-terminus. Herstatin is a soluble negative HER2 regulator due to its ability to disrupt dimers, decrease tyrosine phosphorylation and consequently inhibit the growth of HER2 overexpressing cells. Moreover, thanks to its protective role, it is considered as a growth regulator during normal development (Koletsa et al., 2008). The third HER2 splice variant is the result of an in-frame deletion of exon 16, a 48bp cassette exon which encodes a small region of the extracellular domain, and the translated protein, named Δ16HER2, lacks of 16 amino acids in the juxtamembrane domain (Figure 6). As the juxtamembrane region is rich in cysteine residues, exon 16 skipping leads to the removal of two cysteine residues involved in intramolecular disulphide-bridges. The remaining unpaired cysteine residues are available for intermolecular bonds leading to the formation of disulphide-bridged homodimers and to the constitutive activation of Δ16HER2 receptor (Castiglioni et al., 2006).

The Δ16HER2 receptor is co-expressed in the majority of HER2 positive breast tumors but represents only 4-9% of total HER2 transcripts. However, it plays a critical role in the activation of multiple oncogenic pathways in patients with HER2-overexpressing breast cancer. In particular, it has been reported that the Δ16HER2 cooperates with Src kinase that is considered as a common node involved in trastuzumab resistance mechanism (Zhang et al., 2011). Mitra et al., described that Src kinase co-localized and physically interacts at the cell membrane with Δ16HER2 in a human breast cancer cell line overexpressing the transforming isoform of HER2. Src, in turn, activates multiple oncogenic pathways, including FAK, PI3K and MAP kinase, principally involved in cell motility and invasion (Mitra et al., 2009).

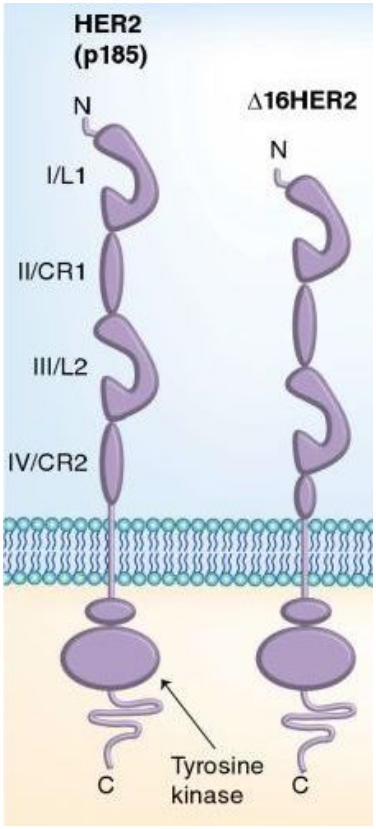

Figure 6. Structure of HER2 and Δ16HER2 variant (Wang et al. 2013)

Furthermore, the expression of Δ16HER2 variant is sufficient and necessary to drive the oncogenic transformation of immortalized mammary epithelial cell lines owing to a defect in downregulation from the cell surface. Accordingly, Δ16HER2 protein has not been detected in the endosomal compartment while the activated form of wild-type HER2 is rapidly degraded. The constitutive plasma membrane localization of the spliced HER2 has been hypothesized to be the responsible for the tumor resistance to TDM-1 treatment (Turpin et al., 2016). Regarding the possible role of Δ16HER2 in the response to trastuzumab, contrasting data exist in literature. Mitra and co-workers provide *in vitro* evidences that Δ16HER2 expression is an important genetic event driving trastuzumab-refractory breast cancer. Nevertheless, trastuzumab binds similarly to Δ16HER2 and wild-type HER2 (Mitra et al., 2009). On the contrary, a recent work proved that spontaneous tumor growth in transgenic mice overexpressing Δ16HER2 was impaired by trastuzumab administration (Castagnoli et al., 2014).

1.5 Δ16HER2 transgenic mouse model

A transgenic mouse model for breast cancer was recently generated to study and support the *in vitro* evidences that Δ16HER2 splicing variant could represent the predominant oncogenic form of HER2. The Δ16HER2 transgenic mouse harbors a bicistronic expression cassette containing the human Δ16HER2 gene and the firefly luciferase gene (Figure 7). The murine mammary tumor virus (MMTV) promoter, which is regulated by hormones, drives its expression, mainly in the mammary tissue. The transgene has a single site of insertion on murine chromosome 5, in an intergenic region that contains neither genes nor regulatory sequences. The great distance between the transgene and two genes located downstream and upstream the insertion site, ensures that the insertion itself does not affect the tumorigenesis.

Other transgenic mouse models of HER2-overexpressing breast cancer were developed in the past. One of these models is the transgenic mouse harboring the full length human HER2 gene under the control of the MMTV promoter (MMTV-WT hHER2), developed by Finkle and colleagues.

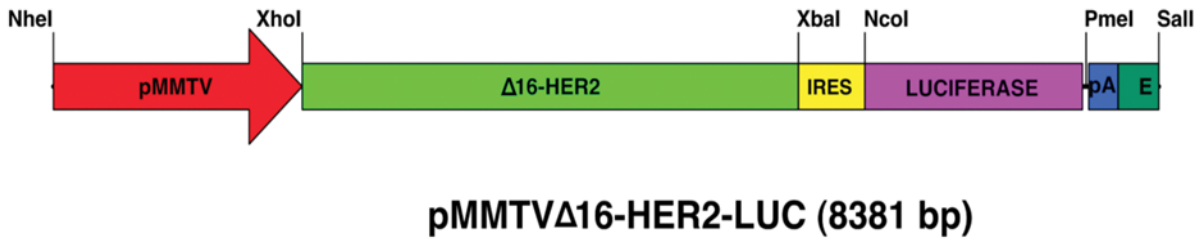

Figure7. Human Δ16HER2-LUC transgene (Marchini et al.,2011).

Interestingly, the sequencing of the human HER2 transcripts from murine mammary primary tumors revealed an in-frame 15-pb deletion in the wild-type HER2 juxtamembrane region that seems to be necessary to initiate the malignant transformation. Similarly, with what occurs with the Δ16HER2 variant, the deletion resulted in the repositioning of two cysteines, eventually affecting the cysteine-mediated receptor dimerization. These data support the hypothesis that Δ16HER2 protein could represent the main mediator of HER2 oncogenesis. Compared with the wild-type human HER2-overexpressing mouse models, Δ16HER2 mice show higher tumor incidence, faster tumor growth and shorter latency period. Only five copies of the transgene are sufficient to induce transformation of mammary epithelial cells in 100% of mice carrying the Δ16HER2, whereas 30–50 wild-type HER2 transgene copies were reported to be necessary to induce breast cancer in about 80% of MMTV-wild-type hHER2 transgenic mice. Furthermore, Δ16HER2 transgenic females develop multifocal asynchronous mammary tumors with an average latency of 15.11±2.5 weeks, classified as invasive HER2-positive adenocarcinoma, while MMTV-wild-type hHER2 transgenic mouse models develop

HER2-overexpressing breast tumors with a significantly longer latency period (28.6 weeks) and less in number. Δ16HER2 tumor-bearing transgenic females develop lung metastases beginning at 25 weeks of age, suggesting particularly aggressive tumor behavior upon expression of the Δ16HER2 splicing variant. The histological features of these pulmonary lesions are consistent with the primary breast tumor origin, with robust positive staining for HER2 (Marchini et al., 2011). In conclusion, MMTV-WT hHER2 mice provide evidences that WT hHER2 expression is not sufficient "per se" to drive malignant transformation and it requires activating mutations to become frankly oncogenic. On the contrary, Δ16HER2 isoform owns stronger oncogenic properties and is sufficient alone to transform mammary epithelium *in vivo*.

1.6 $p27^{kip1}$

$p27^{kip1}$, encoded by CDKN1B gene, is an intrinsically unstructured, multifunctional protein that influences several biological functions ranging from cell cycle regulation to cellular migration and transcriptional regulation. $p27^{kip}$ (here after p27) belongs to the Cip/Kip family of cyclin-dependent kinase (CDK) inhibitors, that includes $p21^{cip1}$, $p57^{kip2}$ and $p27^{kip1}$, all characterized by the presence of a conserved amino-terminal region containing the cyclin and CDK binding domains.

p27 plays a crucial role in the G1 to S phase transition by regulating cyclin E-CDK2 and cyclin A-CDK2 complex activities by binding both cyclin and CDK subunits, thus blocking the cell cycle progression (Figure 8). The crystal structure of human p27 bound to the phosphorylated cyclinA-CDK2 complex revealed that p27 binds the complex as an extended structure interacting with both cyclin A and CDK2. With cyclin A, it binds in a groove formed by conserved cyclin box residues. With CDK2, it binds and rearranges the amino-terminal lobe and also inserts into the catalytic cleft, mimicking the ATP (Russo et al., 1996). It has been demonstrated that overexpression of p27 causes the arrest of cycling cells in G1 phase (Polyak et al., 1994; Toyoshima and Hunter, 1994), while Coats and colleagues showed how a protein reduction hinders the ability of fibroblasts to exit the cell cycle in growth factor deprived conditions, as normal cells do (Coats et al., 1996). In early G1 phase, p27 promotes the assembly and the nuclear importation of cyclin D-CDK4/6 complex, supporting the stabilization of cyclin D. The mitogen induction carried out by cyclin D determines the cell cycle progression both by the activation of CDK4 and by impounding p27, that is maintained in this way displaced from its principal target, cyclin E-CDK2. Cyclin E-CDK2 complex then targets p27 to ubiquitin dependent degradation through its nuclear phosphorylation in Threonine 187 (Sherr and Roberts, 1999), thus reinforcing CDK4 activity to complete Rb phosphorylation.

A large body of literature studying the regulation of p27 during cell cycle, highlighted a regulatory role for p27 also in G2-M transition. In line, p27 was historically known as universal CDKs inhibitor, able to down-regulate *in vitro* not only cyclin E/A-CDK2 activity but also CDK1 (Toyoshima et al., 1994) and Nakayama and colleagues showed *in vivo* how p27 accumulation at G2/M transition induces a strong decrease in CDK1 associated kinase activity. The prolonged G2 arrest induced by p27, through the suppression of CDK1 activity, was shown to be responsible for the centrosome duplication, cell endoreplication and polyploidy (Nakayama et al., 2004). Later, others proposed a different explanation to the mitotic defect, suggesting that p27 could be involved in the prevention of CDK1 expression instead of directly inhibit the activity (Serres et al., 2012; Sharma et al., 2012).

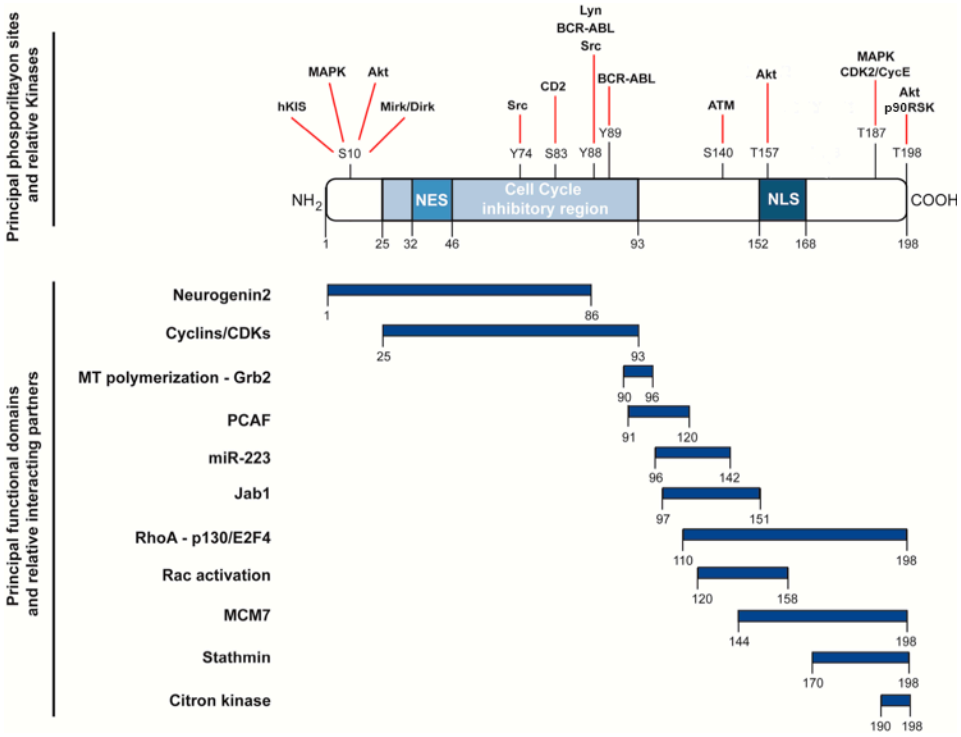

Figure 8. Schematic representation of the main functional domains and phosphorylation sites of p27 (Adapted from Cusan et al., 2018).

The abundance of p27 within the cell is controlled by multiple mechanisms that operate at level of its synthesis (transcription/translation) and, particularly, its stability, degradation and localization. Although mRNA levels are usually constant throughout the cell cycle, p27 protein expression in normal cells is finely regulated. p27 levels increase in response to various stimuli that inhibit cell proliferation, such as cell-cell contact, loss of adhesion to extracellular matrix, cell differentiating stimuli and TGFβ (Transforming growth factor β), INF-γ (Interferon-γ), c-AMP, rapamicin and lovastatin treatments (Belletti et al., 2005). Exit from the quiescent G0 state requires the down-regulation of p27, which in turn results in CDKs activation. p27 can also be regulated by protein sequestration into higher order complexes with cyclin D-CDK4 after activation of the MAPK pathway, that promotes cyclin D transcription (Susaki and Nakayama, 2007). For instance, the proto-oncogene c-Myc, by increasing the expression of cyclin D and cyclin E, is responsible for p27 sequestration and this molecular event appears essential for Myc-induced cell cycle progression (Vlach et al., 1996). Moreover, p27 can be displaced in the cytoplasm, with consequent progression in cell cycle, after phosphorylation of Serine 10 by KIS (kinase-interacting Stathmin) or by MAPK and/or phosphorylation of Threonine 198 by Akt or RSK (Belletti et al., 2005; Philipp-Staheli et al., 2001).

The translocation of p27 from the nucleus to the cytoplasm is followed by its degradation by the ubiquitin-proteasome pathway by the KPC complex (Kip1 ubiquitination-promoting complex), consisting of KPC1 and KPC2 proteins, that interacts with and ubiquitinates p27 in the cytoplasm (Kamura et al., 2004; Kotoshiba et al., 2005). The nuclear export of p27 by CRM1 is necessary for

KPC-mediated proteolysis and the recognition by CRM1 needs p27 phosphorylation on Ser10 (Boehm et al., 2002; Kamura et al., 2004). However, p27 proteolysis is cytoplasmatic and KPC-dependent in early G1, but it is nuclear in late S/G2 phase. In S/G2 phase, degradation is mediated by an SCF ubiquitin ligase, composed by Skp1, a cullin subunit called CulI, Rbx1/Roc1 and the F-box protein Skp2 that specifically recognizes p27. Skp2 binds to p27 and promotes its degradation when the protein is phosphorylated on the conserved Thr187 by cyclinE-CDK2 or cyclinA-CDK2 complexes (Hara et al., 2001). Several distinct kinases determine p27 phosphorylation status during cell cycle. The phosphorylation at Ser10 plays a critical role to decrease p27 nuclear abundance, thereby allowing for the initial activation of cyclin-CDKs complexes (Besson, 2006; Ishida et al., 2000; Rodier et al., 2001). This serine is a substrate for at least four kinases, after mitogenic stimuli. These include human Kinase Interacting with Stathmin (hKIS) (Boehm et al., 2002; Vervoorts and Lüscher, 2008), MAPK (Rodier et al., 2001), Akt/PKB (Vervoorts and Lüscher, 2008) and Mirk/Dirk1B (Besson, 2006). The T187 of p27 is phosphorylated by the cyclin E-CDK2 and cyclinB-CDK1 (Sheaff et al., 1997; Vlach, 1997), and leads to its degradation *via* the cytosolic ubiquitin-proteasome system (Grimmler et al., 2007; Hara et al., 2001). It has been reported that, under high glucose stimulation, MAP kinases ERK1/2 phosphorylate p27 at S10, T187 and S178 in mesangial cells, both *in vitro* and *in vivo* (Wolf et al., 2003). Other phosphorylation sites of p27 are the T157 and the T198, both regulated by AKT. The T157 residue, mapping within the NLS of p27, is phosphorylated by AKT that causes retention of p27 in the cytoplasm, precluding p27-induced G1 arrest (Liang et al., 2002; Shin et al., 2002; Viglietto et al., 2002). AKT phosphorylates p27 also at T198. Once phosphorylated on this residue, p27 is recognized by the 14-3-3 family of proteins and retained in the cytoplasm (Fujita, 2002). Moreover, it has been demonstrated that phosphorylation at T198 is able to regulate p27 stability, localization and interaction with Stathmin, interfering with p27 ubiquitination and p27 role in cell motility (Schiappacassi et al., 2011). The tyrosines Y74, Y88 and Y89, located in the CDK-binding domain, are phosphorylated preferentially in active proliferating cells, converting p27 to a non-inhibitory state (James et al., 2008). Grimmler group has reported that the residue Y88 can be phosphorylated by the Src-family kinase Lyn and by the oncogene product BCR-ABL. Once phosphorylated on Y88, CDK2 efficiently phosphorylates p27 on T187, promoting in turn its SCF-Skp2-dependent degradation, suggesting an explanation for premature p27 elimination in cells transformed by these activated tyrosine kinases (Grimmler et al., 2007). The oncogenic kinase Src regulates p27 stability through its phosphorylation not only at Y88 but also at Y74 and, to a less degree, at Y89, facilitating again p27 proteolysis (Chu et al., 2007). p27 could be phosphorylated at serine 83 by CK2 (Tapia et al., 2004) in cardiomyocites stimulated by angiotensin II, a major cardiac growth factor, inducing its proteasomal degradation (Hauck et al., 2008). Recently, it has been shown that serine in position 140 can be phosphorylated by ATM kinase after DNA damage induced by ionizing γ-radiation, stabilizing p27 for G1/S cell cycle checkpoint activation (Cassimere et al., 2016).

1.6.1 $p27^{kip1}$ in tumors

The importance of p27 in the regulation of exit from and entry into cell cycle and its impact in tumorigenesis was revealed by the generation of p27-deficient mice, that will be discussed below. Although p27 is well known to be a tumor suppressor gene, inactivating mutations and loss of heterozygosity of CDKN1B are observed at very low frequency in most human cancers. An increased body of literature reports frequent p27 functional inactivation in human cancers (Figure 9). Unlike prototypic tumor suppressor genes (e.g. TP53 and RB), p27 does not appear to follow the Knudson's "two-hit" theory, behaving as haplo-insufficient tumor suppressor gene (Fero et al., 1998). Complete loss of p27 expression is not uncommon in human malignancies, but silencing or mutations of both alleles are very rare, which is consistent with the notion that p27 loss in tumors is mainly due to an accelerated proteolysis. Accordingly, a plethora of studies shows the involvement of p27 protein reduction or loss in many tumors, such as carcinomas of the colon, breast, prostate, lung and ovary as well as brain tumors, lymphomas and soft tissue sarcomas (Belletti et al., 2005). Multivariate analysis showed that reduced levels of p27 are of independent prognostic significance for many of these tumors. Yet, apparently in contrast with these data, some tumors may contain high levels of p27, suggesting that mechanisms other than protein degradation allow transformed cell to circumvent p27 growth inhibition.

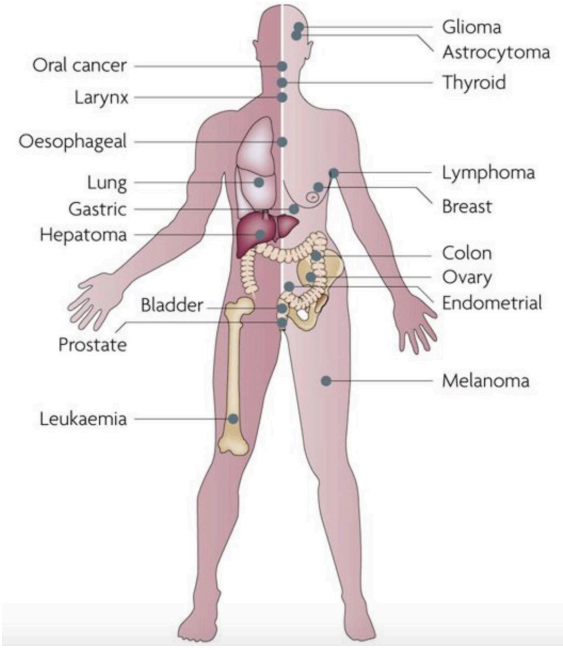

Figure 9. The majority of human malignancies in many organ sites, show reduced p27 protein levels (Chu et al, 2008).

In the last few years, mutations in CDKN1B gene were unexpectedly identified as driver mutations in selected types of cancer, eliciting a particular clinical interest. The advent of massive parallel sequencing that allowed to analyze the cancer genome at very high sensitivity seemed to subvert the

notion that deletion, methylation or mutations of CDKN1B gene are very rare events and indicate that this gene could be mutated with higher frequency than previously thought in prostate cancer (PC), small intestine neuroendocrine tumors (SI-NET) and luminal breast cancer (Cusan et al., 2018). Mutations of CDKN1B in luminal breast cancer occur, in more than half of the cases, in the C-terminal portion of the protein, suggesting that, beyond the classical cyclin/CDK binding domains located at the N-terminus, tumor suppressive activities are also present in the C-terminus (Belletti and Baldassarre, 2012; Koboldt et al., 2012; Stephens et al., 2012).

A retrospective analysis of p27 expression in 2,031 breast cancer samples from a randomized clinical trial, demonstrated that reduced p27 was an independent prognostic factor for reduced overall survival (Porter et al., 2006). In another work including 500 patients with premenopausal ER+ BC, low p27 strongly correlated with poor survival, showing the predictive potential of p27 in a prospective trial (Pohl, 2003). Through meta-analysis of 20 studies, Guan *et al.* correlated p27 expression and clinical outcome of BC including overall survival (OS), disease-free survival (DFS) and relapse-free survival (RFS). A total of 60% of the studies showed a significant association between p27 high expression and OS, whereas 25% and 60% studies demonstrated a correlation between p27 high expression and DFS and RFS, respectively (Guan et al., 2010). Together, these data indicate that reduced p27 is an independent prognostic factor for poor OS and shorter DFS. Moreover, reduced p27 levels correlate with lower cyclin D1 (Barnes et al., 2003; Gillett et al., 1999) and with *ERBB2* (the gene encoding for HER2) amplification (Newman et al., 2001; Spataro et al., 2003).

1.6.2 $p27^{kip1}$ as tumor suppressor gene: the Knock-out model

Because of their recessive nature, prototypic tumor suppressor genes require "two-hit" inactivation of both alleles of genes (Knudson et al., 1971). Nevertheless, for many tumor suppressor genes functional loss of only one allele is sufficient to confer a selective advantage for tumor development. The generation of a mouse model lacking one or both copies of *Cdkn1b* (the gene encoding for mouse p27) permitted the evaluation of p27 haplo-insufficiency in tumorigenesis. Mice lacking one copy of *Cdkn1b*, develop spontaneous tumors late in life and are highly sensitive to tumor induction when challenged with carcinogens, displaying increased tumor frequency and decreased latency. Thus, the model demonstrated that a reduce dosage of p27 was sufficient to contribute to tumor susceptibility (Fero et al., 1998). A similar dosage effect occurs in human tumors, where loss or decrease of p27 protein expression, rather than a complete loss, is frequently observed and correlates with poor patient survival.

In 1996, different groups described the phenotypic evolution of $p27^{-/-}$ mice. Significant increase in body size was observed in $p27^{-/-}$ mice, while p27 heterozygous mice were intermediate in size. The weight difference was not evident at birth, became significant between 2 and 3 weeks postnatally, was maximal by 10 weeks of age, and was maintained throughout adulthood. This is consistent with the fact that the expression level of p27 in day 10 embryos seems to be barely detectable. $p27^{-/-}$ mice weighted 20-40% more than sex-matched control and the difference was slightly more pronounced in females (Fero et al., 1996; Nakayama et al., 1996; Kiyokawa et al., 1996).

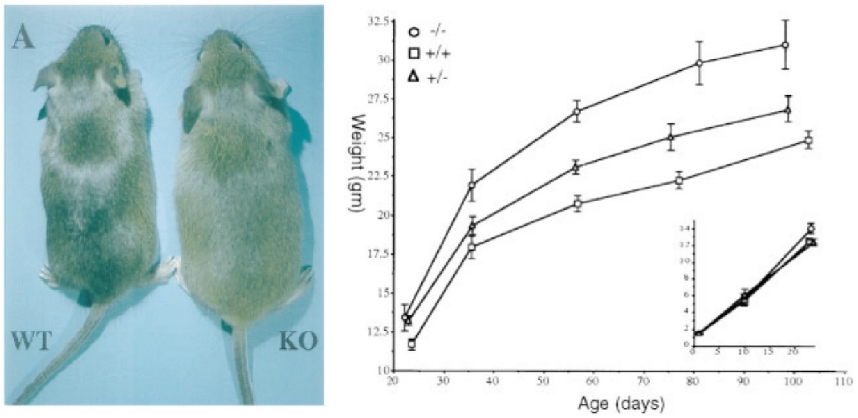

Figure 10. Increased Growth of p27-Deficient Mice (adapted from Fero et al. 1996)

The group of Fero reported that the majority of tissues obtained from $p27^{-/-}$ mice displayed normal histologic characteristics (Fero et al. 1996) and the Nakayama group found that there was tissue specificity with respect to the abundance of p27 protein: lymphocytes, gonad cells, and neurons appeared to express p27 at high levels, whereas liver, kidney, skeletal muscle and fibroblasts had a relatively small amount of p27. Consistent with the abundance of p27 in these tissues, the major abnormalities that occurs in $p27^{-/-}$ mice were an enlargement of thymus, testis, ovaries and adrenal medulla and the possible overgrowth of the neuroepithelium in retina. Analysis of enlarged thymi from 4 weeks of age mice, revealed that number of thymocytes was more elevated respect to control mice. Nevertheless, CD4/CD8 and αβ T cell receptor (TCR) profile of the lymphocytes were within the normal range, and the architecture was relatively normal in spite the increased size, suggesting that lymphoid malignancy was unlikely to account for swelling of the thymus. Compared with the abnormality in the thymus, changes in peripheral lymphoid organs were less striking. Mice with larger body size contained more T cells in their spleen and lymph nodes by up to 2-fold. In contrast, the number of B cells found in spleen, lymph nodes and bone marrow from these mice was normal (Nakayama et al., 1996). Kiyokawa and colleagues, established that there was also an increased number of splenic T cells in $p27^{-/-}$ mice, that might occur either during maturation in the thymus or following antigen exposure in the periphery (Kiyokawa et al., 1996).

Further, adult p27$^{-/-}$ mice displayed 2- to 5- fold enlargement of intermediate lobe of pituitary gland (Fero et al.,1996). Histologic analysis revealed marked expansion of intermediate lobe and development of adenomatous, neoplastic transformation of the pars intermedia cells, while the pars nervosa and the distalis often resulted compressed and displaced, without compromising the cytoarchitectural features. Using antibodies to the anterior pituitary hormones thyroid-stimulating hormone, follicle-stimulating hormone (FSH), luteinizing hormone (LH), prolactin, and growth hormone (GH), Fero and colleagues demonstrate identical patterns of histochemical staining in the pars distalis of the control and knockout mice. None of the hormones reported was expressed in cells of the adenomatous tumor tissue. The significance of the hyperplasia restricted to this area was unclear, but it has been already reported in mice that have lost heterozygosity at the Rb locus (Jacks et al., 1992; Hu et al., 1994).

Another well-established characteristic of p27$^{-/-}$ mice, is the hyperplasia of genitals. Testis and ovaries have been found about 2-fold larger in p27$^{-/-}$ mice. No abnormalities in development or function of spermatids accompany male phenotype, in agreement with the fact that p27 disruption does not impinge on fertility. In contrast, female knockout mice were found not to be able to carry to term a pregnancy. Secondary ovarian follicles developed, but did not progress to form corpora lutea. Gonadotropin production did not appear to be impaired, because normal levels of FSH. LH-producing cells were visualized in the anterior pituitary, and both basal and peak serum levels of hormones was normal.

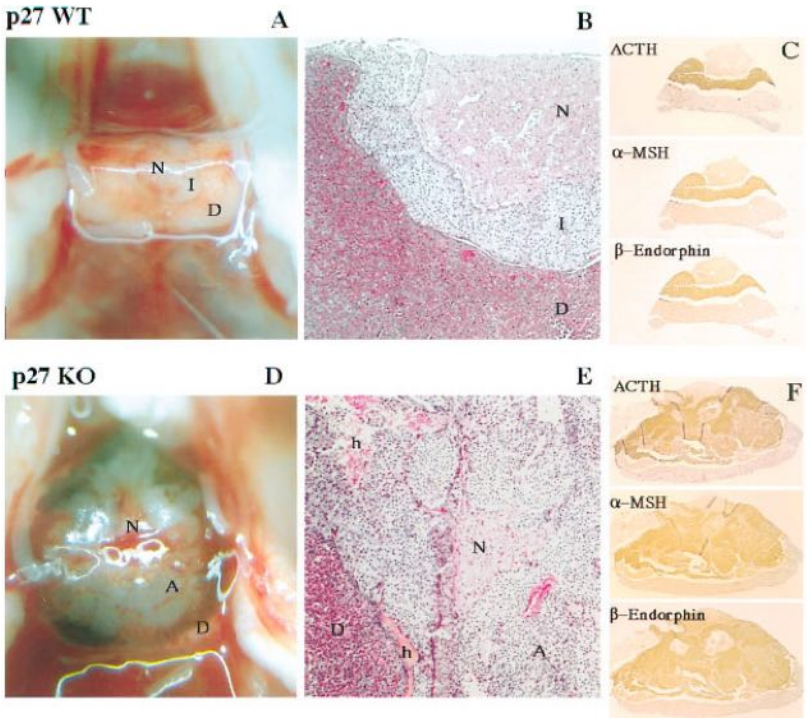

Figure 11. Pituitary Tumorigenesis in p27$^{-/-}$ mice (adapted from Fero et al. 1996)

One clue to the origin of the infertility may be that p27 protein was highly expressed in corpora lutea of control mice. Thus, p27 deficiency may impair relative resistance to the action of LH on the mature follicle. In accord, exogenous administration of gonadotropins induced ovulation, differentiation of corpora lutea, and early development of viable embryos in knockout females. The embryos implanted but did not develop to term in the knockout females, raising the possibility that the loss of p27 caused a second block to development intrinsic to the uterus.

The necessity for precise temporal and spatial control of proliferation during mammary development argues that the expression, localization, and activity of cell cycle regulatory molecules will likewise be tightly regulated. Immunohistochemical investigation of p27 expression revealed that approximately 90% of mammary epithelial cells display nuclear p27 positivity at estrus (Davison et al., 2003). However, this value declines to approximately 60% on days 2–4 of pregnancy, increases at day 6 to approximately 80%, but subsequently falls to below 70% at day 12. The pattern of p27 expression during pregnancy is thus biphasic, and there is a striking inverse relationship between p27 expression and DNA synthesis, as measured by BrdU positivity (Davison et al., 2003). In another study, p27 expression was low during both pregnancy and lactation but increased during involution (Kong et al., 2002). Interestingly, although the regulation of p27 protein levels commonly occurs via altered protein stability, transcript profiling of various stages of mammary gland development indicates decreased p27 mRNA levels during pregnancy compared with virgin or involuting glands (Master et al., 2002), suggesting that at least some of the decrease in p27 expression during pregnancy may be due to decreased transcription.

The correlation between p27 expression and proliferation during pregnancy and the genetic interaction between cyclin D1 and p27 in control of mammary development suggest that p27 may play an important role in mammary development. Consequently, several groups have directly examined this issue, using mice lacking one or both p27 alleles. For reasons which are not presently clear, these studies have yielded apparently divergent results. The infertility of p27-null female mice necessitates transplantation of p27-null mammary tissue onto immunocompromised or syngeneic hosts before development during pregnancy can be studied. Some laboratories, using two different strains of p27-null mice, have documented normal development of transplanted p27-null epithelium during pregnancy, such that alveolar development was indistinguishable from parallel transplants of wild-type epithelium (Davison et al., 2003; Geng at al., 2001). Further examination of the transplanted p27-null epithelium revealed increased proliferation during pregnancy that was balanced by increased apoptosis (Davison et al., 2003). However, impaired development of p27-null epithelium has also been observed (Muraoka et al., 2001).

As reported before, the deregulation of p27 protein in human cancer has been associated with ErbB2 oncogene amplification (Newman et al., 2001; Spataro et al., 2003). Intriguingly, several lines of evidence suggest a relationship between ErbB2 and p27 that may be important in the initiation or progression of breast cancer (Hulit et al., 2002). ErbB2 overexpression and activation reduce p27 stability, while tyrosine receptor inhibition enhances p27 stability and association with cyclin E-CDK2, leading to inhibition of proliferation (Lane et al., 2000; Yang et al., 2000; Lenferink et al., 2001). Experiments on MEC (Mouse Epithelial Cells) derived from p27-null mice displayed impaired response to ErbB2 over-expression, resulting in reduced proliferation and anchorage-indipendent growth capability. Moreover, p27-null MECs formed only small colonies in Matrigel overlay assay which maintained ductal morphology after ErbB2 expression (Muraoka et al., 2002). Complementary experiments have indicated that p27 gene dosage affects ErbB2-mediated oncogenesis *in vivo*. In p27 deficient MMTV-neu transgenics, epithelial development was enhanced and areas of hyperplasia developed in both p27-heterozygous and p27-null animals. However, development of the MMTV-neu/p27-null epithelium was still impaired compared with the other p27 genotypes. Although in p27-null animals the tumor latency was greater than wild-type (~19 months *vs* ~16 months), loss of one p27 allele significantly shortened Neu-induced tumor latency (to ~7 months) and increased the number of tumors per animal (Muraoka et al., 2002). Similarly, another laboratory also found that ErbB2-induced tumorigenesis was accelerated in p27-heterozygous animals (Hulit et al. 2002). The increased tumor latency in p27 deficient animals was unexpected, since decreased p27 expression is a response to ErbB2 overexpression, with the implication that lack of p27 impinges on the resistance to ErbB2-driven transformation.

Several lines of evidence indicate that p27 is an important effector of growth arrest in response to breast cancer therapies, with the implication that reduction in p27 expression may impair the response to these treatments (Carrol et al., 2003; Donovan et al., 2001; Cariou et al., 2000). Recent clinical data also indicate that breast cancer patients with low p27 expression responded poorly to combined hormonal therapy (tamoxifen plus goserelin) and hence have reduced relapse-free and overall survival (Pohl et al., 2003). Since decreased p27 expression *in vitro* has also been reported to confer resistance to inhibitors targeting erbB receptors (Lenferink et al., 2001; Busse et al., 2000), it is conceivable that breast cancers with low p27 levels may respond poorly to these therapies.

2. AIMS

Breast Cancer (BC) is one of the most common malignancy worldwide. Introduction of targeted therapy and early diagnosis improved the survival rates. Nonetheless, BC still remains one of the main causes of women cancer death, because of the high unpredictability of patient response to targeted therapy and chemotherapy. BC heterogeneity plays a key role in treatment response. Moreover, the complexity and heterogeneity of the disease seem to reflect the hierarchical organization of the mammary gland. Various molecular subtypes of BC have been recently characterized and, among them, HER2 positive BC accounts for 15-20% and is usually associated with poor prognosis. Δ16HER2 splicing variant, represents only 4-9% of total HER2 transcripts in HER2 positive BC and is characterized by the lack of exon 16 and by enhanced transforming activity respect the full length form.

Inactivating mutations and loss of heterozygosity of CDKN1B, the gene encoding for the cell cycle inhibitor $p27^{Kip1}$, are observed in several human cancers, including BC, where has been reported that the decreased protein expression is associated with poor prognosis. Controversial preclinical evidences have been reported on the role of p27 in HER2 BC.

In this PhD project we aim to clarify how the presence/absence of p27 impacts on Δ16HER2-driven breast tumorigenesis and the impact of this protein in mammary gland architecture.

To this aim, we generated the FVB-Δ16HER2/Cdkn1b knockout colony and characterized tumor onset and progression, evaluating different stages of mammary tumorigenesis and dissemination. Moreover, taking advantage of syngeneic injection experiments, we evaluated the cell autonomous or cell non-autonomous role of p27 in the context of Δ16HER2-driven tumorigenesis. Thus, we analyzed the growth factors and cytokines that are found in the microenvironmental compartment to assess if there are variation in molecule levels due to the presence/absence of p27 that could explain the different behavior of tumor progression.

3. MATERIAL AND METHODS

3.1 In Vivo experiments

Animal experimentation was approved by the Italian Ministry of Health (#616/2015-PR) and by our Institutional Animal Care and Use Committee (OPBA). In vivo experimentation was conducted strictly complying with OPBA and internationally accepted Institutional Animal Care and Use Committee guidelines for animal research and with the 3R principles. Mice were housed in CRO of Aviano animal facility, at 22°C with 40-60% of humidity, under pathogen free conditions and under a 12-hour dark/light cycle. All mice were monitored twice per week and euthanized when required in accordance to the ‘‘AVMA guidelines on Euthanasia’’.

MMTV-Δ16HER2 Cdkn1b knock out (p27KO) colony was generated by intercrossing FVB male mice expressing Δ16HER2 variant (Marchini et al., 2011) with FVB female mice heterozygous for p27 gene to obtain the MMTV-Δ16HER2 p27 heterozygous mice and, subsequently, the MMTV-Δ16HER2 p27KO colony. PCR analysis on genomic DNA was performed to evaluate the expression of p27 and Δ16HER2. DNA was extracted from tail biopsies using MyTaq^{TM} Extract-PCR Kit (Bioline), and was routinely used for genotyping by PCR.

Primers used (12 μM, Sigma-Aldrich) and their sequence are listed below:

- Δ16HER2 Fw: 5’-GGTCTGGACGTGCCAGTGTGA-3’
- Δ16HER2 Rv: 5’-GATAGAATGGCGCCGGGCCTT-3’
- p27 KO Fw: 5’-CCTTCTATCGCCTTCTTG-3’
- p27 WT Fw: 5’-GGACGGTCGTATCCTTATGAATCC-3’
- p27 Rv: 5’-TGGAACCCTGTGCCATCTCTAT-3’

PCR products were detected by agarose gel electrophoresis. Gel was prepared using TBE-buffer 1X (Tris 54 Mm, EDTA 0.5 M pH8 20 mM, boric acid 27.5 mM) and added with MIDORI^{Green} Advance DNA stain (Nippon Genetics).

3.1.1 Analysis of tumor onset and progression in transgenic mouse models

Δ16HER2 positive female mice were monitored by palpation once per week to determine precisely the tumor onset. Transgenic mice were monitored starting from 8 weeks of age. Primary tumors were measured and tumor volume were calculated as follows:

$$(Length \times Width^2)/2$$

Mice were euthanized at the endpoint of the experiment, at 9, 13, 16 and 20 weeks of age, depending on the tumorigenesis stage examined. During the necroscopy, tumors and mammary glands were collected for subsequent analyses.

3.1.2 Cell extraction from tumors and injection experiments

After tumors removal, some representative pieces were collected. Tumor connective capsule were removed and the tissue were properly minced using sterile scalpels until finely chopped. Tumor digestion were performed by adding a mix of Collagenase and Hyaluronidase enzymes (C&H STEMCELL technologies 10X, 3000 U/mL collagenase and 1000 U/mL hyaluronidase) opportunely diluted in HBSS buffer (Hank's Balanced Salt Solution 1X GIBCO Invitrogen). The digesting solution was incubated for an hour at 37°C. To obtain a better digestion, the solution was passed through a 23G syringe every 30 minutes of incubation. Finally, the digested solution was centrifuged at 2200g for 5 minutes; the supernatant was discarded, while the cell pellet was seeded in Dulbecco's modified Eagle's medium (DMEM) with 4500 mg/L and L-glutamine and sodium bicarbonate (Sigma-Aldrich) supplemented with 20% of FBS (Fetal Bovine Serum, Gibco) and 1% P/S (Penicillin/Streptomycin, Lonza). After 48 hours, the culture medium was changed and, within some days, tumor epithelial cells reached confluence. For injection experiments, Δ16HER2-p27 wild type (WT) or knock out (KO) epithelial cells extracted from mammary tumors were detached using TryPLE™ Express (Sigma-Aldrich) and counted using Trypan blue exclusion test. Aliquots of $3x10^5$ cells were injected in female FVB Δ16HER2 negative mice, WT or KO for Cdkn1b gene. The injection was performed bilaterally in the fat pad of thoracic mammary glands of properly anesthetized mice. Tumor onset and growth was weekly monitored by palpation and measurements. Tumor volume was determined as described above. Mice were sacrificed at the experimental end point or when tumor volume was incompatible with ethical recommendation.

3.1.3 Isolation of primary mammary epithelial cultures

To isolate mouse primary mammary epithelial cells (mMECs), third (thoracic) and fourth (abdominal) mammary glands were collected from 9-10-week-old Δ16HER2 WT and p27KO mice, finely minced using scalpels and dissociated in DMEM/F12 (Gibco) supplemented with 2mg/ml Collagenase IV (Roche), 5μg/ml insulin (Sigma), 1% penicillin and streptomycin (PS, Lonza), at 37°C for 1h with moderate shaking. Cells were collected by centrifuging the digested tissue at 1500 rpm for 10 minutes (min) and plated in Ham's F12/M199 (1:1) (Sigma) supplemented with EGF (10ng/ml, Peprotech), insulin (20μg/ml, Sigma), hydrocortisone (500ng/ml, Sigma), cholera toxin (25ng/ml, Sigma), 2% fetal bovine serum (FBS, Carlo Erba), 1% PS.

3.1.4 Murine mammary gland collection and whole mount staining

Virgin female mice were sacrificed at different weeks of age and thoracic and abdominal mammary glands were bilaterally dissected from the skin. Detached glands were immediately spread on a glass slide and fixed in 4% paraformaldehyde (PFA) for two hours at room temperature (RT). Fixed mammary glands were washed in PBS 1X (Phosphate Buffered Saline, Sigma-Aldrich) to remove the excess of PFA and stained with aqueous solution of 2% Carmine (Sigma-Aldrich) and 5% Alum (Sigma-Aldrich) to specifically highlight the epithelial structures. The mounts were then dehydrated using ethanol (EtOH) at increasing concentration (70%, 95% and 99.8%) for 1 hour each. After, glands were put in xylol overnight (ON) at RT. This last step allows the delipidation of the mammary fat pad and increase transparency. Finally, glands were mounted with cover-slips using the mounting media Eukitt and observed under a stereo microscope (Leica M205 FA) at 10X and 20X magnification, as indicated.

3.1.5 Histological and Immunofluorescence (IF) analysis

Murine thoracic or abdominal mammary glands, explanted from 13 and 16 weeks of age, were fixed in formalin ON at 4°C, embedded in paraffin and 2 μm-thick sections were cut with a microtome. Hematoxilin and Eosin (H&E) staining has been performed on both cohort derived specimens according to standard procedures. For evaluation of structural defect and/or neoplastic foci, images at 5X objective has been taken. At least 5 mice/stage/genotype has been considered.

For immunofluorescence analysis, specimens were rehydrated, immersed into 10 mM citrate buffer pH 6.0 and antigens retrieved by boiling in the microwave (550 W, 20 minutes). Samples were slowly cooled down to RT. and permeabilized with 0.2% Triton X-100 (Sigma-Aldrich) in PBS for 5 minutes. After 10% normal goat serum blocking in PBS for 1 hour, incubation with primary antibodies was performed ON at 4°C, followed by incubation with specific secondary antibodies (AlexaFluor® 488-, 568- or 633-conjugated Invitrogen, 1:200), and TO-PRO-3 (Invitrogen) or Propidium iodide (Sigma, 3 μg/ml) + RNase A 100 μg/ml for 1 hour. For evaluation of $pSTAT5^{Y694}$, was used 1mM pH8 EDTA buffer for antigen retrieval, while permeabilization was performed at -20°C using methanol for 10 minutes. For Ki-67 immunofluorescence analysis, specimens were permeabilized with 0.4% Triton X-100 in PBS for 10 minutes. Then, samples were blocked with 10% normal goat serum in PBS with 0.1% Triton X-100 for 20 minutes, and incubated ON at RT with anti-Ki67 antibody (rabbit, Abcam, 1:200). Incubation with anti-rabbit AlexaFluor® 488-conjugated (Invitrogen) and TO-PRO-3 (Invitrogen) or propidium for 1 hour.

Primary antibodies used were: $pSTAT5^{Y694}$ (Cell Signaling Technology, #9314), PrlR (Invitrogen, #359200), β-Casein (Santa Cruz, sc-166530, H4), β-Catenin (BD Transduction Laboratories,

#610154), RAB5 (Cell Signaling Technology, #3547), Cytokeratin 8 (Biolegend, #904804), Cytokeratin 14 (Biolegend, #905301), ZO-1 (Cell Signaling Technology, #8193), Ki67 (Abcam, #ab15580), HER2 (Abcam, #ab134182).
Samples were analyzed using a confocal laser-scanning microscope (TSP2 or TSP8, Leica) interfaced with a Leica fluorescent microscope. Collected images were analyzed using the LAS (Leica) and the VolocityR (PerkinElmer) softwares.

3.2 In Vitro experiments

3.2.1 Cell culture

Normal mouse mammary epithelial cells, NMuMG, were obtained from American Type Culture Collection (ATCC® CRL-1636™) and cultured in DMEM with 4500 mg/L and L-glutamine and sodium bicarbonate, supplemented with 10% FBS and 1% P/S. Cells were cultured at 37°C in a humidified chamber containing 5% CO2. HEK293-FT (Invitrogen) cells (used for lentiviral production) were maintained in DMEM supplemented with non-essential amino acids, sodium pyruvate, glutamine and 10% FBS, 1% P/S and, when necessary, 1% G418 (Sigma-Aldrich). HEK293 cells (ATCC) were used for adenoviral production and grown in DMEM supplemented with 10% FBS (Carlo Erba). All cell lines were routinely tested to exclude Mycoplasma contamination (MycoAlertTM, Lonza). p27-silenced cells were generated by adenoviral transduction. Control (Ad Neg) and mouse p27 (Ad msh-p27) sh-RNA adenoviruses were generated using the BD Knockout Adenoviral RNAi System 2 (BD biosciences) following the manufacturer's procedures and inserting the appropriate sequence. For mouse p27 sh-RNA the target sequence was 5'-AGACAATCAGGCTGGGTTA -3', for and the scramble sh-RNA sequence, used as control, was 5'-GTCCCATGAAGCTGAGGTC-3'. Recombinant replication defective viruses were generated and amplified in HEK 293 cells. Viral stock was determined by Adeno-X Rapid Titer Kit, following the manufacturer's instruction (Clontech). NMuMG overexpressing Δ16HER2 were obtained by transfecting a pcDNA3CMVΔ16HER2 expression vector (Marchini et al., 2011), using FuGENE HD (Promega), following the manufacturer's instructions. Δ16HER2-expressing cells were selected in complete medium supplemented with 50μg/ml G418.

3.2.2 Three-dimensional culture of murine mammary epithelial cells

Three-dimensional culture was performed following the protocol reported by others (Debnath et al., 2003), and partially modified (Belletti et al., 2008, Segatto et al., 2019). Mammary epithelial cells (mMECs), were extracted as reported above, and embedded as a single cell suspension in Matrigel

(Cultrex). Growth Factor Reduced Basement Membrane Extract (GFR-BME, 2%) (Trevigen), mixed with the appropriate medium and added when necessary with PRL (200ng/ml, Peprotech), and layered on the top of a bottom layer of polymerized matrix (GFR-BME, 8.5mg/ml) (Trevigen). Cells were incubated at 37°C in 5% CO2 for 7 to 10 days, depending on the growth rate. At the appropriate time point, the number of acinar structures was determined and images were collected to calculate colony areas using Volocity ® (PerkinElmer) software. Acini polarity and morphology were analyzed following immunofluorescence staining of apicobasal markers (see below).

3.2.3 PrlR internalization and stability

NMuMG cells were transduced with Ad sh-CTR or Ad sh-p27, and seeded on coverslips. 48 hours after transduction, cells were serum starved in 0.1% BSA for 4 hours, then kept on ice for 5 minutes and treated with murine recombinant Prl (200ng/ml, Peprotech). After 1hours on ice, cells were washed to remove unbound Prl and incubated at 37°C. At indicated time points (5, 10, 20, 40 and 60 minutes), coverslips were washed and immunofluorescence analysis was performed, as described above.

For stability experiment, NMuMG cells were transduced with Ad sh-CTR or Ad sh-STM, as described above, and 48 hrs after transduction were serum starved ON and stimulated with Prl (200ng/ml, Peprotech) in the presence of cycloheximide (50µg/ml, Sigma). At the indicated time points, cells were collected, lysed and analyzed by Western Blot.

3.2.4 ELISA assay

Levels of murine prolactin (Cusabio), IGFBP-5 (Cusabio), PENTRAXIN (Cusabio), CXCL9 (Abcam) and OPN (MyBiosource) were measured in serum specimens and mammary gland derived protein lysates from Δ16HER2 WT or p27KO virgin female mice collected at necroscopy at 13 weeks of age and 16 weeks of age, following manufacturer's instructions.

3.2.5 Immunofluorescence analysis

For cultured cell IF, cells were plated on glass coverslips, fixed in 4% PFA for 10 min and permeabilized with 0.2% Triton X-100 (Sigma) for 5 min before primary and secondary antibody incubation, performed as reported above.

IF analysis on three-dimension Matrigel cultured mMEC was performed as described (Debnath et al., 2003; Belletti et al., 2008). Primary antibodies incubation was performed ON at 4°C, followed by 1h at RT with secondary antibody (AlexaFluorR 488-, 546-, 568- or 633-conjugated, Invitrogen). 30 min

at RT of TO-PRO-3 (Invitrogen) has been used to counterstain nuclei. Staining of conjugated antibodies was performed 1h at RT after the incubation with secondary antibodies.
Primary antibodies used were: pSTAT5^{Y694} (Cell Signaling Technology, #9314), PrlR (Invitrogen, #359200), β-Catenin (BD Transduction Laboratories, #610154), RAB5 (Cell Signaling Technology, #3547), Cytokeratin 8 (Biolegend, #904804), Cytokeratin 14 (Biolegend, #905301), ZO-1 (Cell Signaling Technology, #8193), Phalloidin AF647 (Invitrogen, #A22287). Samples were analyzed using a confocal laser-scanning microscope (TSP2 or TSP8, Leica) interfaced with a Leica fluorescent microscope. Collected images were analyzed using the LAS (Leica) and the VolocityR (PerkinElmer) softwares.

3.2.6 RNA extraction and qRT-PCR

RNA extraction from mammary glands was performed using Trizol solution (Roche Applied Science Mannheim). Murine mammary tissue homogenization was achieved by grinding the frozen tissue using the gentle MACS™ Octo Dissociator (MACS Miltenyi Biotec). Total RNA was quantified by spectrophotometry using NanoDrop 3300 (Thermo Fisher Scientific Inc.). For gene expression analysis, RNA was retro-transcribed with GoScript™ Reverse Transcription Mix, Random Primers (Promega), according to provider's instructions. Absolute quantification of targets was evaluated by qRT-PCR, using 2X SsoFast EvaGreen ready-to-use reaction cocktail (SsoFast™ EvaGreen® Supermix, Bio-rad). All the primers used for gene expression analysis are purchased from Sigma-Aldrich and are reported in the table below. Incorporation of the EvaGreen dye into the PCR products was monitored in real time PCR, using the CFX96 Touch Real-Time PCR Detection System (Bio-Rad). Ct values were converted into attomoles and normalized expression was evaluated by using mGAPDH, or mPLK as housekeeping genes.

Primer	*Sequence 5'-3'*
Murine β-casein For	ACATTTACTGTATCCTCTGAGACTG
Murine β-casein Rev	AGATGGTTTGAGCCTGAGCA
Murine WAP For	GATCAGTAGTACCGGGCCGT
Murine WAP Rev	TCACTGAAGGGTTATCACT
Murine Elf5 For	GTGGCATCAAGAGTCAAGACTGTC
Murine Elf5 Rev	CTCAGCTTCTCGTACGTCATCCTG
Murine Gata3 For	AGCCACATCTCTCCCTTCAG
Murine Gata3 Rev	AGGGCTCTGCCTCTCTAACC
Murine PgR For	TATGGCGTGCTTACCTGTGG
Murine PgR Rev	ACTTACGACCTCCAAGGAGGA
Murine ER α For	CTGGACAGGAATCAAGGTAA
Murine ER α Rev	AGAAACGTGTACACTCCGG
Murine PRL-R For	TGAGGACGAGCGGCTAATG
Murine PRL-R Rev	GGTGTGTGGGTTTAACACCTTGA
Murine PRL For	GATAATTAGCCAGGCCTATCCTGA
Murine PRL Rev	TTGATGGGCAATTTGGCACC
Murine GAPDH For	TGACCACAGTCCATGCCATC
Murine GAPDH Rev	GACGGACACATTGGGGGTAG

3.2.7 Preparation of cell and whole mammary gland lysates and Western Blot analysis

To extract total proteins cells were scraped on ice using an appropriate volume of cold RIPA lysis buffer (NaCl 150 mM, Tris HCl pH8 50 mM, Igepal 1%, Sodium-deoxycholate 0.5%, SDS 0.1% and make up to volume with water), implemented with protease inhibitor cocktail (CompleteTM, Roche) and supplemented with 1 mM Na3VO4 (SIGMA), 10 mM NaF (SIGMA) and 1 mM DTT (SIGMA). Total proteins from whole mammary gland or tumor specimens were extracted by tissue disruption first achieved by using the gentle MACS^{TM} Octo Dissociator (MACS Miltenyi Biotec). Protein concentration was determined using the Bradford protein assay ("Biorad Protein Assay" Bio Rad). For immunoblotting analysis, proteins were separated in 4-20% SDS-PAGE (Criterion Precast Gel, Biorad) and transferred to nitrocellulose membranes (GE Healthcare). Membranes were blocked with 5% dried milk in TBS-0.1% Tween20 or in Odyssey Blocking Buffer (Licor, Biosciences) and incubated at 4°C overnight with primary antibodies.

Primary antibodies used were: pSTAT5^{Y694} (Cell Signaling Technology, #9314), PrlR (Invitrogen, #359200), CDK2 (Santa Cruz, sc-163AC), p27 (BD Transduction Lab, #610191), STAT5A (BD Transduction Lab, #610242), HER2 (Abcam, #ab134182), JAK2 (Santa Cruz, sc-390539), pJAK2 Tyr1007/1008 (Cell Signaling, #3771), Cyclin D3 (Cell Signaling, #2936), β-Tubulin (Sigma, #T8203), Vinculin (Santa Cruz, sc7649, N19). Membranes were washed in TBS-0.1% Tween20 and

incubated 1 hour at RT with IR-conjugated (AlexaFluor680, Invitrogen or IRDye 800, Rockland) secondary antibodies for infrared detection (Odyssey Infrared Detection System, LI- COR) or with the appropriate horseradish peroxidase-conjugated secondary antibodies (GE Healthcare) for ECL detection (Clarity Western ECL Substrate, BioRad). Band quantification was performed using the Odyssey v1.2 software (LI- COR) or the QuantiONE software (Bio-Rad Laboratories). The Re-Blot Plus Strong Solution (Millipore) was used to strip the membranes, when reblotting was needed.

3.2.8 Flow cytometry

Single-cell suspensions of peripheral derived immune cells or primary cells freshly extracted from Δ16HER2 WT and p27KO mammary gland as reported above, were stained with CD45 (BD Bioscience, #553077), CD3 (BD Bioscience, #555274), CD8 (BD Bioscience, #561093), CD11b (BD Bioscience, #557397), Ly6G/6C (BD Bioscience, #553129), and CD45-R (BD Bioscience, #553087) antibodies, then washed in wash buffer (PBS 1X containing 0,5% BSA and 2mM EDTA) and centrifuged for 6 minutes at 1500 rpm. A subsequent incubation of 15 minutes in dark was necessary for CD45 antibody with Streptavidin AF700 (Invitrogen), and washing cycle was performed again. Thus, cells were resuspended in 200 µl of wash buffer. Prior to sorting, DAPI (BD Biosciences) was added to distinguish dead and live cells. After excluding $DAPI^+$ and $CD45^-$ cells, cells were gated into different populations to evaluate $CD3^+$ and $CD8^+$, $Ly6G/6C^+$ and $CD11b^+$, $CD3^-$ and $CD45\text{-}R^+$ circulating and infiltrating cells. Sorting was performed using a BD LRSFortessa™ X-20 (BD Biosciences). FACSDiva™ Software was used for post-analysis.

3.3 Statistical analysis

All graphs and statistical analyses were performed using PRISM (version 6.01, GraphPad, Inc.). Data were examined using the Student's t test, One-Way Anova or Two-Way Anova, as appropriate and indicated in each figure. A minimum of three biologically independent specimens was used for statistical significance. Differences were considered significant at $P<0.05$.

4. RESULTS

- **4.1 Generation and characterization of the FVB MMTV-Δ16HER2/Cdkn1BKO mouse model**

Given the relevance of p27 and HER2 in breast cancer (BC), we decided to exploit the FVB-MMTV-Δ16HER2 transgenic model (Marchini et al. 2011) to investigate the potential impact of their crosstalk during BC initiation and progression. These transgenic female mice develop spontaneous multifocal mammary tumors with a latency of 15-weeks an average. After confirming that our FVB-MMTV-Δ16HER2 colony shares the same characteristics of the one reported in the original study (onset at 12-19 weeks; 15.5 weeks on average), we established the FVB-Δ16HER2/Cdkn1b knockout colony, intercrossing mice from Δ16HER2 colony with mice from our FVB-Cdkn1b colony and generated FVB-Δ16HER2/Cdkn1b wild-type (Δ16HER2 WT), FVB-Δ16HER2/Cdkn1b heterozygous (Δ16HER2 p27Het) and FVB-Δ16HER2/Cdkn1b knockout (Δ16HER2 p27KO) mice. Then, we started the characterization of Δ16HER2 WT, Δ16HER2 p27Het and Δ16HER2 p27KO mice, evaluating the onset of palpable tumors and following the tumor growth.

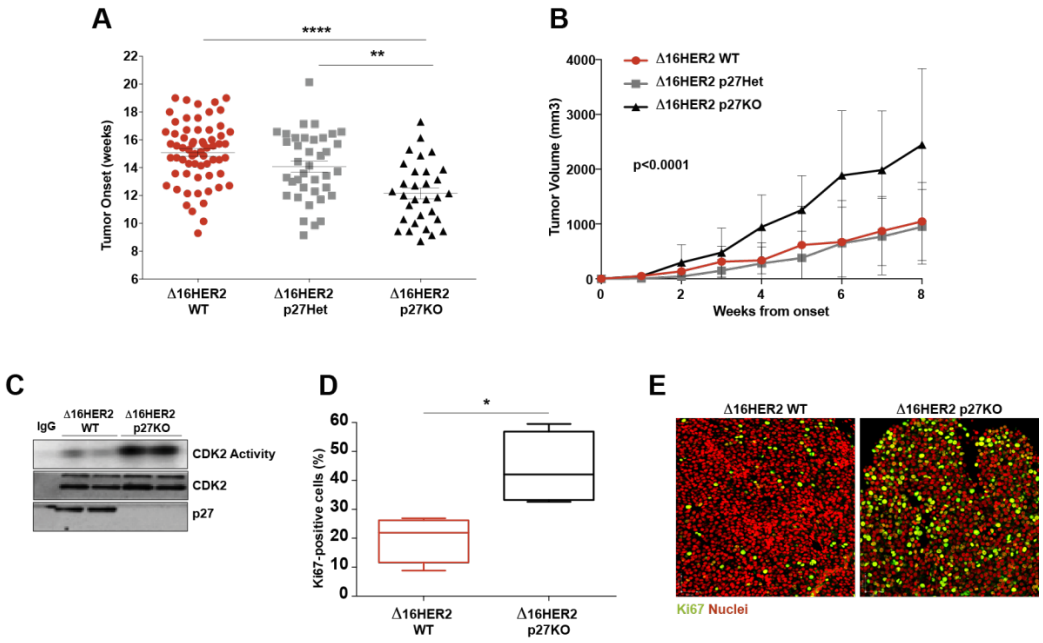

Figure 1. Loss of p27 induces an impairment in tumor onset and an increase in tumor growth rate in Δ16HER2-driven tumorigenesis. **A** and **B**, Graphs report the onset (**A**) and the growth (**B**) of palpable tumors derived from Δ16HER2 WT (15,09 weeks), p27Het (14,07 weeks) and p27KO (12,45 weeks) female mice. Mice were monitored twice a week, and tumors were followed up and measured for 8 weeks after tumor appearance. Results are from at least n=30 mice for each cohort. **C**, CDK2 Kinase assay performed on tumor protein lysates extracted from MMG tumors of 16 weeks of age Δ16HER2-positive p27 WT or KO female mice. Each lane corresponds to a different mouse. **D** and **E,** Graph (**D**) and representative images (**E**) of Ki67-positive cells (green), evaluated by immunofluorescence analysis, in sections from the same samples described in C. Nuclei were stained with propidium iodide (red). Results are from $n = 5$ mice/genotype. In all graphs, significance was calculated by One-Way Anova, Two-Way Anova or Student's t test, as appropriate, and is indicated by a $P < 0.05$.

The ablation of p27 in female transgenic mice induced a marked anticipation of palpable mammary tumors appearance compared to the Δ16HER2 WT counterpart (12.77 weeks *vs* 15.09 weeks). In contrast with the reported haploinsufficient role of p27 for tumor suppression, in this model of Δ16HER2-driven BC loss of only one copy of Cdkn1b gene (Δ16HER2 Het) did not significantly accelerate onset of tumors (14.07 weeks *vs* 15.09 weeks) (Figure 1A). We followed-up mice measuring palpable lesions twice a week and observed that the growth rate in Δ16HER2 KO tumors was dramatically increased compared the other two genotypes (Figure 1B). These results are well in line with the established role of p27 as inhibitor of cell cycle progression, but are in contrast with the studies reporting an impaired development of MMTV-Neu/p27-null epithelium and an augmented Neu-induced tumor latency in p27-null animals (Muraoka et al., 2002). Analysis of CDK2 kinase activity in tumors collected from 16 weeks-old Δ16HER2 WT and Δ16HER2 KO mice, revealed, as expected, that CDK2 is more active in absence of p27 (Figure 1C). Staining for Ki67 proliferation marker in tumor sections obtained from the same lesions used for CDK2 activity confirmed the above-mentioned increase in tumor proliferation, highlighting a 2-fold increase in Ki67 positive cells in Δ16HER2 KO tumors compared with Δ16HER2 WT one (Figure 1D-E).

To characterize if and how p27 impinges on tumor appearance, progression and dissemination in Δ16HER2 mouse model, we collected tumors, organs and tissues known to be affected by Δ16HER2-driven transformation. Therefore, mice were sacrificed at different stages, from early to advanced phases of tumorigenesis, and tumors and organs were collected at necroscopy: i) at 13 weeks of age, for the analyses of early transformation; ii) 16 weeks of age, for the analyses of small palpable tumors; iii) 20 weeks of age, for the analyses of frank tumors; iv) 30 weeks of age, for the analyses of metastatic dissemination.

In accord with Arteaga's group data, the analysis of Hematoxylin and Eosin (H&E) stained mouse mammary gland (MMG) sections in 13 weeks of age mice (early stage of tumorigenesis) revealed the presence of a lower number of pre- and neoplastic lesions in Δ16HER2 p27KO mammary glands compared to Δ16HER2 WT (Figure 2A). These data were confirmed in the 16 and 20 weeks cohorts (Figure 2B-C). Yet, tumors in both cohorts were significantly bigger in size in Δ16HER2 p27KO mice (Figure 2D-E), in accord with the higher CDK2 kinase activity (Figure 1C). The analyses of Δ16HER2 p27Het haploinsufficient mice revealed that tumors number and weight was exactly midway between Δ16HER2 WT and Δ16HER2 p27KO.

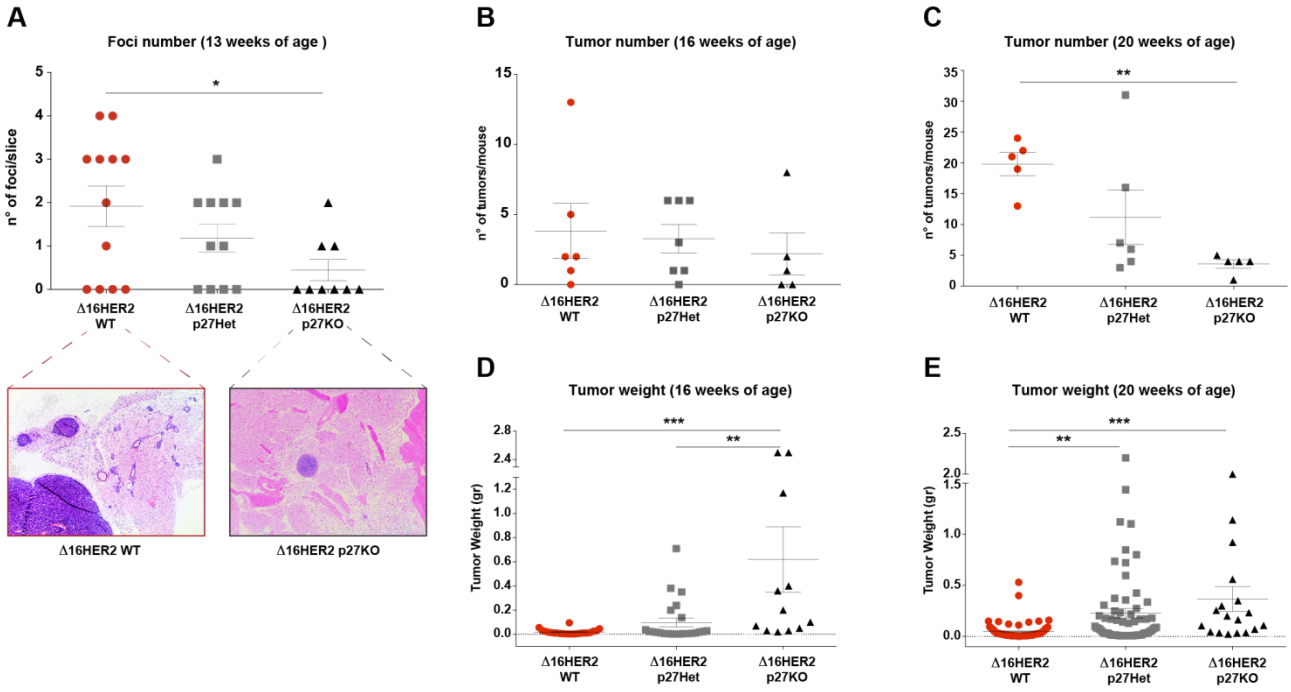

Figure 2. Δ16HER2 p27KO mice present an increase in tumor mass coupled with a significant impairment in tumor number. **A,** Graph reports the number of neoplastic foci detected per hematoxylin and eosin–stained section of mammary glands collected from Δ16HER2 WT or p27KO mice at 13 weeks of age, as indicated. Representative images of hematoxylin and eosin–stained mammary glands, taken with a 5X objective, are reported at the bottom of the graph. At least $n = 5$ mice/genotype were scored. **B** and **C,** Graphs report the number of tumors detected in Δ16HER2-positive, p27 WT, Het and KO mice of 16 weeks of age (**B**) and 20 weeks of age (**C**), as reported, at necropsy examination (from 1 to 5–6 weeks from palpable tumor appearance). At least 6 mice/group were evaluated. **D** and **E**, Graphs report the weight of same tumors as in B and C, as reported. In all graphs, significance was calculated by One-Way Anova and is indicated by a $P < 0.05$.

Last, we analyzed the cohort collected at late stage of tumor progression (30 weeks of age, or 11 weeks from tumor appearance), to evaluate the impact of p27 loss in the Δ16HER2-driven metastatic process. To this aim, tumors and organs known to be potentially targeted during the dissemination steps, such as liver, lungs, bones and brain, have been collected and evaluated for the presence of metastatic lesions. In line with what observed for previous cohorts, the number of tumors developed in Δ16HER2 p27KO mice was significantly lower than in Δ16HER2 WT and Δ16HER2 p27Het, (Figure 3A). Also, data from tumor weight were in line with the results obtained above (data not shown).

As far as distant organ dissemination, preliminary data obtained from H&E staining of lung sections revealed a lower number of metastatic foci in Δ16HER2 p27KO respect to Δ16HER2 WT control mice (Figure 3B). However, the analyses to evaluate the role of p27 in the metastatic process are still ongoing.

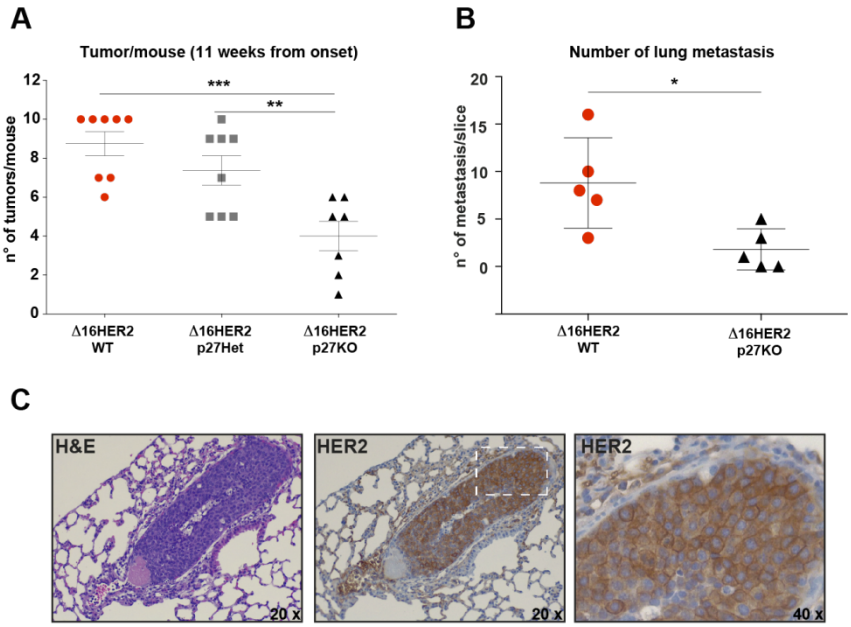

Figure 3. KO of p27 strongly impinges both on neoplastic lesion number and dissemination in later stages of Δ16HER2-driven tumorigenesis. **A**, Graph reports the number of tumors explanted at time of necroscopy from Δ16HER2 WT, p27Het or p27KO mice mammary glands at late tumorigenesis stages (10–11 weeks from palpable lesion appearance), as indicated. **B** and **C**, Graph (**B**) and representative images (**C**) of metastatic foci detected per hematoxylin and eosin–stained section of FFPE lung sections collected from Δ16HER2 WT or p27KO mice from the same cohort as A, as indicated. Representative images of hematoxylin and eosin–stained lung sections, and IHC staining of Δ16HER2 expression, taken with a 20X and 40X objective, are reported in C. At least $n = 5$ mice/genotype were scored. In all graphs, significance was calculated by One-Way Anova or Student's t test, as appropriate, and is indicated by a $P < 0.05$.

H&E staining of Δ16HER2 p27KO lung section revealed that spotted lesions, positive for HER2 (IHC), were usually located in proximity or into blood vessels, suggesting that p27KO cancer cells were still entrapped in the blood vessels and did not extravasate nor settle in the new organ (Figure 3C). However, these results will need to be further validated by the completion of the analyses in this cohort.

Our mouse colony displays expression of the Δ16HER2 transgene under the MMTV promoter and the KO of p27 gene operates in all tissues. Therefore, the phenotypic results that we observe could be dependent on tumor cells (cell autonomous) or could be due to cell non-autonomous mechanisms, involving the stromal cells or the immune cell infiltrates in the MMG or, even, cells or factors operating from distant districts.

To discriminate among cell autonomous and non-autonomous function of p27 in Δ16HER2-driven tumorigenesis, we performed the syngeneic injections of mammary epithelial cells harvested from Δ16HER2 WT and Δ16HER2 p27KO tumors, in mammary fat pads (MFP) of FVB WT or FVB p27KO *non* transgenic recipient mice.

Data collected highlighted a marked anticipation in tumor onset when Δ16HER2 p27KO-derived tumor cells were injected in p27KO background (5.3 weeks after injection). The injection of the same Δ16HER2 p27KO-derived cells in WT recipient mice resulted in an onset (6.7 weeks after injection) anticipated but more similar to both the combination of Δ16HER2 WT-derived tumor cells injected in WT (8 weeks after injection) or p27KO (7.5 weeks after injection) background (Figure 4A). These data indicated that ablation of p27 in both the epithelial and stromal components were necessary to significantly affect tumor appearance. Surprisingly, looking at the tumor growth rate of syngeneic tumors we observed a significant increase in tumor growth when both Δ16HER2 WT and Δ16HER2 p27KO derived cells were implanted in p27KO mice (Figure 4B, compare dark red and black lines), when compared to the growth rate of both cell types implanted in WT MFP (Figure 4B, compare red and grey lines). Molecular analyses on explanted tumors revealed that CDK2 activity was augmented in Δ16HER2 p27KO cells independently on the genotype of implanted animals, although a tendency for higher CDK2 activity when cells were implanted in the p27KO background could be observed (Figure 4C). Ki67 staining of tumor sections, reported in Figure 4D-E, indicated an increased cell proliferation of Δ16HER2 p27KO cells in p27KO background respect to all other combinations. These results suggest that, on one side, ablation of p27 in the tumor cells (donors) plays critical and cell cycle related roles and, on the other, its loss in the mammary microenvironment (recipients) also plays an important role in tumor onset and progression, supporting both cell autonomous and non-autonomous contributions of p27 in this context.

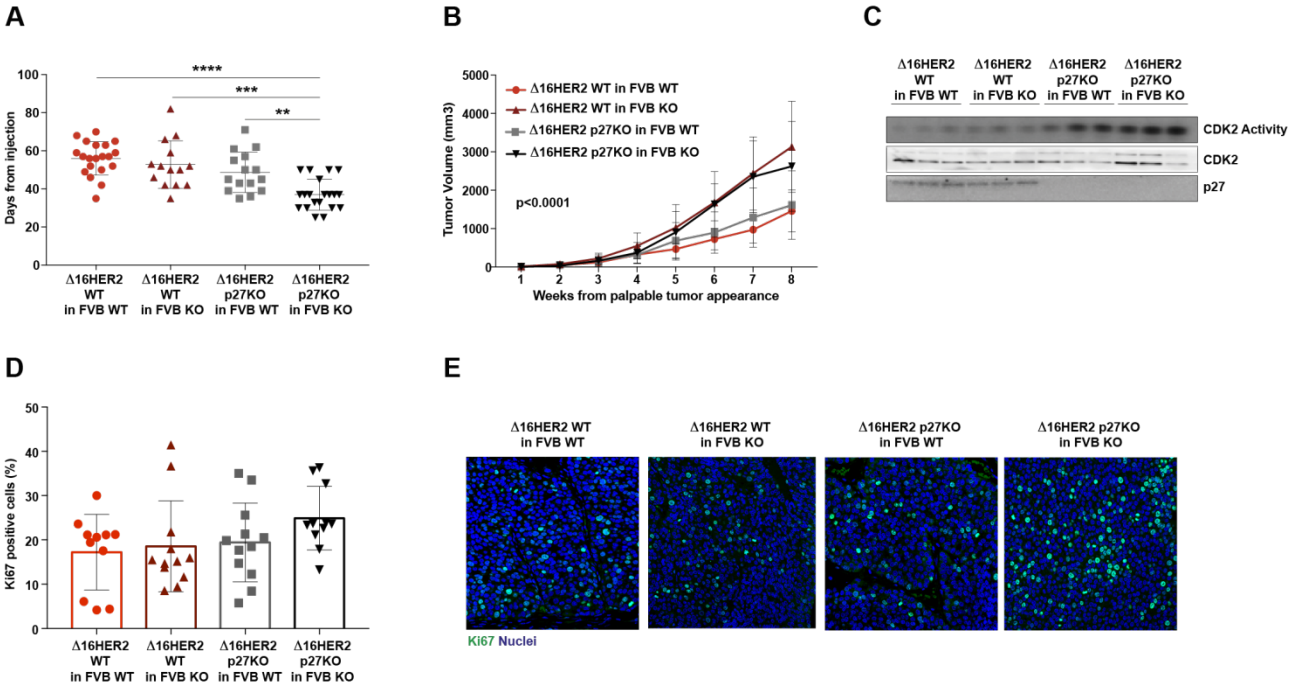

Figure 4. Ablation of p27 impacts on tumor onset and tumor growth mainly by cell non-autonomous mechanism **A** and **B**, Graphs report the onset (**A**) and growth (**B**) of palpable tumors derived from syngeneic injection experiments. Tumors from Δ16HER2-positive, WT or p27KO mice (donors) were disaggregated and plated as primary cultures. Upon achievement of confluence, 3×10^5 cells were injected in mammary fat pad of Δ16HER2-negative, WT or p27KO mice (recipients). At least 5 mice/group and three different cell populations/group were utilized. **C**, CDK2 Kinase assay performed on protein lysates extracted from MMG tumors explanted at time of necroscopy from FVB WT or p27KO recipient, injected with Δ16HER2 WT or p27KO primary epithelial cells, as reported. Each lane corresponds to a different mouse. **D** and **E,** Graph (**D**) and representative images (**E**) of Ki67-positive cells (green), evaluated by immunofluorescence analysis, in sections from the same samples described in C. Nuclei were stained with TO-PRO-3 (blue). Results are from $n = 5$ mice/genotype. In all graphs, significance was calculated by One-Way Anova or Two-Way Anova, as appropriate, and is indicated by a $P < 0.05$.

- **4.2 Characterization of Δ16HER2 mammary gland architectural development**

Based on these evidences, we reasoned that p27 absence could also have a role in the development of mammary gland in the context of Δ16HER2 expression. Many studies indicate that the ErbB family, and in particular HER2, play an important role in MMG development during puberty and ductal elongation, while the role of p27 in MMG development is still not completely understood. We thus characterized the mammary gland architectural and functional development in our Δ16HER2 p27KO colony. The mammary gland development is a multistage process that occurs mainly under the influence of hormonal cues, particularly during puberty, and completes during pregnancy and lactation. Pregnancy stage could not be evaluated because p27KO female mice are sterile (Fero et al., 1996; Nakayama et al., 1996; Kiyokawa et al., 1996). We thus collected MMG from virgin female mice of the different genotypes, starting from the 9 weeks of age, then 13 weeks of age and, finally, 16 weeks of age. Mammary architecture in young adult stage (9 weeks of age) did not evidence morphological and developmental differences between WT and p27KO Δ16HER2 female mice (data not shown) and at 16 weeks of age MMG of p27KO mice were already altered by tumor infiltration due to the high penetrance of Δ16HER2 tumors (Figure 2). For these reasons we first focused our analyses on the mammary gland morphology from virgin female mice of 13 weeks of age that only had early neoplastic lesions (Figure 2).

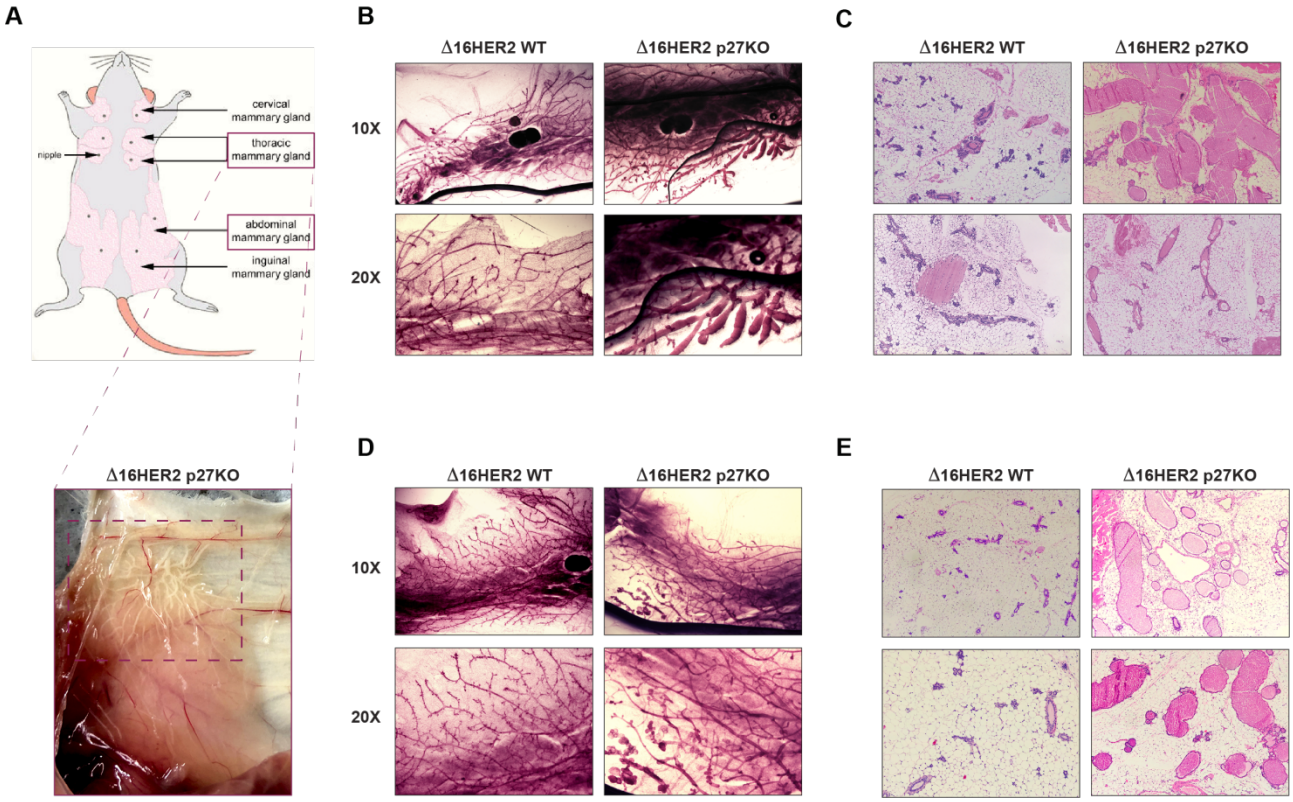

Figure 5. Loss of p27 causes structural abnormalities and lactating-like phenotype in Δ16HER2 expressing mammary gland. **A**, Schematic representation of mouse mammary gland anatomy (top). Purple squared mammary glands are those used for the subsequent analysis. Representative image of Δ16HER2 p27KO mammary gland is reported at the bottom of the scheme. Enlarge ducts and milky fluids are encased in purple dashed-line. **B**, Carmine Alum stained whole mount of mammary glands collected from Δ16HER2-positive, p27 WT or KO virgin female mice at 13 weeks of age. Representative images have been taken with a 10X (top) and 20X (bottom) objective. At least 5 mice/genotype were analyzed. **C**, Hematoxylin and eosin–stained FFPE mammary gland sections from the same mice as in B. Representative images have been taken with a 5X objective. **D**, Carmine Alum stained whole mount of mammary glands collected from Δ16HER2-positive, p27 WT or KO virgin female mice at 16 weeks of age. Representative images have been taken with a 10X (top) and 20X (bottom) objective. At least 5 mice/genotype were analyzed. **E**, Hematoxylin and eosin–stained FFPE mammary gland sections from the same mice as in D. Representative images have been taken with a 5X objective. Whole mount structural analysis and hematoxylin and eosin staining were performed on 9 weeks of age cohort, which did not reveal significant structural differences.

Whole mount analyses of the mammary glands showed that Δ16HER2 p27KO mice had structural defects in duct branching. As shown in Figure 5B, Δ16HER2 p27KO MMG presented hypertrophic ducts and alveoli-like structure, not present in the branched ductal tree of Δ16HER2 WT mice (Figure 5B, see 10X and 20X). Intriguingly, we also observed the presence of milky fluid in Δ16HER2 p27KO mammary glands (Figure 5A). H&E staining confirmed the striking structural difference in MMG from Δ16HER2 p27KO mice, highlighting the presence of swollen ducts and acini structures that appeared filled with proteinaceous material and fatty vesicles, highly reminiscent of a lactating phenotype (Figure 5C).

These data were confirmed by the analysis of 16 weeks of age Δ16HER2 p27KO MMG showed the same phenotype, only more exacerbated, both at whole mount examination and H&E staining, while

the Δ16HER2 WT gland continue to maintain normal ductal structures and side branching (Figure 5D-E).

Since the above-mentioned observations evoked a lactation-like phenotype, we moved our attention on those signaling pathways that are responsible for the maturation of mammary gland. It is well known that the preparation and maturation of the MMG for lactation is finely regulated by Signal Transducer and Activator of Transcription 5 (STAT5), that is considered the master regulator of alveolar development and whose activity is critical in the MMG for the synthesis of milk proteins. The transcriptional activity of STAT5 depends on its dimerization (homo- or hetero-) and nuclear translocation, which in turn depends on its activation through the phosphorylation, by Janus Kinase 2 (JAK2), of specific tyrosine residue (Y694) located on the C-terminus of the protein. After JAK2 phosphorylation, STAT5 dissociates from the cytokine receptor it is finally available for dimerization and nuclear translocation. In the nucleus, STAT5 dimers bind to its responsive elements, and induce the transcription of specific genes (Figure 6A). Western blot analysis on the protein lysates derived from Δ16HER2 WT and p27KO mammary glands explanted at 13 weeks of age and 16 weeks of age confirmed that despite total protein was equally expressed, the phosphorylation of STAT5 in tyrosine 694 was higher in Δ16HER2 p27KO respect the WT counterpart (Figure 6B-C). Immunofluorescence analysis of $STAT5^{Y694}$ reinforced and confirmed these finding showing that Δ16HER2 mammary glands derived from p27 ablated mice displayed diffuse and significantly elevated levels of activated STAT5 (*p=0.021*). These data suggested that hyper activation of STAT5 could be responsible for the hypertrophic phenotype observed in mammary gland of Δ16HER2 p27KO mice (Figure 6D). Accordingly, when Δ16HER2 WT and p27KO virgin female mice from 13 and 16 weeks of age cohort were stained for milk protein β–casein, a known STAT5 target gene, this was found to be expressed in luminal compartment of Δ16HER2 p27KO but not WT glands, (Figure 6E see enlargements in the lower panels).

Quantitative RT-PCR on the same samples, demonstrated that the higher expression of the milk proteins β–casein and Whey Acidic Protein (WAP) in the Δ16HER2 p27KO glands was due to a higher mRNA expression, confirming that STAT5 transcriptional activity is augmented in Δ16HER2 MMG in the absence of p27. It is interesting to note that the evaluation of STAT5 activation at the 9 weeks of age stage, did not evidence any difference between Δ16HER2 WT and p27KO mice (data not shown), suggesting that the occurrence of structural and molecular alteration of p27KO MMG could be due, at least in part, to the appearance of neoplastic HER2 positive lesions.

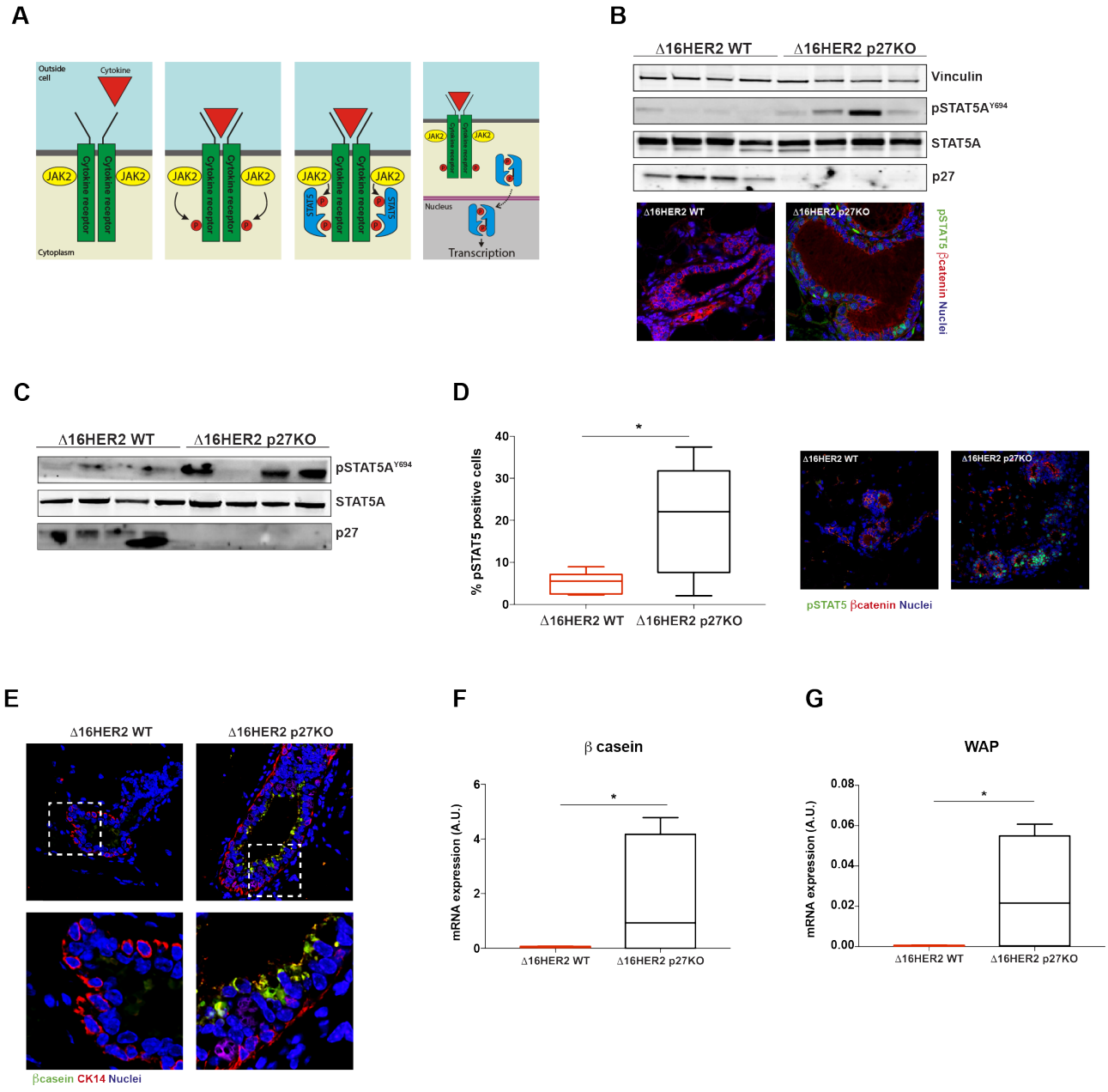

Figure 6. Δ16HER2 p27KO lactating-like mammary glands display aberrant activation of PRL-R/JAK2/STAT5 axis. **A**, Schematic representation of PRL-R pathway. **B**, Western blot analysis (top) of protein lysates extracted from MMG of Δ16HER2 WT and p27KO mice at 13 weeks of age. Each lane corresponds to a different mouse. Vinculin was used as loading control. Bottom, representative images of immunofluorescence analysis of pSTAT5^{Y694} (green), β-catenin (red), and nuclei (TO-PRO-3, blue), performed on FFPE sections of MMG collected from same aged Δ16HER2 WT and p27KO virgin female mice. **C**, Western blot analysis of protein lysates extracted from MMG of Δ16HER2 WT and p27KO mice at 16 weeks of age. Each lane corresponds to a different mouse. **D**, Graph (right) and representative images (left) of immunofluorescence analysis of pSTAT5^{Y694} (green), β-catenin (red), and nuclei (TO-PRO-3, blue), performed on FFPE sections of same samples as in C. Right, graph report the quantification of the percentage of positive stained cells to pSTAT5^{Y694} (green). **E**, Representative images of immunofluorescence analysis of milk protein β-casein (green), cytokeratin14 (red) and nuclei (TO-PRO-3, blue), performed on FFPE sections of 16 weeks of age Δ16HER2 WT and p27KO derived mammary glands. Analysis has been performed also on 13 weeks of age MMG derived cohort. Bottom, enlargement of the white dashed-line region. **F** and **G**, qRT-PCR analysis of STAT5 target genes β-casein (**F**) and WAP (**G**) in MMG collected Δ16HER2 WT and p27KO 13 and 16 weeks of age virgin mice. Normalized mRNA level of β-casein and WAP is reported. At least four mice/stage/genotype were analyzed. In all graphs, significance was calculated by Student's *t* test and is indicated by a $P < 0.05$.

- **4.3 Analysis of circulating and mammary gland microenvironmental factors**

Data collected so far in syngeneic injection experiments (Figure 4) and in the evaluation of mammary gland architecture (Figure 5), suggested that the local microenvironment could be altered in Δ16HER2 p27KO mice. We first focused our attention on the release of secreted growth factors and cytokine in the microenvironment of p27KO mammary gland that could be involved in the paracrine crosstalk of tumor cells with local microenvironment and that eventually may impact in different aspects of mammary gland transformation, tumor appearance and progression, and modulation of immune recruitment, infiltration and response.

Since our data indicated that phenotypic differences between WT and p27KO in term of tumor development and mammary gland development become evident at 13 weeks of age we used this cohort of mice to evaluate the expression of 200 growth factors and cytokines in the mammary gland protein lysates and in serum samples.

First, we tested these samples in a commercially available array comprising 200 cytokines and identified 15 growth factors/cytokines differentially expressed in Δ16HER2 WT *versus* Δ16HER2 p27KO serum and/or protein lysates from mammary glands (Figure 7A).

In serum samples, 10 cytokines were significantly increased in Δ16HER2 p27KO mice. These include AREG, Fractalkine (CX3CL1), MIP-3b (CCL19), TACI (TNFRSF13B), TECK (CCL25), that are known to be involved in cell survival, motility, EMT and that are up-regulated in different types of cancer, including breast cancer. Biological processes enrichment analysis indicated that seven out of ten altered cytokines played a role in regulation of immune cell chemotaxis or migration. For instance, CCL1, CCL19, CCL25 and CX3CL1 regulate monocyte, lymphocytes, neutrophils and granulocytes chemotaxis and are also involved in interferon-gamma response (Figure 7B). Next, pathway enrichment analyses highlighted a possible alteration of NF-kappa B, IL-12-related pathway, IL-23-related pathway or IL-35-related pathway, all related to immune cells regulation (Figure 7C).

Given the implication of most of the altered molecules in the immune regulation processes, we next evaluated the composition of circulating immune cells in blood samples from Δ16HER2 p27KO virgin female mice compared to the Δ16HER2 WT counterpart. Complete blood count with formula revealed no significant differences between WT and p27 in the total number of platelets, red (RBC) and white blood cell (WBC) but demonstrated a significant increase neutrophil and monocyte number (Figure 7D) that was in accord with the increased cytokines expression observed in Δ16HER2 p27KO serum samples.

In mammary gland lysates, we found five cytokines significantly altered in Δ16HER2 p27KO mice compared to the WT counterpart (Figure 7A). Among these, we found two cytokines that are involved

in the regulation of mammary gland transformation during lactation and involution: Prolactin (PRL), the hormone responsible for the maturation of alveolar structures and production of milk protein through the activation of the signaling mediated by prolactin receptor (PRL-R), and IGFBP5, that plays a critical role in mammary gland development, particularly in the clearance of mammary epithelial cells that takes place during the involution stage post-lactation.

In order to confirm the interesting results obtained in the cytokine array, we decided to focus on cytokines differentially expressed in the mammary gland, using commercially available ELISA assays for IGFBP-5, Pentraxin 3, CXCL9 and Prolactin. Unfortunately, we could not find a validated ELISA for murine GAS6. Moreover, we included in the validation experiments also osteopontin (OPN), significantly altered in sera, since its tumor derived expression has been previously related to mammary gland inflammation and tumor progression (Sharon et al., 2015). The evaluation of the expression of these cytokines was performed on an enlarged cohort of sera and mammary gland protein lysates, derived from Δ16HER2 WT and p27KO mice of both 13 and 16 weeks of age. By this approach, 2 out of the 5 tested cytokines were not confirmed, namely IGFBP-5 and Pentraxin 3 (Figure 7 E-I). Of note, CXCL9 levels were found significantly increased only in serum from Δ16HER2 p27KO mice (Figure 7I) and a very significant increase in osteopontin (OPN) levels was observed in Δ16HER2 p27KO mammary gland lysates, but not in serum (Figure 7L-M). A clear increase of Prolactin (PRL) was confirmed in mammary gland lysates from Δ16HER2 p27KO virgin female mice compared to Δ16HER2 WT controls (Figure 7N). It is well known that PRL is a crucial hormone operating mainly during mammary gland maturation for lactation. The major source of this pleiotropic polypeptide hormone is represented by the lactotropic cells located in the anterior pituitary gland, which produces prolactin in response to hormonal signals including dopamine (or less frequently oxytocin, estrogen and progesterone). We thus expected that the up-regulation of PRL in mammary gland lysates was paralleled by an equivalent increase in serum samples derived from Δ16HER2 p27KO. Unexpectedly, circulating PRL was not significantly increased but, rather, slightly decreased in the serum of these mice (Figure 7O).

Overall, the obtained results support the possibility that alteration of cytokines expression could be responsible for the regulation of mammary gland development, eventually explaining the tumoral and lactation-like phenotypes observed in the mammary gland of Δ16HER2 p27KO mice.

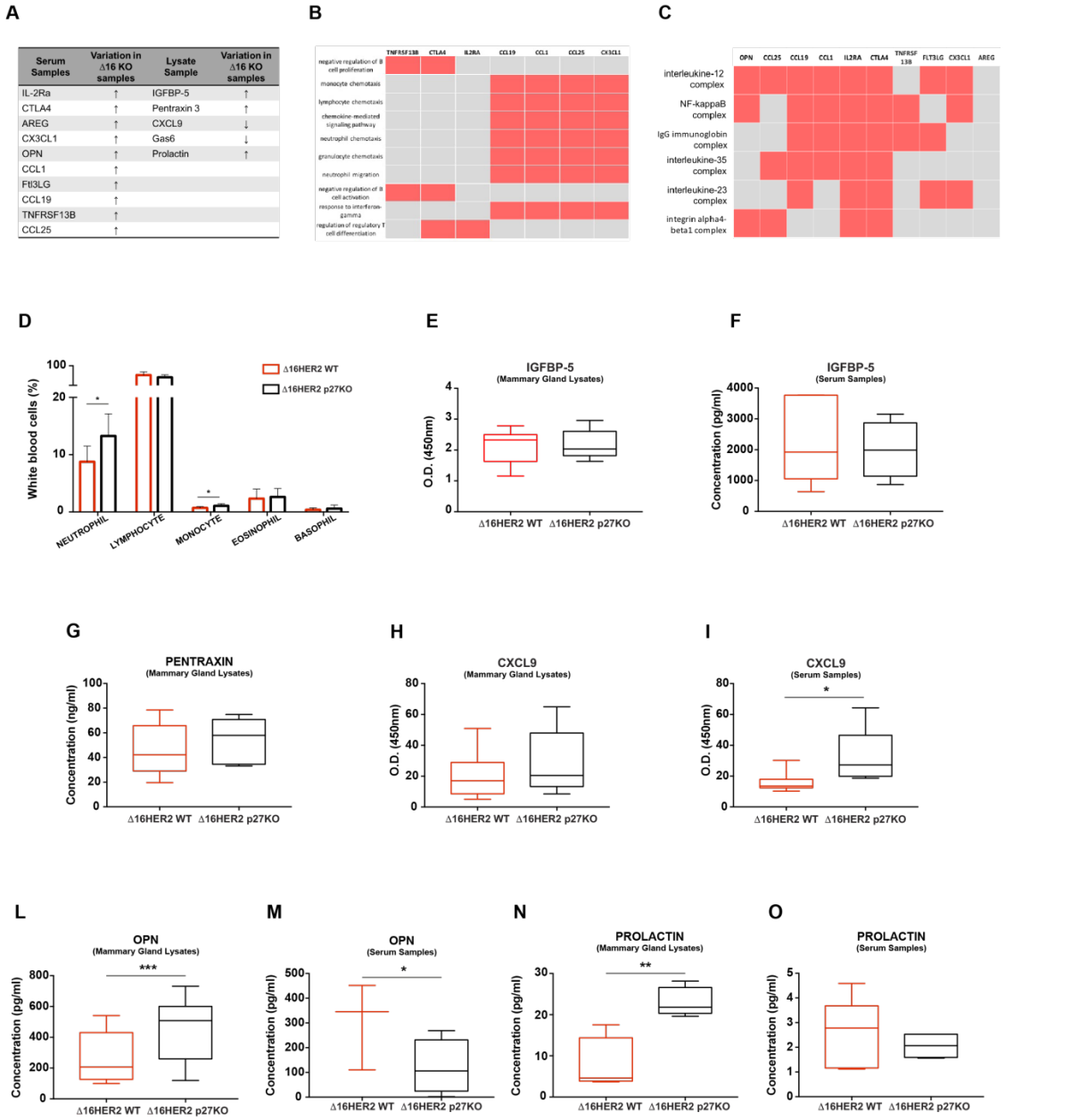

Figure 7. Ablation of p27 profoundly impinges on cytokine production in mammary microenvironment. **A**, Table reports the 15 cytokines out of 200 found altered from cytokine array performed on serum samples and mammary protein lysates from Δ16HER2-positive WT or KO for p27. **B**, Enrichment analysis for biological processes on serum altered cytokines. Serum cytokines derived from the cytokine array performed on same samples as in A, have been analyzed using Enrichr program. **C**, Enrichment analysis for biological complexes in which altered cytokine are involved. Serum and MMG cytokines derived from the cytokine array performed on same samples as in A, have been analyzed using Enrichr program. **D**, WBC differential count of peripheral blood from 13 weeks of age Δ16HER2 WT and p27KO virgin female mice, sampled from submandibular vein. Results are from n = 6 mice/genotype. **E** and **F**, Graphs report the result of confirmation Elisa assay for IGFBP-5 performed on mammary gland derived lysates (**E**) and serum samples (**F**) from 13 weeks of age and 16 weeks of age Δ16HER2 WT and p27KO virgin female mice. **G**, Graph reports the result of confirmation Elisa assay for PTX3 performed on same samples as (**E**). **H** and **I**, Graphs report the result of confirmation Elisa assay for CXCL9 cytokine performed on mammary gland derived lysates (**H**) and serum samples (**I**) from same samples as (**E**) and (**F**). **L** and **M**, Graphs report the result of confirmation Elisa assay for OPN performed on mammary gland derived lysates (**L**) and serum samples (**M**) from same samples as (**E**) and (**F**). **N** and **O**, Graphs report the result of confirmation Elisa assay for PRL performed on mammary gland derived lysates (**N**) and serum samples (**O**) from same samples as (**E**) and (**F**). All results derived from at least 5 mice/stage/genotype. In all graphs, significance was calculated by Student's t test and is indicated by a $P < 0.05$

- **4.4 Dissection of PRL and PRL-R pathway in mammary glands of Δ16HER2 p27KO virgin female mice**

Converging collected evidences support a pivotal role for PRL-PRL-R pathway in mammary gland development and transformation of Δ16HER2 p27KO mice. These include not only the higher expression of PRL in p27KO mammary gland lysates but also the observed hyper phosphorylation of STAT5 (Figure 6) that likely represent the readout of increased activation of the PRL-R-JAK-STAT axis.

First, we tried to understand how PRL expression was differentially regulated in our model. As mentioned above, PRL levels were increased in Δ16HER2 p27KO MMG (Figure 7N-O) but not in the serum of the same mice, suggesting that the source of PRL was not the anterior part of the pituitary gland. To assess this possibility, we performed RNA extraction from pituitary glands and mammary tissues collected from 13 weeks of age Δ16HER2 virgin female mice of both genotypes and carried out qRT-PCR to measure PRL mRNA levels. PRL mRNA levels were very high in pituitary extracts, as expected, but, contrarily to what observed in MMGs, were higher in Δ16HER2 WT respect to p27KO samples (Figure 8A; $p=0.05$). This result was in line with the observed decreased levels of circulating PRL in Δ16HER2 p27KO mice. Conversely, in the mammary gland PRL mRNA expression was significantly increased in Δ16HER2 p27KO compared to WT samples (Figure 8B), suggesting that the increased PRL levels observed in p27KO mice were due to an increased local production.

In accord with the increased PRL levels in the MMG, we also observed an increased expression and activation of JAK2 and a variable increase of PRL-R expression in MMG lysates of p27KO mice using western blot analyses (Figure 8C).

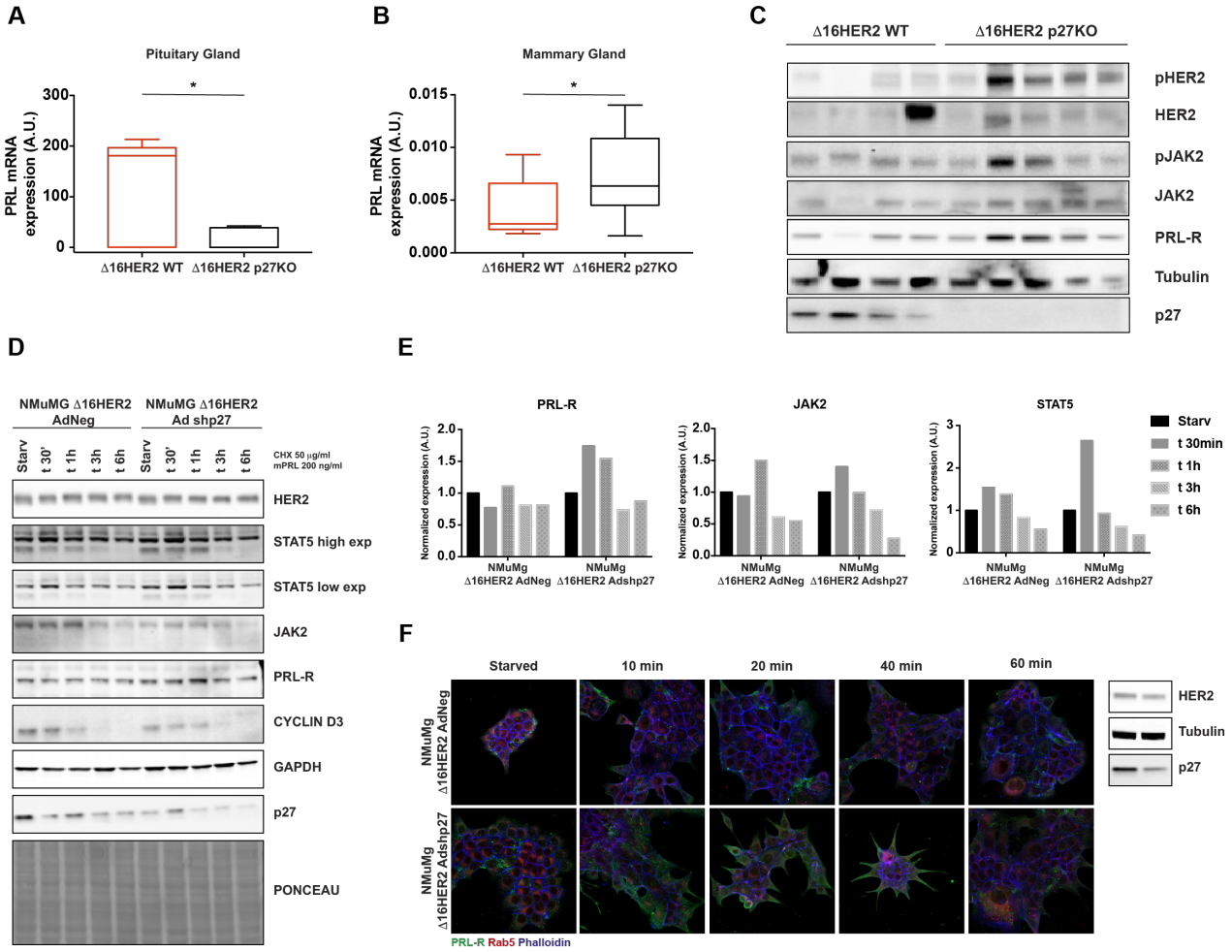

Figure 8. p27 absence causes an increase in PRL-R levels and protein stability after prolactin stimulus. **A** and **B**, qRT-PCR analysis of prolactin (PRL), in pituitary gland and mammary gland explanted from Δ16HER2 WT and p27KO 13 weeks of age virgin female mice. Normalized mRNA level of PRL is reported. At least 4 mice per genotype were analyzed. **C**, Western blot analysis of protein lysates extracted from MMG of Δ16HER2 WT and p27KO mice at 13 weeks of age. Each lane corresponds to a different mouse. Tubulin blot was used as loading control. **D** and **E**, Western blot analysis (**D**) of PRL-R pathway members in NMuMG control cells (AdNeg) or silenced for p27 (shp27). Cells were serum starved overnight, treated with cycloheximide (CHX; 50 μg/mL) for 2 hours and then stimulated with murine PRL (200 ng/mL) for indicated times. GAPDH was used as loading control. Graphs in (**E**) report the quantification of the bands corresponding to PRL-R, JAK2 and STAT5 normalized by the Ponceau staining of the lysates. **F**, Analysis of PRL-R internalization and trafficking in NMuMG cells control cells (AdNeg) or silenced for p27 (Ad mshp27). Cells were serum starved for 4 hours and stimulated with murine PRL (200 ng/mL) for 1 hour on ice. Cells were then incubated at 37°C for the indicated time and immunostained with PRL-R (green), RAB5 (red), and phalloidin (blue). Right, silencing control of cells used for PRL-R immunostaining. In all graphs, significance was calculated by Student's *t* test and is indicated by a $P < 0.05$

To better dissect, at molecular level, the players responsible for PRL-R pathway signaling hyperactivation in Δ16HER2 p27KO mammary glands we moved to *in vitro* models.

We exploited the murine epithelial cell line NMuMG (Normal Murine Mammary Gland) and generated stable clones overexpressing the human Δ16HER2 oncogene, in which p27 expression could be efficiently silenced by adenoviral transduction. First, we wondered whether PRL-R, JAK2 or STAT5 protein expression and stability was different in control and p27 silenced cells. Using cycloheximide, an inhibitor of protein synthesis, in combination with PRL treatment we looked at the protein stability at different time points, by western blot analysis (Figure 8D). By this approach we did not observed major differences in PRL-R, JAK2 and STAT5 expression or stability in Δ16HER2 sh-p27 NMuMG cells (Figure 8D and E). Next, we used immunofluorescence analyses to verify if, upon PRL stimulation, PRL-R was differentially localized and/or regulated in the absence of p27. To this aim we collected cells at different time points after prolactin stimulation and performed immunofluorescence analysis for different markers of the endocytic pathway (Figure 8F). Since prolactin receptor is a highly polarized molecule that needs to be located on the basal membrane of the mammary tissue to correctly signal through the epithelial structure, to mimic this condition we stimulated epithelial cells cultured as clusters isolated one from the other, in which PRL-R assumes a polarized-like distribution on the membrane of the external ring of cells composing the cluster (see Figure 8F, starved cells) (Segatto I et al., 2019). We observed that in Δ16HER2-p27 silenced cells prolactin receptor persisted longer in time and lost its receptor polarization in the outer membrane of cell clusters. In fact, while in control NMuMg cells PRL-R returned to basal levels 40 minutes after the stimuli and maintained its polarized localization in the external membrane, in shp27 NMuMg PRL-R decreased later (60 minutes) and the positive signal was intense and widespread in the cells composing the cluster (Figure 8F).

Considering the fundamental role of cell polarity in the mammary tissue organization, we decided to investigate further this phenotype, by using a more physiological assay. We set up the three-dimensional (3D) embedded culture of primary murine mammary epithelial cells (mMECs) from transgenic mice, to better study the involvement of p27 in the mammary acini formation assay. This assay mimics and recapitulates in culture how mammary cells organize in the real tissue and can thus allow the monitoring of the structural changes that occur within the mammary gland during development. Modulation of mPRL concentration in culture medium also permitted the monitoring of acini formation in the two genotypes using different culture conditions. After 10 days of 3D-culture the mammary acini structures were fully grown within the Matrigel, thus allowing the possibility to study the differences between Δ16HER2 WT and p27KO mMECs, by morphological and immunofluorescence analyses.

Both number and area of the mammary acini grown in 3D Matrigel reflected what we have previously observed *in vivo*, that loss of p27 led to a significant decrease in the number of acini compared to the WT control, coupled with a significant increase in the size of these acini, both in absence and in presence of exogenous mPRL stimulus (Figure 9A-C). Moreover, the addition of exogenous prolactin to p27 KO epithelial cells, but not to WT matched control, resulted in a 3.9-fold increase in the formation of abnormal acini structures, defined as branched acini that resembled the anomalous ductal branching observed in transgenic p27KO mammary gland (Figure 9D).

Immunofluorescence analysis evaluating the expression and localization of PRL-R and ZO-1 (a luminal marker of cell-cell junctions and polarity) showed that Δ16HER2 WT cells stimulated with mPRL displayed a well-organized prolactin receptor localization at the plasma membrane of the cells (red signal in Figure 9E, left panel). Furthermore, ZO-1 (green signal) was found to be expressed in the luminal compartment of the mammary-like acini structures, demonstrating, as expected, a normal conformation and organization of mammary epithelial cells. In contrast, in mammary acini formed by Δ16HER2 p27KO mMEC, only few cells were positive for PRL-R and these cells were aberrantly localized both in the basal and in the luminal compartments, highlighting an abnormal distribution of the receptor and polarization of mammary structure (Figure 9E, see right panel). Moreover, ZO-1 expression was almost undetectable and equally located both in the luminal and basal membranes.

These data suggested that p27 absence in PRL stimulated Δ16HER2 mMECs resulted in a profound alteration of luminal-basal polarization. To better dissect this possibility, we repeated the experiment and compared untreated versus treated condition. Then, we stained for the luminal marker ZO-1, β-catenin and cytokeratins 8 and 14. As reported in Figure 9F, in prolactin-free condition Δ16HER2 p27KO mammary epithelial cells organized in aberrant tubular structures that resembled ductal rather than acini-like structure, contrarily to the WT cells that formed organized acini. p27KO spheres presented an inner luminal compartment that positively stained for the ZO-1 antibody, encircled in a double layer of basal membranes marked by β-catenin (Figure 9F).

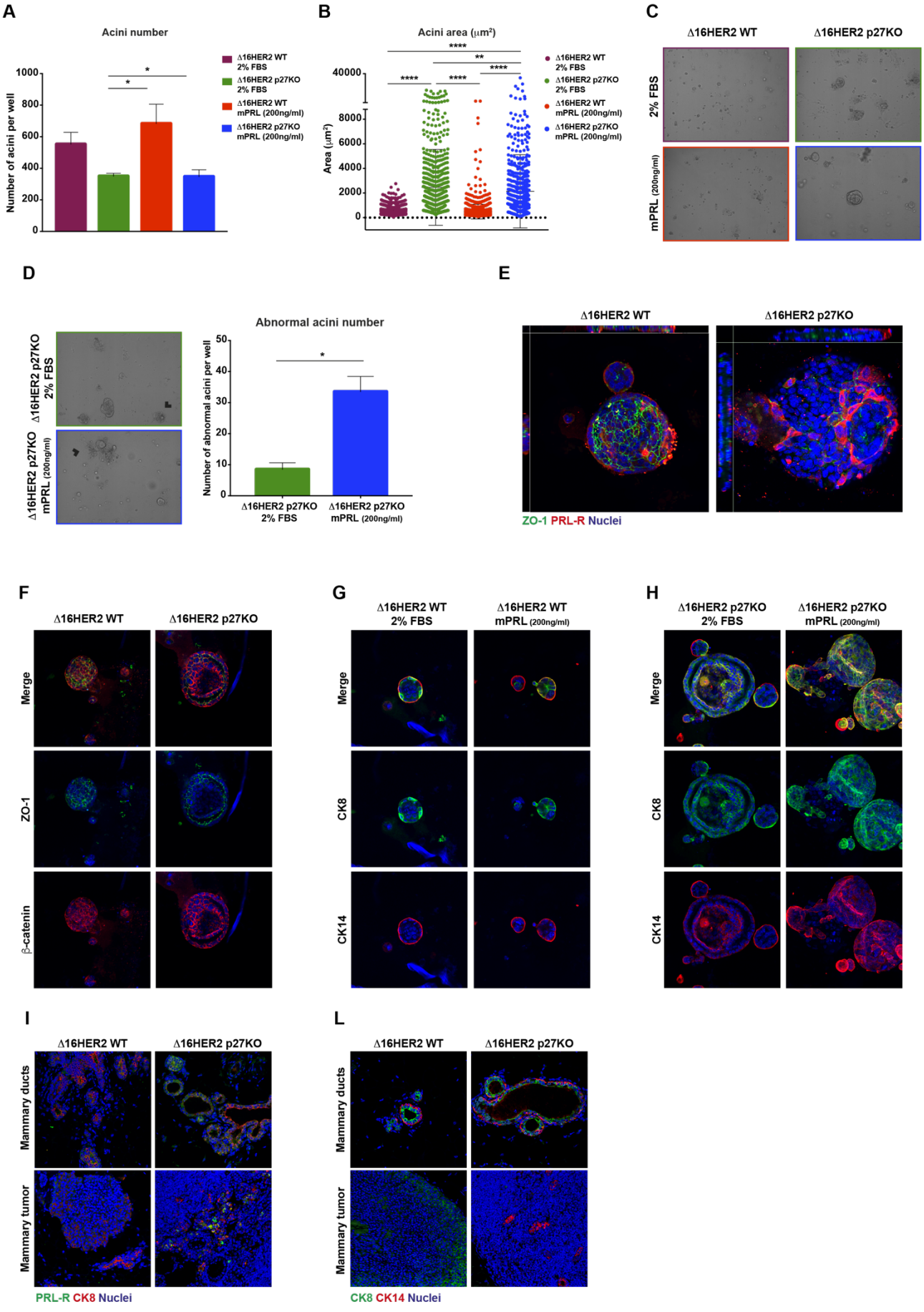
A
Acini number
Number of acini per well
1000
800
600
400
200
0
*
*
Δ16HER2 WT 2% FBS
Δ16HER2 p27KO 2% FBS
Δ16HER2 WT mPRL (200ng/ml)
Δ16HER2 p27KO mPRL (200ng/ml)
B
Acini area (μm²)
Area (μm²)
40000
8000
6000
4000
2000
0
****
**
****
****
****
C
Δ16HER2 WT
Δ16HER2 p27KO
2% FBS
mPRL (200ng/ml)
D
Abnormal acini number
Δ16HER2 p27KO 2% FBS
Δ16HER2 p27KO mPRL (200ng/ml)
Number of abnormal acini per well
50
40
30
20
10
0
*
Δ16HER2 p27KO 2% FBS
Δ16HER2 p27KO mPRL (200ng/ml)
E
Δ16HER2 WT
Δ16HER2 p27KO
ZO-1 PRL-R Nuclei
F
Δ16HER2 WT
Δ16HER2 p27KO
Merge
ZO-1
β-catenin
G
Δ16HER2 WT 2% FBS
Δ16HER2 WT mPRL (200ng/ml)
Merge
CK8
CK14
H
Δ16HER2 p27KO 2% FBS
Δ16HER2 p27KO mPRL (200ng/ml)
Merge
CK8
CK14
I
Δ16HER2 WT
Δ16HER2 p27KO
Mammary ducts
Mammary tumor
PRL-R CK8 Nuclei
L
Δ16HER2 WT
Δ16HER2 p27KO
Mammary ducts
Mammary tumor
CK8 CK14 Nuclei

Figure 9. Loss of p27 alters mammary epithelial cells polarization in Δ16HER2 overexpressing conditions. **A**, Acini formation assay in 3D Matrigel of mouse mammary primary epithelial cells (mMEC) extracted from 13 weeks of age Δ16HER2 WT and p27KO mice. Ten days after Matrigel embedding, with or without exogenous PRL (200 ng/mL) administration, the number of acini/field was counted. **B** and **C**, Colony area (**B**) of experiment described in A measured using the Volocity software and expressed in μm^2. Each dot corresponds to one acinus. Representative images (**C**) of colonies from Δ16HER2 WT and p27KO mice 3D cultured as described in A. **D**, Graph (right) reports the augmented number of abnormal structured acini. Left, representative images of the same structures counted in graph. Arrowheads, tubular structures spreading from mammary epithelial derived acini. **E**, Representative confocal images of mMEC grown in 3D-matrigel, as described in A. ZO-1 (green), PRL-R (red) and nuclei (TO-PRO-3, blue). Cross-section elaboration was obtained using the Volocity software to evaluate the correct polarization of luminal marker ZO-1 and the basal localization of PRL-R. **F**, Representative immunofluorescence analysis of ZO-1 (green), b-catenin (red) and nuclei (TO-PRO-3, blue) in Δ16HER2 p27KO 3D cultured mMEC in 2% FBS culture. **G**, Representative images of immunofluorescence analysis of cytokeratin 8 (luminal marker, green), cytokeratin14 (basal marker, red) and nuclei (TO-PRO-3, blue) in Δ16HER2 WT 3D cultured mMEC in 2% FBS culture condition (left) and after administration of exogenous prolactin (right). **H**, Representative images of immunofluorescence analysis of luminal CK8 (green), basal CK14 (red) and nuclei (TO-PRO-3, blue) in Δ16HER2 p27KO 3D cultured mMEC in 2% FBS culture condition (left) and after administration of exogenous prolactin (right). **I**, Representative images of immunofluorescence analyses of FFPE mouse mammary glands and tumors collected from Δ16HER2 WT or p27KO mice of 16 weeks of age, as indicated. Tissue sections were immunostained for PRL-R (green), luminal cytokeratin 8 (red), and nuclei (TO-PRO-3, blue). At least 4 mammary glands/genotype were analyzed. **L**, Representative images of immunofluorescence analyses of FFPE mouse mammary glands and tumors collected from Δ16HER2 WT or p27KO mice of 16 weeks of age, as indicated. Tissue sections were immunostained for cytokeratin 8 (luminal marker, green), cytokeratin 14 (basal marker, red), and nuclei (TO-PRO-3, blue). At least 4 mammary glands/genotype were analyzed. In all graphs, significance was calculated by One-Way Anova or Student's *t* test, as appropriate, and is indicated by a $P < 0.05$.

The results obtained with the cytokeratins 8 and 14 staining, accepted markers of luminal and basal cells, respectively, reinforced the above data. While WT Δ16HER2 MMEC formed acini with a defined compartmentalization of the luminal CK8 and the basal CK14 expression, Δ16HER2 p27KO cells formed tubular-like structures profoundly altered in polarity organization. The addition of PRL worsened this abnormal phenotype, leading to the formation of tubular elongated structures and collapsed acini, eventually bearing the colocalization of the two cytokeratines widespread between the luminal-basal layers (Figure 9H). Intriguingly, a slight alteration of green (CK8) and red (CK14) signals compartmentalization could be observed also in some of analyzed Δ16HER2 WT spheres exposed to exogenous mPRL (Figure 9G).

Taken together these observations indicated that the presence of the oncogene Δ16HER2 combined with the lack of p27, caused a strong defect in the polarity program of mammary epithelial cells, leading to loss of epithelial cell ability to form normal acinar spheres, which was worsened by the exogenous stimulation with PRL.

To confirm these data derived from 3D-culture of ex vivo cultured mMECs, we next analyzed PRL-R and cytokeratins in the mammary glands from Δ16HER2 13 weeks of age cohort of both genotypes (early stage of tumorigenesis). In mammary glands from Δ16HER2 WT mice PRL-R was weakly expressed and restricted to few cells, while in MMG from Δ16HER2 p27KO mice PRL-R staining was largely diffused and localized inside the disorganized luminal cells that formed the ductal structures (Figure 9I, upper pictures). Analysis of tumor lesions revealed that WT cells presented diffuse and peripheral staining of CK8, but no PRL-R expression and that Δ16HER2 p27KO tumors displayed small subgroups of cells that were co-stained for luminal cytokeratin 8 and PRL-R (Figure 9I). Moreover, the combined staining of mammary glands with CK8 and CK14 revealed that hypertrophic ductal structures that characterize mammary glands from Δ16HER2 p27KO mice, displayed a dramatic loss of the double layered structure of the acini and showed an altered staining of cytokeratins, when compared with WT controls (Figure 9L, see upper panels).

The analysis of mammary foci from the same glands also highlighted profound differences in cytokeratins staining. As already reported (Segatto et al., 2010), Δ16HER2 WT tumors were positive for the luminal marker CK8, while Δ16HER2 p27KO tumors completely lost the expression of CK8, acquiring instead a spotted expression of the basal CK14 (Figure 9L, lower panels).

Taken together all these data, we can conclude that loss of p27 in Δ16HER2-driven breast cancer profoundly impacts on local PRL production and PRL-R pathway activation accompanied by an altered polarity of mice mammary gland, eventually leading to a luminal to basal transition in neoplastic foci.

- **4.5 Loss of p27 in Δ16HER2 overexpressing mice causes an increase in immune cells recruitment**

The role of prolactin in mammary gland structural changes during lactation has been long established, but recent studies underlined the crucial involvement of prolactin hormone also in immune regulation. PRL is recognized as a cytokine produced in a large variety of extra-pituitary sites, including neurons, prostate, decidua, mammary epithelium, endothelial cells, skin cells, and immune cells. In fact, not only prolactin is important to maintain immune competence, but also plays an important role in animal and human immune response (Ben-Jonathan et al., 1996; Bouchard et al., 1999; Walker et al. 2000). Intriguingly, a role for both immune innate and adaptive populations has been assigned during mammary gland development and involution (Coussens et al., 2011; Plaks et al., 2015). In this context, Dill and Walker recently demonstrated the implication of prolactin in migration of immune cells, showing that prolactin administration to adult female mice increased immune cell infiltration throughout the mammary gland, and that the expression and depletion of some chemoattractants produced by epithelial cells are regulated by prolactin in the mammary tissue (Dill and Walker, 2017). We thus hypothesized that the significant increase in expression of prolactin registered in p27KO mammary glands (Figure 7N and 8B) could be due to the recruitment of a specific immune cell population that infiltrates the gland and that, directly or indirectly, could be responsible of local prolactin secretion.

To evaluate the possible impingement of immune population on mammary prolactin levels, we examined the RNA from MMGs of 13 weeks of age Δ16HER2 WT and p27KO female mice. MMGs were processed to separate the epithelial and stromal cells from the immune infiltrating cells. qRT-PCR analysis of prolactin mRNA expression evidenced that a significant extent of the prolactin present in the MMG derived from immune infiltrating cells, both in Δ16HER2 WT and p27KO samples. A significant increase was observed in immune infiltrating cells derived from p27KO mammary tissue, suggesting an important role for this cell population in the higher expression of local prolactin observed in these mice (Figure 10A).

A slight increase in prolactin production was observed also in transgenic p27KO epithelial and stromal compartment compared to the WT counterpart. Looking at PRL-R, we detected a significant increase in Δ16HER2 p27KO-derived epithelial and stromal cells, while no differences were detected in mammary immune infiltrating ones (Figure 10B).

To better assess if differences existed in circulating and/or mammary gland-infiltrating immune populations between Δ16HER2 WT and p27KO mice, 13 weeks of age mice were sacrificed to obtain matched samples of peripheral blood and mammary gland. Specimens were examined by FACS analysis, using a panel of antibodies able to identify the different immune sub-population.

We found interesting differences both in blood and in mammary tissue revealing that three immune populations were significantly altered in Δ16HER2 p27KO mice, namely neutrophils, T lymphocytes and, particularly, $CD8^+$ cells. Lymphocytes normally represent 70% to 80% of the white blood cell (WBC) in healthy wild-type mice, while neutrophils represent 20% to 30% of the WBC and are the most common circulating granulocytes (O'Connell et al., 2015). In our model, while total lymphocytes perfectly follow the percentage reported in literature, we detected a 1.5-fold increase in $CD3^+$ population in Δ16HER2 p27KO compared to the WT, and, by deeper examination of T lymphocytes population, a 2.7-fold increase in $CD8^+$ subset in the same samples. Moreover, we found a 2-fold increase of circulating granulocytes in p27KO samples, in particular of neutrophils, that confirmed the data collected by blood sampling of 13 weeks of age mice reported in Figure 7D.

Then, we analyzed the matched mammary glands from WT and p27KO transgenic mice for the $CD45^+$ gated population (Figure 10C). A comparable T lymphocyte infiltration was observed in both WT and p27KO mammary gland extracts, accounting for approximately 70% of the total $CD45^+$ population and no significant difference was found in granulocytes infiltration, except for a slight increase in neutrophils in Δ16HER2 p27KO mice. However, within the T lymphocytes total population, we identified a 2-fold increase in the so called "likely-active T lymphocytes" ($CD3^+$, $CD11b^+$) population in Δ16HER2 p27KO MMG (Figure 10D). Considering that 13 weeks of age represents a pre-neoplastic condition, we did not expect to find any increase in these cells that are typically recruited and responsible for the immune response to an oncogenic signaling. However, it is conceivable that the anticipation of tumor onset in p27KO mice induces an anticipation of the recruitment of the immune cells to the site in which the oncogenic signaling and, consequently, the appearance of the tumor foci originates. As confirmation of this possibility, IHC analysis of 16 weeks of age mammary glands from both Δ16HER2 WT and p27KO, representing a more advanced stage of tumorigenesis, revealed a 2 fold increase in positive staining for granzyme B (GMZB) in transgenic p27KO mice (Figure 10E), a serine proteinase typically found in granules of natural killer and cytotoxic T cells that, together with the pore forming protein perforin, induces apoptosis in target cells.

Taken together, these results suggest that anticipated oncogene activation in Δ16HER2 p27KO MMG promotes the recruitment of activated T cells that, in turn, induce increased local production of PRL. Matching these results with the fact that PRL-R protein is more expressed in p27KO MMG, there is a molecular explanation for the lactating-like phenotype observed in p27KO virgin mice. However, since we also observed a basal subversion of the immune cell compartment in the circulation of Δ16HER2 p27KO mice, we cannot exclude that this alteration is the one that *in primis* promotes the anticipation of the tumor onset and the consequent acquisition of the lactating-like phenotype. Future

experiments will likely shed light on the actual driving event that leads to the strong tumoral phenotypes that we observe in p27 KO transgenic animals and described in this thesis.

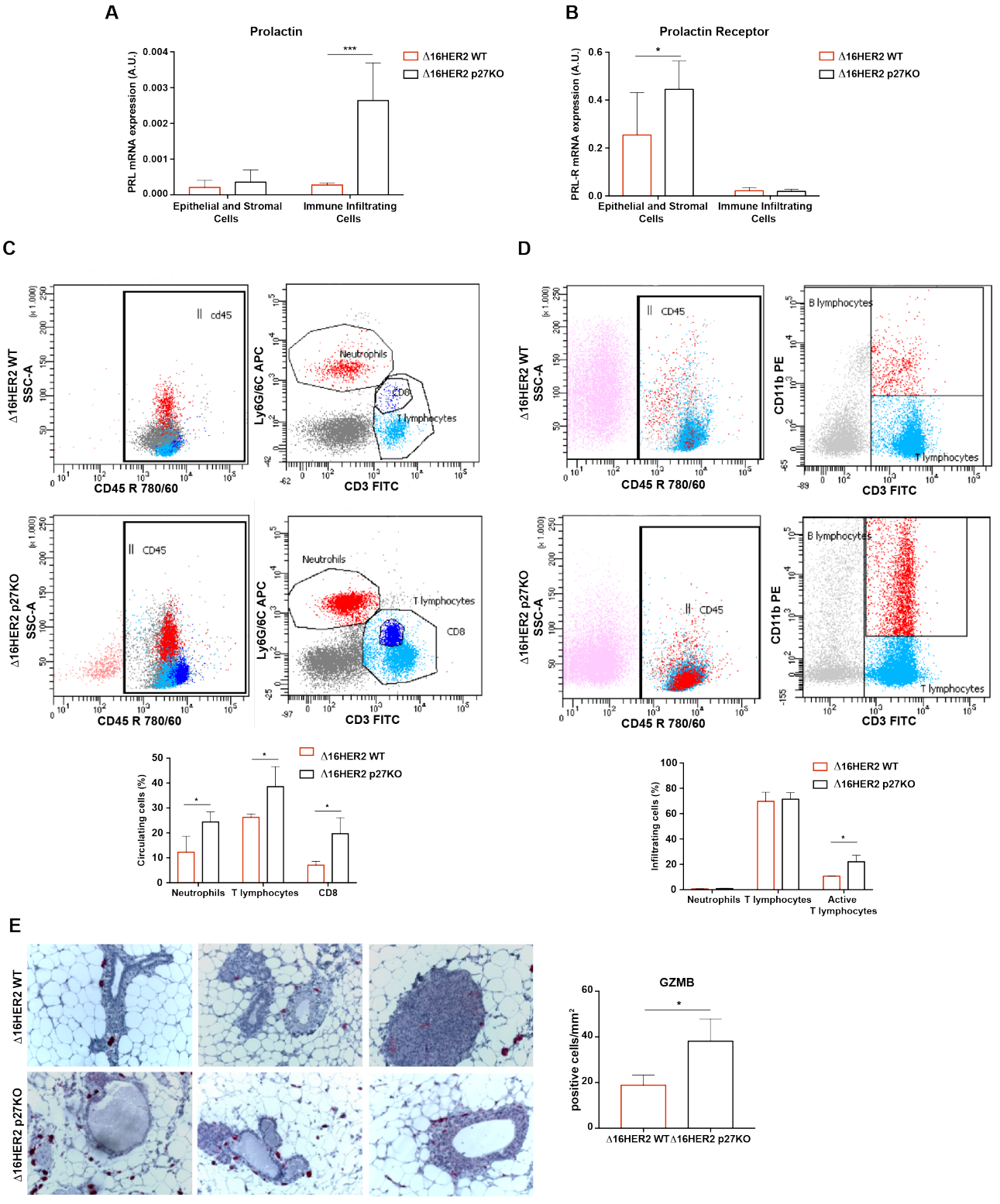
A
Prolactin
PRL mRNA expression (A.U.)
0.004
0.003
0.002
0.001
0.000
***
Δ16HER2 WT
Δ16HER2 p27KO
Epithelial and Stromal Cells
Immune Infiltrating Cells
B
Prolactin Receptor
PRL-R mRNA expression (A.U.)
0.6
0.4
0.2
0.0
*
Δ16HER2 WT
Δ16HER2 p27KO
Epithelial and Stromal Cells
Immune Infiltrating Cells
C
Δ16HER2 WT SSC-A
CD45 R 780/60
cd45
Ly6G/6C APC
CD3 FITC
Neutrophils
CD8
T lymphocytes
Δ16HER2 p27KO SSC-A
CD45
Circulating cells (%)
Δ16HER2 WT
Δ16HER2 p27KO
Neutrophils
T lymphocytes
CD8
D
Δ16HER2 WT SSC-A
CD45 R 780/60
CD45
CD11b PE
B lymphocytes
T lymphocytes
CD3 FITC
Δ16HER2 p27KO SSC-A
Infiltrating cells (%)
Neutrophils
T lymphocytes
Active T lymphocytes
E
Δ16HER2 WT
Δ16HER2 p27KO
GZMB
positive cells/mm²
Δ16HER2 WT
Δ16HER2 p27KO

Figure 10. Ablation of p27 in Δ16HER2-positive mice result in increased circulating and mammary gland infiltrating immune cells. **A** and **B**, qRT-PCR analysis reporting the normalized expression of prolactin (**A**) and prolactin receptor (**B**), on cells explanted MMG from Δ16HER2 WT (red) and p27KO (black) 13 weeks of age virgin female mice. Mammary glands were explanted and properly digested with collagenase IV digestion mix in order to separate epithelial and stromal compartment from immune infiltrating cells. In A PRL mRNA level were normalized on housekeeping gene and on the levels of RNA extracted from each cell population. At least 4 mice per genotype were analyzed. **C**, Representative dot-plot of FACS analysis performed on immune cells extracted from peripheral blood from 13 weeks of age Δ16HER2 WT and p27KO mice. Blood was collected by intracardiac sampling at time of necroscopy and properly processed to obtain the purified circulating immune cells. Right, dot-plots report the alterations found in neutrophils (red gated), T lymphocytes (light-blue gated) and $CD8^+$ T lymphocyte subset (blue gated). Immune sorting analysis were performed on $CD45^+$ gated population (left). Bottom, graph reports the percentage of immune circulating cells. **D**, Representative dot-plot of FACS analysis performed on mammary derived cells extracted from 13 weeks of age Δ16HER2 WT and p27KO mice. Mammary glands were properly digested with collagenase IV digestion mix to obtain the purified epithelial and stromal cells, and immune infiltrating cells. Right, dot-plots report the alterations found in T lymphocytes (light-blue gated) and likely-activated T lymphocyte cells (red gated). Immune sorting analysis were performed on $CD45^+$ gated population (left). Bottom, graph reports the percentage of mammary gland immune infiltrating cells. **E**, Representative image (right) and quantification (left) of immunohistochemistry analysis for serine protease granzyme B in 16 weeks of age FFPE mammary gland sections from Δ16HER2 WT and p27KO mice, 400X enlargement. In all graphs, significance was calculated by One-Way Anova or Student's *t* test, as appropriate, and is indicated by a $P < 0.05$.

5. DISCUSSION

The mammary gland is a highly dynamic tissue, capable of profound changes during its full development, when the cells of the mammary gland proliferate, differentiate or apoptose in response to different stimuli, giving rise to significant remodeling of the glandular tissue architecture. In a similar way, the mammary tissue responds to changes induced by aberrantly activated programs during breast cancer onset and progression (Visvader, 2009; Inman et al., 2015). Several recent studies indicate that, in mammary gland, the organization of luminal epithelial cells into apical-basal polarized structures provides a tumor-suppressive function and that disruption of polarity complexes is implicated in promoting hyperplasia, invasion and metastasis (Catterjee and McCaffrey, 2014; Rejon et al., 2016). Therefore, understanding the mechanisms underlying the mammary gland hierarchy and polarity in this highly organized tissue will contribute to our knowledge of the early stages leading to the pathogenesis of breast cancer.

The cyclin-dependent kinase inhibitor p27Kip1 (p27) is a well-known tumor suppressor gene, that exerts its key role through canonical functions in cell cycle regulation and other so called non-canonical functions (Sharma and Pledger, 2016). The role of p27 as tumor suppressor gene has been largely studied thanks to the generation of p27-deficient mice models. Moreover, inactivating mutations and loss of heterozygosity of CDKN1B have been observed in human cancers, including breast cancer, in which decreased protein expression is associated with poor prognosis. Given the high proliferative rate of mammary tissue and the ability of cyclin-dependent kinase (CDK) inhibitor p27 to negatively regulate cyclin/CDK function, the role of this protein in the regulation of mammary gland fate has been largely investigated, giving rise however to controversial results. Some investigations have demonstrated reduced cyclin D1 expression and consequent lack of lobuloalveolar development in p27-deficient mice, but others have found increased cyclin E-CDK2 activity and increased proliferation, balanced by increased apoptosis (Muraoka et al.,2001; Kong et al., 2002; Davison et al., 2003). The deregulation of p27 protein in human cancer has been associated with ErbB2 oncogene amplification (Newman et al., 2001; Spataro et al., 2003). Intriguingly, several lines of evidence suggest a relationship between ErbB2 and p27 that may be important in the initiation or progression of breast cancer (Hulit et al. 2002).

Here, to study the role of p27 in mammary tumor development and progression we exploited a mouse model expressing a highly aggressive variant of HER2 oncogene, the FVB-MMTV Δ16HER2 and intercrossed these mice with the Cdkn1b (p27 gene) KO colony. Loss of p27 leads to anticipation of tumor onset and acceleration of tumor growth, accompanied by a strong increase in CDK2 activity and proliferation, in line with the canonical role of p27 in inhibiting the cell cycle (Figure 1). Intriguingly, and partially unexpectedly, despite the tumor volume perfectly resemble the highly proliferating phenotype of Δ16HER2 p27KO tumor cells, the number of pre-neoplastic lesions and,

subsequently, of frank tumors that these mice develop is significantly lower in Δ16HER2 p27KO mice compared to the WT counterpart (Figure 2). Further, the capability to disseminate in distant organs, in particular to lungs, seems to be partially impaired in Δ16HER2 p27KO. Not only the number of metastatic lesions was lower, but they were mainly located within the blood vessels instead of the lung parenchyma, as observed in WT counterpart, suggesting that p27KO tumor cells could have a defect in the extravasation process and/or in regrowing at distant sites (Figure 3). These data are partially in contrast with data reporting the correlation of p27 down-regulation in colorectal adenocarcinomas and the ability to metastasize (Thomas et al., 1998), and in line with a recent study where high levels of autoantibodies against p27 significantly correlates with poor overall and event-free survival of high-risk osteosarcoma patients, and an augmented risk of pulmonary metastases when p27 overexpressed (Li et al., 2016).

These phenotypes are complicated and may be the result of different processes that go on together. In literature, in the context of mammary gland transformation CDKN1B alteration seems to be mainly restricted to the luminal subtype. A role for CDKN1B in the maintenance of luminal progenitor cells has been proposed in both humans and ACI rats where p27 absence results in the reduction of luminal progenitor cells (Choudhury et al., 2013 and Ding et al., 2019). It has been proposed that the reduction of luminal progenitors might then result in decreased progenitor cell transformation and, eventually, in the reduction of luminal breast cancer risk (Choudhury et al., 2013 and Ding et al., 2019). Yet, these points will need to be better clarified in appropriate models of luminal breast cancer. Our results, showing an anticipated appearance of palpable tumors combined with a decreased number of transformed foci, support the possibility that a lower number of luminal progenitors are present in the mammary gland of Δ16HER2 p27KO mice. Whether these progenitor cells are more or less susceptible of transformation is something that will be better evaluated in future studies. In any case, p27 null tumors rapidly grow and disseminates within the mammary gland. This of course might represent a cell autonomous role for p27 in the control of breast cancer onset.

However, using several approaches, we have also elucidated that p27 impacts on tumor onset mainly through cell non-autonomous mechanism. The syngeneic injection experiments demonstrated that loss of p27 in the mammary microenvironment of the recipient mouse, has an impact both in tumor appearance and tumor growth, more than loss of p27 in Δ16HER2 mMECs (Figure 4). This result suggests an important role for p27 in the mammary niche, in which different cell populations, such as normal epithelial, stromal cells and immune cells, can contribute to cytokine and growth factor production eventually impinging on Δ16HER2 mMECs engraftment, growth and tumor onset and progression (Figure 7).

The perturbation of the mammary microenvironment could be, at least in part, the explanation for the mammary gland phenotype that we observe in Δ16HER2 p27KO virgin female mice (Figure 5). The features we observed are typical of a lactating mammary tissue, in which ductal and alveolar structures are massively remodeled and transformed under the control of circulating and locally produced hormones and by the timely expression of hormonal-receptors (Macias and Hink, 2012). This phenotype also resembles the one recently observed in Cdkn1B KO ACI rats that showed altered pregnancy-related differentiation (Ding et al. 2019). Even in that case cell non-autonomous mechanisms have been proposed to explain the effects of p27 on mammary gland development (Ding et al. 2019).

Due to the clear lactation-like phenotype we observed and to the results of the cytokine array, we have focused on prolactin and prolactin receptor pathway, master regulator of lactation and highly deregulated in Δ16HER2 p27KO virgin female mice. The alteration of both PRL and PRL-R resulted in the aberrant activation of JAK2 and STAT5 and, consequently, increase transcription of milk proteins β-casein and WAP (Figure 6). Our findings also highlighted that this pathway activation was switched on by concomitant activation of the oncogene (Δ16HER2), suggesting that Δ16HER2 and JAK2 could be "partners in crime" in the exacerbated lactating-like phenotype that we observed in Δ16HER2 p27KO mice. Both JAK2 and STAT5 play a well-established role in breast cancer. Recently, it has been reported that JAK2 represents an important player in initiation of ErbB2-associated breast cancer but constitutive activation of HER2 signaling is able to override the functional role of JAK2 (Sakamoto et al., 2009). Given this evidence, we will need to better understand if there is a functional interaction between Δ16HER2 and the kinase JAK2, and if this relation is critical for developing the lactation-like phenotype and for Δ16HER2-driven breast cancer.

The association of prolactin receptor with breast tumorigenesis remains unclear, as studies that have focused on this association have had limited sample size and/or information about tumor characteristics (Faupel-Badger et al., 2014). In our model of Δ16HER2-driven breast cancer, we find that PRL-R expression is increased in the absence of p27, likely for higher transcription in epithelial cells, and it is also abnormally localized in the mammary epithelial cells of acinar structures, possibly leading to the loss of polarity phenotype that we observed in Δ16HER2 p27KO mMEC in Matrigel and in MMGs (Figure 9) that lost the proper glandular architecture and partially passed from a luminal to basal state. Since the tissue architecture is fundamental for the maintenance of the correct mammary function it is conceivable that this subversion underlies the functional defects that we observed in MMG *in vivo* (Chatterjee and McCaffrey, 2014; Rejon et al., 2016).

Correlation studies of PRL and PRL-R in association with human breast cancer have predominantly focused on circulating PRL levels (Faupel-Badger et al., 2014). Previous studies have found an

association between elevated circulating prolactin levels and increased risk of breast cancer (Vonderhaar, 1999; Clevenger et al., 2003). PRL stimulates breast cancer cell proliferation, migration, and survival by binding to the cell-surface prolactin receptor. The binding of PRL to its receptor activates downstream signaling cascades, influencing several cell functions (Bole et al., 1998). In this thesis, we demonstrate that the levels of circulating PRL are not significantly different in Δ16HER2 WT *vs* p27KO serum samples, but strongly increased within the mammary tissue of p27KO transgenic female mice, thus excluding that this difference was due to an altered production by the pituitary gland (Figure 8). It is well known that PRL can also be secreted in several extra-pituitary locations, including mammary epithelium, ovary, placenta, neurons, endothelium, skin cells, adipose tissue, prostate, spleen, bone marrow and immune cells. Since we observed an increased immune infiltrate in the mammary tissue of Δ16HER2 p27KO mice, we looked at the PRL expression in this population present within the MMGs. The results clearly demonstrated that these cells are the main contributors to the local PRL present in MMGs and could also contribute to further immune recruitment and chemotaxis. Many literature data report that PRL has a bioactive function acting as a hormone and a cytokine and that it exerts a great influence on both cell and humoral immunity (Borba et al., 2019). PRL receptors are expressed in a great variety of immune cells, including macrophages, monocytes, lymphocytes, granulocytes, natural killer cells and thymic epithelial cells. It has been shown that PRL is important to maintain immune competence, is involved in immune response (Ben-Jonathan et al., 1996; Bouchard et al., 1999; Walker et al. 2000) impairs B cell receptor-mediated clonal deletion, deregulate receptor editing, decrease the threshold for activation of anergic B cells and finally interfere with B cell tolerance induction. Likewise, the increase of local PRL is able to enhance cytokine production and the expression of T-cells markers on mitogen stimulated normal $CD8^+$ T-cells and their cytotoxic activity, indirectly support our findings in the context of the cell non-autonomous role of p27 in Δ16HER2 expressing mammary tissue.

In our model, we identified an infiltrating $CD11b^+$ immune population, defined as likely-activated T-lymphocytes, that was greatly increased in Δ16HER2 p27KO mammary glands. The presence of these infiltrating cells could represent either the cause or the effect of the augmented PRL levels in the MMG. Moreover, since immune innate and adaptive populations are associated with mammary gland development and involution (Coussens et al., 2011; Plaks et al., 2015), it will be also important to establish whether the presence of this altered immune infiltrate in p27KO mice is responsible for the anticipated tumor onset. Further studies, aimed at a deeper characterization of these immune population, will be needed to fully elucidate this aspect of Δ16HER2 mammary tumorigenesis in p27KO background.

Another interesting aspect is the specific role of the Δ16HER2 isoform as an immunogen for the recruitment of immune infiltrate. Bartolacci et al., recently demonstrate that phage-based vaccines are able to trigger a protective anti-Δ16HER2 humoral response, demonstrating the immunogenicity of the splicing variant Δ16HER2, able to recruit $CD3^+$ cells to the tumor (Bartolacci et al., 2018). Moreover, our group has recently demonstrated that, after DNA damage, p27 expression is important for preserving genomic integrity and for the apoptosis of aberrant cells (Berton et al., 2017). Putting these two aspects together, it is conceivable that, in the context of p27 loss, emerging tumor foci acquire a "T cell inflamed" phenotype ("hot tumors") eventually leading to the decreased number of mammary tumors that we observe in Δ16HER2 p27KO animals.

So, the immunogenic capability of the oncogene capable to lead to the higher infiltration of activated T-cells in the mammary gland of Δ16HER2 p27KO mice, and the genomic instability caused by the loss of the cell cycle inhibitor p27 could account for the lower number of developed tumor foci as the results of a higher tumor control by the immune system. Even though previously reported observations reinforce the possible crucial role of immune system in limiting tumor growth in p27KO transgenic mice, this possibility should be better dissected in future studies.

Overall, we have fully characterized the phenotypes descending from p27 ablation in Δ16HER2-driven mammary tumorigenesis. The results collected so far reveal a complex crosstalk between the Δ16HER2 transformed epithelial cells and the surrounding mammary microenvironment and demonstrate that, in the absence of p27, the Δ16HER2 oncogene activates earlier in epithelial cells, leading to anticipation of tumor onset and to recruitment of immune infiltrating cells, responsible, in turn, for the local production of prolactin. These early events result in the increased and more sustained activation of PRL-R signaling cascade, thus leading to abnormal mammary tissue architecture and to the appearance of a lactating-like phenotype.

Further studies will be necessary to elucidate the nature and the function of immune cells involved in this phenotype and to understand the molecular mechanism that underlies the anticipated activation of Δ16HER2 oncogene when p27 was ablated. Given that PRL/PRL-R axis is currently proposed as a new possible target for anticancer therapies for BC patients (*e.g.* Prolanta), our results could have a high and immediate translational relevance for BC patients that display low or undetectable levels of p27 expression.

6. REFERENCES

1. Ali, S. & Coombes, R. C. Endocrine-responsive breast cancer and strategies for combating resistance. *Nat. Rev. Cancer* **2**, 101–112 (2002).
2. Andrechek, E. R., White, D. & Muller, W. J. Targeted disruption of ErbB2/Neu in the mammary epithelium results in impaired ductal outgrowth. *Oncogene* **24**, 932–937 (2005).
3. Asselin-Labat, M.-L. *et al.* Gata-3 is an essential regulator of mammary-gland morphogenesis and luminal-cell differentiation. *Nat. Cell Biol.* **9**, 201–209 (2007).
4. Barnes, A. *et al.* Expression of p27kip1 in breast cancer and its prognostic significance. *J. Pathol.* **201**, 451–459 (2003).
5. Bartolacci, C. *et al.* Phage-Based Anti-HER2 Vaccination Can Circumvent Immune Tolerance against Breast Cancer. *Cancer Immunol Res* **6**, 1486–1498 (2018).
6. Belletti, B. *et al.* p27(kip1) functional regulation in human cancer: a potential target for therapeutic designs. *Curr. Med. Chem.* **12**, 1589–1605 (2005).
7. Belletti, B. & Baldassarre, G. New light on p27(kip1) in breast cancer. *Cell Cycle* **11**, 3701–3702 (2012).
8. Ben-Jonathan, N., Mershon, J. L., Allen, D. L. & Steinmetz, R. W. Extrapituitary prolactin: distribution, regulation, functions, and clinical aspects. *Endocr. Rev.* **17**, 639–669 (1996).
9. Berton, S. *et al.* Loss of p27kip1 increases genomic instability and induces radio-resistance in luminal breast cancer cells. *Sci Rep* **7**, (2017).
10. Besson, A. *et al.* A pathway in quiescent cells that controls p27Kip1 stability, subcellular localization, and tumor suppression. *Genes Dev.* **20**, 47–64 (2006).
11. Blows, F. M. *et al.* Subtyping of breast cancer by immunohistochemistry to investigate a relationship between subtype and short and long term survival: a collaborative analysis of data for 10,159 cases from 12 studies. *PLoS Med.* **7**, e1000279 (2010).
12. Boehm, M. *et al.* A growth factor-dependent nuclear kinase phosphorylates p27(Kip1) and regulates cell cycle progression. *EMBO J.* **21**, 3390–3401 (2002).
13. Bole-Feysot, C., Goffin, V., Edery, M., Binart, N. & Kelly, P. A. Prolactin (PRL) and Its Receptor: Actions, Signal Transduction Pathways and Phenotypes Observed in PRL Receptor Knockout Mice. *Endocr Rev* **19**, 225–268 (1998).
14. Borba, V. V., Zandman-Goddard, G. & Shoenfeld, Y. Prolactin and autoimmunity: The hormone as an inflammatory cytokine. *Best Practice & Research Clinical Endocrinology & Metabolism* 101324 (2019) doi:10.1016/j.beem.2019.101324.
15. Bouchard, B., Ormandy, C. J., Di Santo, J. P. & Kelly, P. A. Immune system development and function in prolactin receptor-deficient mice. *J. Immunol.* **163**, 576–582 (1999).
16. Brisken, C. *et al.* Prolactin controls mammary gland development via direct and indirect mechanisms. *Dev. Biol.* **210**, 96–106 (1999).
17. Brisken, C. *et al.* A paracrine role for the epithelial progesterone receptor in mammary gland development. *Proc. Natl. Acad. Sci. U.S.A.* **95**, 5076–5081 (1998).
18. Brown, L. F. *et al.* Expression and distribution of osteopontin in human tissues: widespread association with luminal epithelial surfaces. *Mol. Biol. Cell* **3**, 1169–1180 (1992).
19. Busse, D. *et al.* Reversible G(1) arrest induced by inhibition of the epidermal growth factor receptor tyrosine kinase requires up-regulation of p27(KIP1) independent of MAPK activity. *J. Biol. Chem.* **275**, 6987–6995 (2000).
20. Cancer Genome Atlas Network. Comprehensive molecular portraits of human breast tumours. *Nature* **490**, 61–70 (2012).

21. Cariou, S. *et al.* Down-regulation of p21WAF1/CIP1 or p27Kip1 abrogates antiestrogen-mediated cell cycle arrest in human breast cancer cells. *Proc. Natl. Acad. Sci. U.S.A.* **97**, 9042–9046 (2000).
22. Carroll, J. S. *et al.* p27(Kip1) induces quiescence and growth factor insensitivity in tamoxifen-treated breast cancer cells. *Cancer Res.* **63**, 4322–4326 (2003).
23. Cassimere, E. K., Mauvais, C. & Denicourt, C. p27Kip1 Is Required to Mediate a G1 Cell Cycle Arrest Downstream of ATM following Genotoxic Stress. *PLoS ONE* **11**, e0162806 (2016).
24. Castagnoli, L. *et al.* Activated d16HER2 homodimers and SRC kinase mediate optimal efficacy for trastuzumab. *Cancer Res.* **74**, 6248–6259 (2014).
25. Castiglioni, F. *et al.* Role of exon-16-deleted HER2 in breast carcinomas. *Endocr. Relat. Cancer* **13**, 221–232 (2006).
26. Chatterjee, S. J. & McCaffrey, L. Emerging role of cell polarity proteins in breast cancer progression and metastasis. *Breast Cancer (Dove Med Press)* **6**, 15–27 (2014).
27. Cheang, M. C. U. *et al.* Ki67 index, HER2 status, and prognosis of patients with luminal B breast cancer. *J. Natl. Cancer Inst.* **101**, 736–750 (2009).
28. Choudhury, S. *et al.* Molecular profiling of human mammary gland links breast cancer risk to a p27+ cell population with progenitor characteristics. *Cell Stem Cell* **13**, 117–130 (2013).
29. Chu, E. Y. *et al.* Canonical WNT signaling promotes mammary placode development and is essential for initiation of mammary gland morphogenesis. *Development* **131**, 4819–4829 (2004).
30. Chu, I. M., Hengst, L. & Slingerland, J. M. The Cdk inhibitor p27 in human cancer: prognostic potential and relevance to anticancer therapy. *Nat. Rev. Cancer* **8**, 253–267 (2008).
31. Clevenger, C. V., Furth, P. A., Hankinson, S. E. & Schuler, L. A. The role of prolactin in mammary carcinoma. *Endocr. Rev.* **24**, 1–27 (2003).
32. Coats, S., Flanagan, W. M., Nourse, J. & Roberts, J. M. Requirement of p27Kip1 for restriction point control of the fibroblast cell cycle. *Science* **272**, 877–880 (1996).
33. Coussens, L. M. & Pollard, J. W. Leukocytes in mammary development and cancer. *Cold Spring Harb Perspect Biol* **3**, (2011).
34. Cui, Y. *et al.* Inactivation of Stat5 in mouse mammary epithelium during pregnancy reveals distinct functions in cell proliferation, survival, and differentiation. *Mol. Cell. Biol.* **24**, 8037–8047 (2004).
35. Cusan, M. *et al.* Landscape of CDKN1B Mutations in Luminal Breast Cancer and Other Hormone-Driven Human Tumors. *Front Endocrinol (Lausanne)* **9**, 393 (2018).
36. Davison, E. A. *et al.* The cyclin-dependent kinase inhibitor p27 (Kip1) regulates both DNA synthesis and apoptosis in mammary epithelium but is not required for its functional development during pregnancy. *Mol. Endocrinol.* **17**, 2436–2447 (2003).
37. Dawood, S. Triple-negative breast cancer: epidemiology and management options. *Drugs* **70**, 2247–2258 (2010).
38. Desmedt, C., Sotiriou, C. & Piccart-Gebhart, M. J. Development and validation of gene expression profile signatures in early-stage breast cancer. *Cancer Invest.* **27**, 1–10 (2009).
39. Dill, R. & Walker, A. M. Role of Prolactin in Promotion of Immune Cell Migration into the Mammary Gland. *J Mammary Gland Biol Neoplasia* **22**, 13–26 (2017).
40. Ding, L. *et al.* Deletion of Cdkn1b in ACI rats leads to increased proliferation and pregnancy-associated changes in the mammary gland due to perturbed systemic endocrine environment. *PLOS Genetics* **15**, e1008002 (2019).

41. Donovan, J. C., Milic, A. & Slingerland, J. M. Constitutive MEK/MAPK activation leads to p27(Kip1) deregulation and antiestrogen resistance in human breast cancer cells. *J. Biol. Chem.* **276**, 40888–40895 (2001).
42. Fata, J. E. *et al.* The osteoclast differentiation factor osteoprotegerin-ligand is essential for mammary gland development. *Cell* **103**, 41–50 (2000).
43. Faupel-Badger, J. M. *et al.* Prolactin receptor expression and breast cancer: relationships with tumor characteristics among pre and postmenopausal women in a population-based case-control study from Poland. *Horm Cancer* **5**, 42–50 (2014).
44. Fero, M. L., Randel, E., Gurley, K. E., Roberts, J. M. & Kemp, C. J. The murine gene p27Kip1 is haplo-insufficient for tumour suppression. *Nature* **396**, 177–180 (1998).
45. Fero, M. L. *et al.* A syndrome of multiorgan hyperplasia with features of gigantism, tumorigenesis, and female sterility in p27(Kip1)-deficient mice. *Cell* **85**, 733–744 (1996).
46. Fujita, N., Sato, S., Katayama, K. & Tsuruo, T. Akt-dependent phosphorylation of p27Kip1 promotes binding to 14-3-3 and cytoplasmic localization. *J. Biol. Chem.* **277**, 28706–28713 (2002).
47. Gallego, M. I. *et al.* Prolactin, growth hormone, and epidermal growth factor activate Stat5 in different compartments of mammary tissue and exert different and overlapping developmental effects. *Dev. Biol.* **229**, 163–175 (2001).
48. Geng, Y. *et al*. Deletion of the p27Kip1 gene restores normal development in cyclin D1-deficient mice. *Proc Natl Acad Sci U S A* **98**, 194–199 (2001).
49. Gillett, C. E., Smith, P., Peters, G., Lu, X. & Barnes, D. M. Cyclin-dependent kinase inhibitor p27Kip1 expression and interaction with other cell cycle-associated proteins in mammary carcinoma. *J. Pathol.* **187**, 200–206 (1999).
50. Gouon-Evans, V., Lin, E. Y. & Pollard, J. W. Requirement of macrophages and eosinophils and their cytokines/chemokines for mammary gland development. *Breast Cancer Res.* **4**, 155–164 (2002).
51. Grimmler, M. *et al.* Cdk-inhibitory activity and stability of p27Kip1 are directly regulated by oncogenic tyrosine kinases. *Cell* **128**, 269–280 (2007).
52. Guan, X. *et al.* p27(Kip1) as a prognostic factor in breast cancer: a systematic review and meta-analysis. *J. Cell. Mol. Med.* **14**, 944–953 (2010).
53. Han, Y., Watling, D., Rogers, N. C. & Stark, G. R. JAK2 and STAT5, but not JAK1 and STAT1, are required for prolactin-induced beta-lactoglobulin transcription. *Mol. Endocrinol.* **11**, 1180–1188 (1997).
54. Hara, T. *et al.* Degradation of p27(Kip1) at the G(0)-G(1) transition mediated by a Skp2-independent ubiquitination pathway. *J. Biol. Chem.* **276**, 48937–48943 (2001).
55. Hauck, L. *et al.* Protein kinase CK2 links extracellular growth factor signaling with the control of p27(Kip1) stability in the heart. *Nat. Med.* **14**, 315–324 (2008).
56. Hennighausen, L. & Robinson, G. W. Information networks in the mammary gland. *Nat. Rev. Mol. Cell Biol.* **6**, 715–725 (2005).
57. Hergueta-Redondo, M., Palacios, J., Cano, A. & Moreno-Bueno, G. 'New' molecular taxonomy in breast cancer. *Clin Transl Oncol* **10**, 777–785 (2008).
58. Higgins, M. J. & Baselga, J. Targeted therapies for breast cancer. *J. Clin. Invest.* **121**, 3797–3803 (2011).
59. Holbro, T. & Hynes, N. E. ErbB receptors: directing key signaling networks throughout life. *Annu. Rev. Pharmacol. Toxicol.* **44**, 195–217 (2004).

60. Hulit, J., Lee, R. J., Russell, R. G. & Pestell, R. G. ErbB-2-induced mammary tumor growth: the role of cyclin D1 and p27Kip1. *Biochem. Pharmacol.* **64**, 827–836 (2002).
61. Hynes, N. E. & Watson, C. J. Mammary gland growth factors: roles in normal development and in cancer. *Cold Spring Harb Perspect Biol* **2**, a003186 (2010).
62. Inman, J. L., Robertson, C., Mott, J. D. & Bissell, M. J. Mammary gland development: cell fate specification, stem cells and the microenvironment. *Development* **142**, 1028–1042 (2015).
63. Ishida, N., Kitagawa, M., Hatakeyama, S. & Nakayama, K. Phosphorylation at serine 10, a major phosphorylation site of p27(Kip1), increases its protein stability. *J. Biol. Chem.* **275**, 25146–25154 (2000).
64. Jackson-Fisher, A. J. *et al.* ErbB2 is required for ductal morphogenesis of the mammary gland. *Proc. Natl. Acad. Sci. U.S.A.* **101**, 17138–17143 (2004).
65. Jacquemier, J. *et al.* Association of GATA3, P53, Ki67 status and vascular peritumoral invasion are strongly prognostic in luminal breast cancer. *Breast Cancer Res.* **11**, R23 (2009).
66. James, M. K., Ray, A., Leznova, D. & Blain, S. W. Differential modification of p27Kip1 controls its cyclin D-cdk4 inhibitory activity. *Mol. Cell. Biol.* **28**, 498–510 (2008).
67. Kamura, T. *et al.* Cytoplasmic ubiquitin ligase KPC regulates proteolysis of p27(Kip1) at G1 phase. *Nat. Cell Biol.* **6**, 1229–1235 (2004).
68. Kiyokawa, H. *et al.* Enhanced growth of mice lacking the cyclin-dependent kinase inhibitor function of p27(Kip1). *Cell* **85**, 721–732 (1996).
69. Koletsa, T. *et al.* A splice variant of HER2 corresponding to Herstatin is expressed in the noncancerous breast and in breast carcinomas. *Neoplasia* **10**, 687–696 (2008).
70. Kong, G. *et al.* Functional analysis of cyclin D2 and p27 Kip1 in cyclin D2 transgenic mouse mammary gland during development. *Oncogene* **21**, 7214–7225 (2002).
71. Kotoshiba, S., Kamura, T., Hara, T., Ishida, N. & Nakayama, K. I. Molecular dissection of the interaction between p27 and Kip1 ubiquitylation-promoting complex, the ubiquitin ligase that regulates proteolysis of p27 in G1 phase. *J. Biol. Chem.* **280**, 17694–17700 (2005).
72. Kouros-Mehr, H., Slorach, E. M., Sternlicht, M. D. & Werb, Z. GATA-3 maintains the differentiation of the luminal cell fate in the mammary gland. *Cell* **127**, 1041–1055 (2006).
73. Krege, J. H. *et al.* Generation and reproductive phenotypes of mice lacking estrogen receptor beta. *Proc. Natl. Acad. Sci. U.S.A.* **95**, 15677–15682 (1998).
74. Lane, H. A. *et al.* ErbB2 potentiates breast tumor proliferation through modulation of p27(Kip1)-Cdk2 complex formation: receptor overexpression does not determine growth dependency. *Mol. Cell. Biol.* **20**, 3210–3223 (2000).
75. Lenferink, A. E., Busse, D., Flanagan, W. M., Yakes, F. M. & Arteaga, C. L. ErbB2/neu kinase modulates cellular p27(Kip1) and cyclin D1 through multiple signaling pathways. *Cancer Res.* **61**, 6583–6591 (2001).
76. Li, C. I., Uribe, D. J. & Daling, J. R. Clinical characteristics of different histologic types of breast cancer. *Br. J. Cancer* **93**, 1046–1052 (2005).
77. Li, Y. *et al.* p27 Is a Candidate Prognostic Biomarker and Metastatic Promoter in Osteosarcoma. *Cancer Res.* **76**, 4002–4011 (2016).
78. Liang, J. *et al.* PKB/Akt phosphorylates p27, impairs nuclear import of p27 and opposes p27-mediated G1 arrest. *Nat. Med.* **8**, 1153–1160 (2002).
79. Lilla, J. N. & Werb, Z. Mast cells contribute to the stromal microenvironment in mammary gland branching morphogenesis. *Dev. Biol.* **337**, 124–133 (2010).

80. Lubahn, D. B. *et al.* Alteration of reproductive function but not prenatal sexual development after insertional disruption of the mouse estrogen receptor gene. *Proc. Natl. Acad. Sci. U.S.A.* **90**, 11162–11166 (1993).
81. Lydon, J. P. *et al.* Mice lacking progesterone receptor exhibit pleiotropic reproductive abnormalities. *Genes Dev.* **9**, 2266–2278 (1995).
82. Macias, H. & Hinck, L. Mammary gland development. *Wiley Interdiscip Rev Dev Biol* **1**, 533–557 (2012).
83. Malhotra, G. K., Zhao, X., Band, H. & Band, V. Histological, molecular and functional subtypes of breast cancers. *Cancer Biol. Ther.* **10**, 955–960 (2010).
84. Mani, S. A. *et al.* The epithelial-mesenchymal transition generates cells with properties of stem cells. *Cell* **133**, 704–715 (2008).
85. Marchini, C. *et al.* The human splice variant Δ16HER2 induces rapid tumor onset in a reporter transgenic mouse. *PLoS ONE* **6**, e18727 (2011).
86. Master, S. R. *et al.* Functional microarray analysis of mammary organogenesis reveals a developmental role in adaptive thermogenesis. *Mol. Endocrinol.* **16**, 1185–1203 (2002).
87. Mitra, D. *et al.* An oncogenic isoform of HER2 associated with locally disseminated breast cancer and trastuzumab resistance. *Mol. Cancer Ther.* **8**, 2152–2162 (2009).
88. Moasser, M. M. The oncogene HER2: its signaling and transforming functions and its role in human cancer pathogenesis. *Oncogene* **26**, 6469–6487 (2007).
89. Muraoka, R. S. *et al.* ErbB2/Neu-induced, cyclin D1-dependent transformation is accelerated in p27-haploinsufficient mammary epithelial cells but impaired in p27-null cells. *Mol. Cell. Biol.* **22**, 2204–2219 (2002).
90. Musgrove, E. A., Davison, E. A. & Ormandy, C. J. Role of the CDK Inhibitor p27 (Kip1) in Mammary Development and Carcinogenesis: Insights from Knockout Mice. *J Mammary Gland Biol Neoplasia* **9**, 55–66 (2004).
91. Nakayama, K. *et al.* Mice lacking p27(Kip1) display increased body size, multiple organ hyperplasia, retinal dysplasia, and pituitary tumors. *Cell* **85**, 707–720 (1996).
92. Nakayama, K. *et al.* Skp2-mediated degradation of p27 regulates progression into mitosis. *Dev. Cell* **6**, 661–672 (2004).
93. Nelson, C. M., Vanduijn, M. M., Inman, J. L., Fletcher, D. A. & Bissell, M. J. Tissue geometry determines sites of mammary branching morphogenesis in organotypic cultures. *Science* **314**, 298–300 (2006).
94. Newman, L. *et al.* Correlation of p27 protein expression with HER-2/neu expression in breast cancer. *Mol. Carcinog.* **30**, 169–175 (2001).
95. O'Connell, K. E. *et al.* Practical Murine Hematopathology: A Comparative Review and Implications for Research. *Comp Med* **65**, 96–113 (2015).
96. Olayioye, M. A., Neve, R. M., Lane, H. A. & Hynes, N. E. The ErbB signaling network: receptor heterodimerization in development and cancer. *EMBO J.* **19**, 3159–3167 (2000).
97. Ormandy, C. J., Binart, N. & Kelly, P. A. Mammary gland development in prolactin receptor knockout mice. *J Mammary Gland Biol Neoplasia* **2**, 355–364 (1997).
98. Ormandy, C. J. *et al.* Null mutation of the prolactin receptor gene produces multiple reproductive defects in the mouse. *Genes Dev.* **11**, 167–178 (1997).
99. Parise, C. A., Bauer, K. R., Brown, M. M. & Caggiano, V. Breast cancer subtypes as defined by the estrogen receptor (ER), progesterone receptor (PR), and the human epidermal growth

factor receptor 2 (HER2) among women with invasive breast cancer in California, 1999-2004. *Breast J* **15**, 593–602 (2009).

100. Parmar, H. & Cunha, G. R. Epithelial-stromal interactions in the mouse and human mammary gland in vivo. *Endocr. Relat. Cancer* **11**, 437–458 (2004).
101. Perou, C. M. *et al*. Molecular portraits of human breast tumours. *Nature* **406**, 747–752 (2000).
102. Perou, C. M. & Børresen-Dale, A.-L. Systems biology and genomics of breast cancer. *Cold Spring Harb Perspect Biol* **3**, (2011).
103. Philipp-Staheli, J., Payne, S. R. & Kemp, C. J. p27(Kip1): regulation and function of a haploinsufficient tumor suppressor and its misregulation in cancer. *Exp. Cell Res.* **264**, 148–168 (2001).
104. Piccart-Gebhart, M. J. *et al.* Trastuzumab after adjuvant chemotherapy in HER2-positive breast cancer. *N. Engl. J. Med.* **353**, 1659–1672 (2005).
105. Plaks, V. *et al.* Adaptive Immune Regulation of Mammary Postnatal Organogenesis. *Dev. Cell* **34**, 493–504 (2015).
106. Pohl, G. *et al.* High p27Kip1 expression predicts superior relapse-free and overall survival for premenopausal women with early-stage breast cancer receiving adjuvant treatment with tamoxifen plus goserelin. *J. Clin. Oncol.* **21**, 3594–3600 (2003).
107. Polyak, K. *et al.* p27Kip1, a cyclin-Cdk inhibitor, links transforming growth factor-beta and contact inhibition to cell cycle arrest. *Genes Dev.* **8**, 9–22 (1994).
108. Polyak, K. *et al.* Cloning of p27Kip1, a cyclin-dependent kinase inhibitor and a potential mediator of extracellular antimitogenic signals. *Cell* **78**, 59–66 (1994).
109. Porter, P. L. *et al.* p27(Kip1) and cyclin E expression and breast cancer survival after treatment with adjuvant chemotherapy. *J. Natl. Cancer Inst.* **98**, 1723–1731 (2006).
110. Prat, A. *et al.* Phenotypic and molecular characterization of the claudin-low intrinsic subtype of breast cancer. *Breast Cancer Res.* **12**, R68 (2010).
111. Prat, A. & Perou, C. M. Deconstructing the molecular portraits of breast cancer. *Mol Oncol* **5**, 5–23 (2011).
112. Rakha, E. A., Reis-Filho, J. S. & Ellis, I. O. Basal-like breast cancer: a critical review. *J. Clin. Oncol.* **26**, 2568–2581 (2008).
113. Rejon, C., Al-Masri, M. & McCaffrey, L. Cell Polarity Proteins in Breast Cancer Progression. *Journal of Cellular Biochemistry* **117**, 2215–2223 (2016).
114. Ren, Z. & Schaefer, T. S. ErbB-2 activates Stat3 alpha in a Src- and JAK2-dependent manner. *J. Biol. Chem.* **277**, 38486–38493 (2002).
115. Rittling, S. R. & Novick, K. E. Osteopontin expression in mammary gland development and tumorigenesis. *Cell Growth Differ.* **8**, 1061–1069 (1997).
116. Rodier, G. *et al.* p27 cytoplasmic localization is regulated by phosphorylation on Ser10 and is not a prerequisite for its proteolysis. *EMBO J.* **20**, 6672–6682 (2001).
117. Russo, A. A., Jeffrey, P. D. & Pavletich, N. P. Structural basis of cyclin-dependent kinase activation by phosphorylation. *Nat. Struct. Biol.* **3**, 696–700 (1996).
118. Sasso, M. *et al*. HER2 splice variants and their relevance in breast cancer. J Nucleic Acids Investig. 2011;2(1).
119. Sakamoto, K., Lin, W., Triplett, A. A. & Wagner, K.-U. Targeting janus kinase 2 in Her2/neu-expressing mammary cancer: Implications for cancer prevention and therapy. *Cancer Res.* **69**, 6642–6650 (2009).

120. Schiappacassi, M. *et al.* Role of T198 modification in the regulation of p27(Kip1) protein stability and function. *PLoS ONE* **6**, e17673 (2011).
121. Segatto, I. *et al.* Stathmin is required for normal mouse mammary gland development and Δ16HER2-driven tumorigenesis. *Cancer Res* (2018) doi:10.1158/0008-5472.CAN-18-2488.
122. Serres, M. P. *et al.* p27(Kip1) controls cytokinesis via the regulation of citron kinase activation. *J. Clin. Invest.* **122**, 844–858 (2012).
123. Sharma, S. S., Ma, L., Bagui, T. K., Forinash, K. D. & Pledger, W. J. A p27Kip1 mutant that does not inhibit CDK activity promotes centrosome amplification and micronucleation. *Oncogene* **31**, 3989–3998 (2012).
124. Sharma, S. S. & Pledger, W. J. The non-canonical functions of p27(Kip1) in normal and tumor biology. *Cell Cycle* **15**, 1189–1201 (2016).
125. Sharon, Y. *et al.* Tumor-derived osteopontin reprograms normal mammary fibroblasts to promote inflammation and tumor growth in breast cancer. *Cancer Res.* **75**, 963–973 (2015).
126. Sheaff, R. J., Groudine, M., Gordon, M., Roberts, J. M. & Clurman, B. E. Cyclin E-CDK2 is a regulator of p27Kip1. *Genes Dev.* **11**, 1464–1478 (1997).
127. Sherr, C. J. & Roberts, J. M. CDK inhibitors: positive and negative regulators of G1-phase progression. *Genes Dev.* **13**, 1501–1512 (1999).
128. Shevde, L. A., Das, S., Clark, D. W. & Samant, R. S. Osteopontin: an effector and an effect of tumor metastasis. *Curr. Mol. Med.* **10**, 71–81 (2010).
129. Shin, I. *et al.* PKB/Akt mediates cell-cycle progression by phosphorylation of p27(Kip1) at threonine 157 and modulation of its cellular localization. *Nat. Med.* **8**, 1145–1152 (2002).
130. Silberstein, G. B., Van Horn, K., Shyamala, G. & Daniel, C. W. Essential role of endogenous estrogen in directly stimulating mammary growth demonstrated by implants containing pure antiestrogens. *Endocrinology* **134**, 84–90 (1994).
131. Slamon, D. J. *et al.* Use of chemotherapy plus a monoclonal antibody against HER2 for metastatic breast cancer that overexpresses HER2. *N. Engl. J. Med.* **344**, 783–792 (2001).
132. Sørlie, T. *et al*. Gene expression patterns of breast carcinomas distinguish tumor subclasses with clinical implications. *PNAS* **98**, 10869–10874 (2001).
133. Sorlie, T. *et al.* Repeated observation of breast tumor subtypes in independent gene expression data sets. *Proc. Natl. Acad. Sci. U.S.A.* **100**, 8418–8423 (2003).
134. Spataro, V. J. *et al.* Decreased immunoreactivity for p27 protein in patients with early-stage breast carcinoma is correlated with HER-2/neu overexpression and with benefit from one course of perioperative chemotherapy in patients with negative lymph node status: results from International Breast Cancer Study Group Trial V. *Cancer* **97**, 1591–1600 (2003).
135. Spitale, A., Mazzola, P., Soldini, D., Mazzucchelli, L. & Bordoni, A. Breast cancer classification according to immunohistochemical markers: clinicopathologic features and short-term survival analysis in a population-based study from the South of Switzerland. *Ann. Oncol.* **20**, 628–635 (2009).
136. Stephens, P. J. *et al.* The landscape of cancer genes and mutational processes in breast cancer. *Nature* **486**, 400–404 (2012).
137. Susaki, E., Nakayama, K. & Nakayama, K. I. Cyclin D2 translocates p27 out of the nucleus and promotes its degradation at the G0-G1 transition. *Mol. Cell. Biol.* **27**, 4626–4640 (2007).
138. Tapia, J. C., Bolanos-Garcia, V. M., Sayed, M., Allende, C. C. & Allende, J. E. Cell cycle regulatory protein p27KIP1 is a substrate and interacts with the protein kinase CK2. *J. Cell. Biochem.* **91**, 865–879 (2004).

139. Thomas, G. V. *et al.* Down-regulation of p27 is associated with development of colorectal adenocarcinoma metastases. *Am. J. Pathol.* **153**, 681–687 (1998).
140. Toyoshima, H. & Hunter, T. p27, a novel inhibitor of G1 cyclin-Cdk protein kinase activity, is related to p21. *Cell* **78**, 67–74 (1994).
141. Tsuda, H. *et al.* Detection of HER-2/neu (c-erb B-2) DNA amplification in primary breast carcinoma. Interobserver reproducibility and correlation with immunohistochemical HER-2 overexpression. *Cancer* **92**, 2965–2974 (2001).
142. Turpin, J. *et al.* The ErbB2ΔEx16 splice variant is a major oncogenic driver in breast cancer that promotes a pro-metastatic tumor microenvironment. *Oncogene* **35**, 6053–6064 (2016).
143. Vervoorts, J. & Lüscher, B. Post-translational regulation of the tumor suppressor p27(KIP1). *Cell. Mol. Life Sci.* **65**, 3255–3264 (2008).
144. Viglietto, G. *et al.* Cytoplasmic relocalization and inhibition of the cyclin-dependent kinase inhibitor p27(Kip1) by PKB/Akt-mediated phosphorylation in breast cancer. *Nat. Med.* **8**, 1136–1144 (2002).
145. Visvader, J. E. Keeping abreast of the mammary epithelial hierarchy and breast tumorigenesis. *Genes Dev.* **23**, 2563–2577 (2009).
146. Vlach, J., Hennecke, S., Alevizopoulos, K., Conti, D. & Amati, B. Growth arrest by the cyclin-dependent kinase inhibitor p27Kip1 is abrogated by c-Myc. *EMBO J.* **15**, 6595–6604 (1996).
147. Vlach, J., Hennecke, S. & Amati, B. Phosphorylation-dependent degradation of the cyclin-dependent kinase inhibitor p27. *EMBO J.* **16**, 5334–5344 (1997).
148. Vogel, C. L. *et al.* Efficacy and Safety of Trastuzumab as a Single Agent in First-Line Treatment of *HER2*-Overexpressing Metastatic Breast Cancer. *J. Clin. Oncol.* **20**, 719–726 (2002).
149. Vonderhaar, B. K. Prolactin involvement in breast cancer. *Endocr. Relat. Cancer* **6**, 389–404 (1999).
150. Wagner, K.-U. *et al.* Impaired alveologenesis and maintenance of secretory mammary epithelial cells in Jak2 conditional knockout mice. *Mol. Cell. Biol.* **24**, 5510–5520 (2004).
151. Walker, S. E. & Jacobson, J. D. Roles of prolactin and gonadotropin-releasing hormone in rheumatic diseases. *Rheum. Dis. Clin. North Am.* **26**, 713–736 (2000).
152. Wang, K. X. & Denhardt, D. T. Osteopontin: role in immune regulation and stress responses. *Cytokine Growth Factor Rev.* **19**, 333–345 (2008).
153. Weigelt, B., Baehner, F. L. & Reis-Filho, J. S. The contribution of gene expression profiling to breast cancer classification, prognostication and prediction: a retrospective of the last decade. *J. Pathol.* **220**, 263–280 (2010).
154. Wolf, G., Reinking, R., Zahner, G., Stahl, R. A. K. & Shankland, S. J. Erk 1,2 phosphorylates p27Kip1: Functional evidence for a role in high glucose-induced hypertrophy of mesangial cells. *Diabetologia* **46**, 1090–1099 (2003).
155. Xing, D. *et al.* Estrogen modulates TNF-alpha-induced inflammatory responses in rat aortic smooth muscle cells through estrogen receptor-beta activation. *Am. J. Physiol. Heart Circ. Physiol.* **292**, H2607-2612 (2007).
156. Yang, H.-Y., *et al*. Oncogenic Signals of HER-2/neu in Regulating the Stability of the Cyclin-dependent Kinase Inhibitor p27. *J. Biol. Chem.* **275**, 24735–24739 (2000).
157. Zhang, S. *et al.* Combating trastuzumab resistance by targeting SRC, a common node downstream of multiple resistance pathways. *Nat. Med.* **17**, 461–469 (2011).

Publications

Segatto I, De Marco Zompit M, Citron F, D'Andrea S, Rampioni Vinciguerra GL, Perin T, Berton S, **Mungo G**, Schiappacassi M, Marchini C, Amici A, Vecchione A, Baldassarre G, and Belletti B. Stathmin Is Required for Normal Mouse Mammary Gland Development and Δ16HER2-Driven Tumorigenesis. Cancer Res. 2019 Jan 15;79(2):397-409. doi: 10.1158/0008-5472.CAN-18-2488.

Cusan M*, **Mungo G***, De Marco Zompit M*, Segatto I, Belletti B, and Baldassarre G. Landscape of CDKN1B Mutations in Luminal Breast Cancer and Other Hormone-Driven Human Tumors. Front Endocrinol (Lausanne). 2018 Jul 17;9:393. doi: 10.3389/fendo.2018.00393.

Citron F, Segatto I, Rampioni Vinciguerra GL, Musco L, Russo F, **Mungo G**, D'Andrea S, Mattevi MC, Perin T, Schiappacassi M, Massarut S, Marchini C, Amici A, Vecchione A, Baldassarre G, and Belletti B. "Downregulation of miR-223 expression is an early event during mammary transformation and confers resistance to CDK4/6 inhibitors in luminal breast cancer." Cancer Res. (2019) doi:10.1158/0008-5472.CAN-19-1793.

Acknowledgments

I am grateful to all my group members (SCICC lab), in particular I like to thank Dr. Barbara Belletti, Dr. Ilenia Segatto and Dr. Gustavo Baldassarre for accepting me in the lab and for giving me the opportunity to carry out my PhD project, helping and supporting me.